AD_____

AWARD NUMBER: DAMD17-02-1-0415

TITLE: Tc-99m Labeled and VIP-Receptor Targeted Liposomes for Effective Imaging of Breast Cancer

PRINCIPAL INVESTIGATOR: Hayat Onyuksel, Ph.D.

CONTRACTING ORGANIZATION: University of Illinois
Chicago, Illinois 60612-7205

REPORT DATE: September 2006

TYPE OF REPORT: Final

PREPARED FOR: U.S. Army Medical Research and Materiel Command
Fort Detrick, Maryland 21702-5012

REPORT DOCUMENTATION PAGE

Form Approved
OMB No. 0704-0188

1. REPORT DATE *(DD-MM-YYYY)*	**2. REPORT TYPE**	**3. DATES COVERED** *(From - To)*
01-09-2006	Final	1 Sep 2002 –31 Aug 2006

4. TITLE AND SUBTITLE

Tc-99m Labeled and VIP-Receptor Targeted Liposomes for Effective Imaging of Breast Cancer

5a. CONTRACT NUMBER

5b. GRANT NUMBER
DAMD17-02-1-0415

5c. PROGRAM ELEMENT NUMBER

6. AUTHOR(S)

Hayat Onyuksel, Ph.D.

E-Mail: hayat@uic.edu

5d. PROJECT NUMBER

5e. TASK NUMBER

5f. WORK UNIT NUMBER

7. PERFORMING ORGANIZATION NAME(S) AND ADDRESS(ES)

University of Illinois
Chicago, Illinois 60612-7205

8. PERFORMING ORGANIZATION REPORT NUMBER

9. SPONSORING / MONITORING AGENCY NAME(S) AND ADDRESS(ES)
U.S. Army Medical Research and Materiel Command
Fort Detrick, Maryland 21702-5012

10. SPONSOR/MONITOR'S ACRONYM(S)

11. SPONSOR/MONITOR'S REPORT NUMBER(S)

12. DISTRIBUTION / AVAILABILITY STATEMENT
Approved for Public Release; Distribution Unlimited

13. SUPPLEMENTARY NOTES

14. ABSTRACT
However, current methods of breast cancer detection cannot provide accurate results. This study was conceived to begin to address this issue by developing and testing a novel method of active targeting of radionuclide (Tc-99m) encapsulating sterically stabilized liposomes (SSL) for gamma scintigraphic imaging of breast cancer. This non-invasive imaging modality utilizes both overexpression of vasoactive intestinal peptide (VIP) receptors in breast tumor and distinct biology of the tumors (leaky vasculature) to target specifically to breast cancer. The liposomal imaging agent developed in this study encapsulates multiple molecules of Tc99m for high sensitivity. In addition, its specificity for breast cancer is achieved with a peptide (VIP) the receptors of which are over expressed in breast cancer. Targeting of this novel liposomal imaging agent to breast tumors was tested both in vitro using rat and human breast cancer tissues and in vivo using a carcinogen induced rat breast cancer model. The results showed that significantly more VIP-SSL were bound to carcinogen-induced rat breast cancer tissue sections than SSL without VIP or with non-covalently associated VIP. The imaging results demonstrated that Tc-99m encapsulating VIP-SSL showed a higher tumor-to-background ratio than Tc-99m encapsulating SSL. In addition, the accumulation of Tc-99m encapsulating VIP-SSL was significantly higher than Tc-99m encapsulating SSL in rat breast tumor, suggesting that the presence of VIP did serve the purpose of active targeting of liposomes, confirming the results obtained by imaging studies. In conclusion, the novel breast tumor targeted liposomes developed in this study can provide accurate detection of breast cancer in the clinics. In addition, the same targeted carrier system can be used in the future for the targeted delivery of anticancer agents to breast tumors for safe and effective chemotherapy of breast cancer.

15. SUBJECT TERMS
VIP-R as molecular target for breast cancer

16. SECURITY CLASSIFICATION OF:			**17. LIMITATION OF ABSTRACT**	**18. NUMBER OF PAGES**	**19a. NAME OF RESPONSIBLE PERSON**
a. REPORT	**b. ABSTRACT**	**c. THIS PAGE**			USAMRMC
U	U	U	UU	88	**19b. TELEPHONE NUMBER** *(include area code)*

Table of Contents

INTRODUCTION

Every year about 40,000 women die of breast cancer. Statistics show that early detection and therapy improves breast cancer survival. However, current methods of breast cancer detection cannot provide accurate results. For example, the most commonly used technique, mammography, can only detect one-fourth of all the breast cancers. This study was conceived to begin to address this issue by developing and testing a novel method of active targeting of radionuclide (Tc-99m) encapsulating sterically stabilized liposomes (SSL) for gamma scintigraphic imaging of breast cancer. This non-invasive imaging modality utilizes both overexpression of vasoactive intestinal peptide (VIP) receptors in breast tumor and distinct biology of the tumors (leaky vasculature) to target specifically to breast cancer. The liposomal imaging agent developed in this study encapsulates multiple molecules of Tc99m for high sensitivity. In addition, it should have high specificity for breast cancer because its' surface is modified with a peptide (VIP) the receptors for which are over expressed in breast cancer. This novel targeted liposomal imaging agent was tested both in vitro using rat and human breast cancer tissues and in vivo using a carcinogen induced rat breast cancer model.

BODY

Task 1: Develop labeled VIP-SSL (Year 1)

Preparation of SSL encapsulating Tc-99m:

Sterically stabilized liposomes were prepared by hydration of dried lipid film followed by extrusion, as described before (Dagar, 1998) with modifications. Egg- phosphatidylcholine (PC), cholesterol (CH), polyethylene glycol (molecular weight 2000) conjugated distearyl phosphatidylethanolamine (DSPE-PEG) & dipalmitoyl phosphatidylglycerol (DPPG) in the molar ratio PC: DPPG: DSPE-PEG: CH of 0.50:0.10:0.05:0.35 were dissolved in an organic solvent (chloroform-methanol; 9:1 v/v) & solvent evaporated in a rotary evaporator under vacuum. The dry lipid film was hydrated with isotonic, 50 mM glutathione containing isotonic 0.01 M HEPES buffer (pH 7.4). The dispersion was extruded through polycarbonate filter (100 nm) and unentrapped glutathione removed by gel filtration with isotonic 0.01 M HEPES buffer (pH 7.4) as the eluent. The glutathione containing liposomes, visible as turbid fractions, were pooled. These liposomes were then labeled by first incubating Ceretec® with Tc-99m-pertechnate to form a lipophilic Tc-99m-HMPAO complex. This lipophilic complex was then incubated with preformed glutathione-containing liposomes and the complex, being lipophilic, passed through the bilayer. Tc-99m-HMPAO complex was then trapped irreversibly in the internal aqueous phase of the liposome by reduction of the lipophilic

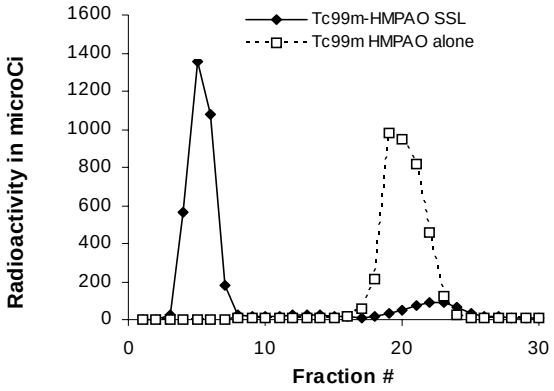

Figure 1: Elution profile of free Tc-99m-HMPAO and Tc-99m-HMPAO encapsulating SSL after gel filtration

complex by glutathione into a hydrophilic one. The free label was then removed by gel filtration. The Tc-99m-HMPAO encapsulating liposomes (turbid fractions with high radioactivity) coming out in the void volume were pooled and used for further studies. The mean size of the prepared liposomes and the radioactivity in each fraction were measured using QuasiElastic Light Scattering and a dose calibrator respectively.

Results: SSL with average size of -100 nm were successfully prepared and a clear separation of the encapsulated Tc-99m-HMPAO was seen as shown in Figure 1.

Conjugation of VIP to DSPE-PEG and insertion into SSL:

An activated DSPE-PEG_{3400} (DSPE-PEG_{3400}-NHS, 1,2-dioleoyl-sn-glycero-3-phosphoethanolamine-n-[poly(ethylene glycol)]-N-hydroxy succinamide) was used to conjugate VIP to DSPE-PEG . This reaction takes place between amines and NHS group, which acts as the linking agent. VIP and DSPE-PEG_{3400}-NHS in the molar ratio of 1:5 (VIP: DSPE-PEG-NHS) were dissolved separately in 0.01 M isotonic HEPES buffer, pH 6.6. DSPE-PEG-NHS solution was added in small increments over 1-2 min to the VIP solution at 48°C with gentle stirring. The reaction was allowed to proceed for 2 h at 4°C and then stopped by adding glycine solution to the reaction mixture to consume the remaining NHS moieties. The conjugation was tested using SOS-PAGE and subsequent staining with first Coomassie Blue R-250 and then silver stain. The bioactivity of the conjugated VIP was tested using an in situ hamster cheek pouch bioassay. The VIP conjugated to DSPE-PEG (DSPE-PEG-VIP) was subsequently used to prepare fluorescent VIP-SSL.

The conditions for DSPE-PEG conjugated VIP insertion into preformed Tc-99m- HMPAO encapsulating SSL were determined by measuring the amount of DSPE-PEG in the preformed liposomes under various conditions and times.

Results: A 1:1 conjugate of DSPE-PEG and VIP was successfully prepared (Figure 2).

In addition in situ bioassay indicated that the bioactivity of VIP was retained after conjugation. DSPE-PEG-VIP was maximally inserted at about 2h. There was no significant increase in insertion into the liposomes after 2h. Hence, 2h incubation at 37°C was considered enough to insert significant amounts of DSPE-PEG-VIP into the preformed SSL.

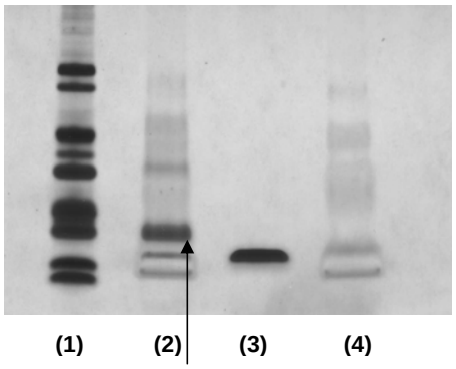

Figure2: SDS-PAGE of the reaction products. (1) Molecular weight standards, (2) Reaction mixture (1:5 VIP: DSPE-PEG_{3400}- NHS, ~2h at 4°C), (3) VIP alone and (4) DSPE-PEG_{3400}-NHS

Characterization of *Tc-99m-HMPAO encapsulating VIP-SSL*

The Tc-99m-HMPAO encapsulating VIP-SSL were characterized in terms of their size, phospholipid and radioactivity content and their labeling efficiency and compared to Tc-99m-HMPAO encapsulating SSL. The release of Tc-99m-HMPAO encapsulating SSL after insertion of conjugate was tested by storing of SSL in the presence and absence of DSPE-PEG_{3400}-NHS at 37°C.

Results: There was no significant difference between Tc-99m-HMPAO encapsulating VIP-SSL and SSL (Table 1) indicating that insertion of VIP did not interfere with the properties of the SSL. No significant leakage of Tc-99m label (Figure 3) and change in size (Before incubation 109±13 nm and after incubation 114±15 nm) was observed, indicating that these liposomes were stable.

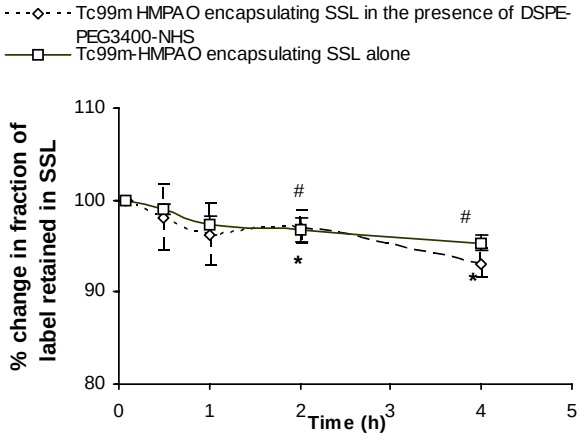

Figure 3: Leakage of encapsulated Tc-99m-HMPAO from sterically stabilized liposomes (SSL) after incubation at 37oC in isotonic 0.01M HEPES buffer (pH 7.4). (* and # ;p<0.05 as compared to 0h)

CHARACTERISTIC	METHOD	Tc-99m-HMPAO encapsulating SSL	Tc-99m-HMPAO encapsulating SSL and VIP-SSL
SIZE	*Qausi - elastic light scattering*	109.81±14.21nm	114.77 ± 13.72 nm
PHOSPHOLIPID CONTENT	*Modified Bartlet Phosphate assay*	3.15±0.23 μmol/mL	3.01 ± 0.48 μmol/mL
RADIOACTIVITY CONTENT	*Atomlab 100 dose Calibrator*	1008± 160μCi/mL	800 ± 113 μCi/mL
LABELING EFFICIENCY	*Atomlab 100 dose Calibrator*	85.7 ± 4.46 %	83.8 ± 2.42 %

Table 1: Characteristics of Tc-99m-HMPAO encapsulating SSL and VIP-SSL (Each value is Mean±standard deviation, n = at least 6)

Status of Task 1: COMPLETED (Year 1)

Task 2: Test the in vitro Targeting of labeled VIP-SSL to VIP-R (Year 1)

For testing the in vitro binding, BODIPY-Chol (a non-exchangeable fluorescent probe) containing liposomes, were prepared using film rehydration-extrusion method, as described above but incorporating the probe at 1: 1500 molar ratio (lipid:probe) in the lipid mixture. DSPE-PEG-VIP was inserted into these fluorescent liposomes to form fluorescent VIP conjugated sterically stabilized liposomes (VIP-SSL).

The rats bearing MNU-induced breast cancer were developed as described below and were euthanized by exposure to carbon dioxide in a closed chamber. Normal and cancerous breast tissues were excised, frozen immediately in liquid nitrogen and stored at 80°C until use. The frozen breast tissue was cut into 20 micron sections and mounted on microscopic slides. They were then fixed with 4% formaldehyde and allowed to air- dry for 10 min. Adjacent 5 micron thick frozen tissue sections, were stained with hemotoxylin and eosin to confirm the presence or absence of cancer in the breast tissue. The presence of VIP-R in these rat breast cancer tissues was confirmed using a fluorescent VIP, Fluo-VIP as described by us recently (Dagar 1999 and 2001). Twenty- micrometer sections of MNU-induced rat breast cancer tissues were cut using a cryotome, placed on a slide, fixed with 4% formalin for 20 min, and then air-dried for 10 min. The BODIPY-Chol containing VIP-SSL were added to the sections and incubated for 1 h at room temperature. At the end of the incubation period, the slides were washed with 0.01 M isotonic HEPES buffer, pH 7.4, four times for 60s each. The slides were then observed with a Zeiss Fluorescence microscope attached to a Zeiss Camera (Carl Zeiss Inc., Thornwood, NY) and photographed.

Results: Figure 4 shows the fluorescence microphotographs of breast cancer tissues. The microphotographs indicate that more VIP-SSL was attached to MNU-induced rat breast cancer tissue sections while SSL without VIP or with non-covalently associated VIP, showed no significant attachment. This data indicated that VIP-SSL were able to bind to breast cancer tissue *in vitro* and it was likely that same would be true *in vivo.*

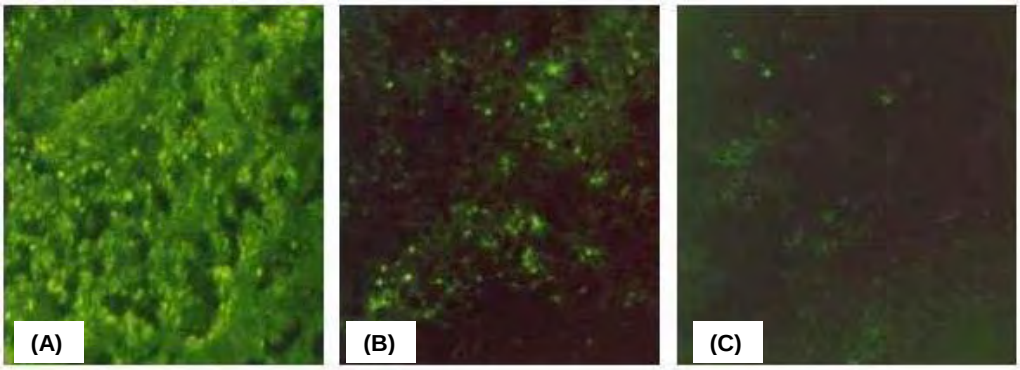

Figure 4: Microphotographs of MNU-induced rat breast tumor tissue sections incubated with fluorescent liposomes A. BOD I PY-Chol incorporating fluorescent VIP-SSL (with covalently attached VIP) B. BODIPY-Chol incorporating fluorescent SSL (without VIP) C. BODIPY-Chol incorporating fluorescent SSL (with non-covalently associated VIP).

Status of Task 2: COMPLETED (Year 1)

Task 3: Determine the biodistribution of labeled VIP-SSL in Breast Cancer Bearing Rats. (Year 2)

Breast cancer induction:

Breast cancer was induced in rats with MNU as previously described (Dagar 1998). Briefly, virgin female Sprague-Dawley rats, 36 days old, weighing -140 g, were anesthetized with ketamine/ xylazine (13.31/1.3 mg per 100 g body weight, i.m.). Each animal received a single intravenous injection of MNU (50 mg/kg body weight) in acidified saline (pH 5.0), via the tail vein. The rats were weighed weekly. They were palpated every week, starting at 3 weeks post-MNU administration. Palpable mammary tumors were detected within 100-150 days after injection. When tumors were ~2cm in diameter they were utilized for the in vivo studies.

Biodistribution studies:

In order to determine the targeting ability of the Tc-99m loaded-VIP-SSL to the breast tumors biodistribution studies were performed on the tumor bearing rats. Rats with induced mammary tumors were divided into two groups of five rats. Each group was injected with 300 μCi as Tc-99m-labeled-VIP-SSL or Tc-99m-labeled-SSL by the tail vein. At 27 h post-injection, the rats were euthanized by an over-dose of ketaminel/xylazine. A blood sample was obtained by cardiac puncture. Tissues (normal breast or breast cancer, liver, spleen, kidneys, calf muscle, heart and lungs) were dissected, washed with saline, dried and transferred to pre-weighed polypropylene tubes and weighed. Their activity was measured using a scintillation gamma counter (Cobra 5005, Packard Instruments). To correct for the physical decay of Tc-99m, a 10 ml aliquot of the injected dose was also counted. The uptake was measured and expressed as percent injected dose per gram of tissue muscles (% I.D./g). The tissue radioactivity amounts, % I.D./g, were compared between formulations (Tc-99m-HMPAO encapsulating SSL or Tc-99m-HMPAO encapsulating VIP-SSL) as well as between normal and tumor bearing rats for each of the formulations using unpaired Student's *t-test. $P<0.05$* was considered significant.

Results: The tissue and tumor distribution of SSL and VIP-SSL in healthy and tumor bearing rats are shown in tables 2 &3 and Figure 5.

The normal breast uptake in healthy rats for both Tc-99m-HMPAO encapsulated SSL and Tc-99m-HMPAO encapsulated VIP-SSL was only 0.04 % 1.0. per gram of tissue (Table 2). In contrast, the breast tumor uptake for Tc-99m-HMPAO encapsulated SSL was about 3 times more than in normal tissues suggesting that the SSL were passively targeted to the breast tumor due the leaky vasculature present in the tumor and the correct size of liposomes (~100 nm). For Tc-99m-HMPAO encapsulated VIP- SSL the uptake was about 6 times more than in normal tissues and 2 times more in the tumors in comparison to SSL (Table 3). This significant increase in accumulation of Tc-99m-HMPAO encapsulated VIP-SSL in breast tumor as compared to SSL indicates success in active targeting resulting in retention of the liposomes by receptor interaction at the tumor site after extravasation leading to significant improvement in the accumulation of SSL into the breast tumor.

There was no major difference in the accumulation of Tc-99m-HMPAO encapsulated SSL and Tc-99m-HMPAO encapsulated VIP-SSL in other tissues (heart, lungs, liver, blood and muscle) on both normal and breast tumor bearing rats.

TISSUE	% I.D. per gram of tissue	
	SSL	VIP-SSL
Normal Breast	0.04 ± 0.00	0.04 ± 0.01
Heart	0.13 ± 0.04	0.18 ± 0.03
Lungs	0.20 ± 0.03	0.31 ± 0.02*
Spleen	9.47 ± 0.96	9.84 ± 0.72
Liver	0.87 ± 0.14	0.88 ± 0.03
Blood	1.10 ± 0.23	0.96 ± 0.06
Kidneys	1.11 ± 0.13	2.42 ± 0.13
Muscle	0.02 ± 0.00	0.02 ± 0.01

Table 2: Biodistribution of Tc-99m-HMPAO encapsulating SSL and Tc-99m-HMPAO encapsulating VIP-SSL in healthy female Sprague-Dawley rat. Each value is Mean ± SEM, n = 3.

TISSUE	% I.D. per gram of tissue	
	SSL	VIP-SSL
Breast tumor	0.13 ± 0.06	0.23 ± 0.02
Heart	0.09 ± 0.02	0.07 ± 0.02
Lungs	0.49 ± 0.32	0.28 ± 0.05
Spleen	10.36 ± 1.60	13.37 ± 1.19
Liver	0.83 ± 0.16	0.90 ± 0.19
Blood	1.44 ± 0.11	1.17 ± 0.26
Kidneys	1.02 ± 0.11	1.57 ± 0.24*
Muscle	0.03 ± 0.01	0.01 ± 0.01

Table 3: Biodistribution of Tc-99m-HMPAO encapsulating SSL and Tc-99m-HMPAO encapsulating VIP-SSL in MNU-induced tumor bearing rats. Each value is Mean ± SEM, n = 5.

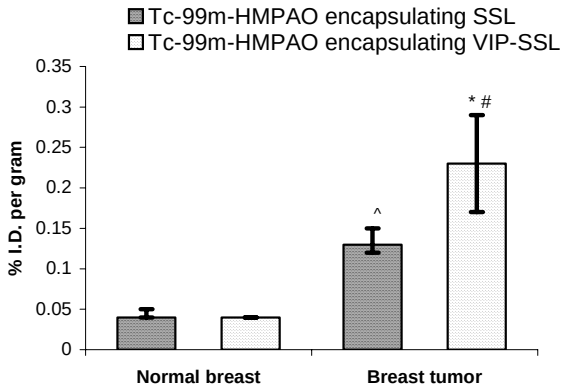

Figure 5: Accumulation of Tc-99m-HMPAO loaded-VIP-SSL and SSL in normal breast tissue and breast cancer tissue. (Values are mean±SEM, n=5). *p<0.05 in comparison to SSL in breast cancer; # p<0.05 in comparison to SSL and VIP-SSL in normal breast, ^p<0.05 in comparison to SSL and VIP-SSL in normal breast

Status of Task 3: COMPLETED (Year 2)

Task 4: Determine the Pharmacokinetics of labeled VIP-SSL in Breast Cancer Bearing Rats (Year 2)

In order to demonstrate the steric stability of the developed liposomes pharmacokinetic studies were performed. Rats with induced mammary tumor were divided into two groups of five rats. Each group was injected with 300 μCi as Tc-99m-labeled VIP-SSL, or SSL, by the tail vein. Two control rat groups without tumors (healthy rats) received SSL or Classical liposomes (non-PEG) similarly. Blood samples, 100μl each were withdrawn from a chronic carotid arterial cannula at 5 min, and 0.5, 1,2,4,8, 12, and 24hr post administration. The radioactivity of each sample was measured and the blood profile of the liposomes determined. Pharmacokinetic parameters were then estimated using Win-Nonlin, version 1.5.

Results: The blood profile of Tc-99m-HMPAO encapsulating SSL in normal rats was evaluated and compared to the behavior of Tc-99m-HMPAO encapsulating liposomes without PEG, i.e. classical liposomes so as to determine whether these SSL are indeed sterically stabilized *in vivo* (Figure 6). Classical liposomes were cleared much faster than SSL and indicating that the presence of PEG on the liposomes did indeed increase the circulation half-life of the liposomes. In tumor bearing rats, the decline in the amount of radioactivity in the blood with time was similar for both Tc-99m-HMPAO encapsulating SSL and Tc-99m-HMPAO encapsulating VIP-SSL, over a 27 h period, as seen in Figure 7, suggesting that the presence of VIP on the surface did not alter the blood behavior of SSL.

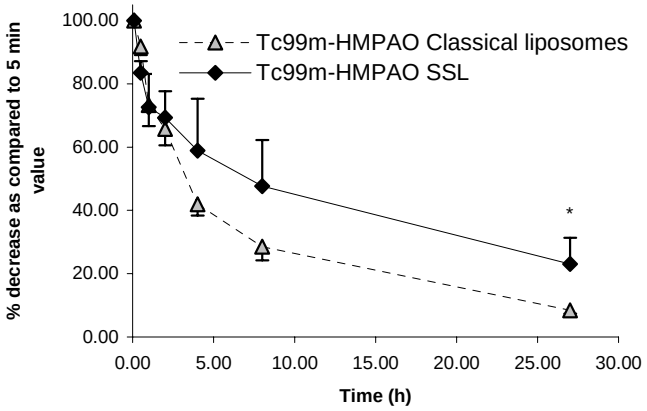

Figure 6: Blood profile of Tc-99m-HMPAO SSL and Tc-99m-HMPAO classical liposomes in normal healthy rats. Each value is mean±SD, n = at least 3. * $p<0.05$ as compared to Tc99m-HMPAO encapsulating CL

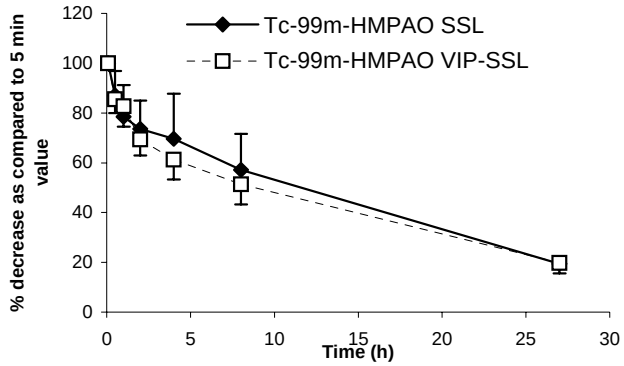

Figure 7: Blood profile of Tc-99m-HMPAO SSL and Tc-99m-HMPAO VIP-SSL in MNU-induced tumor bearing rats. Each value is mean±SD, n = at least 5.

The pharmacokinetic parameters estimated from the blood profile data using Win-Nonlin, version 1.5 is shown in table 4. The half-life of about 14 -16 h for both Tc-99m-HMPAO encapsulating SSL and Tc-99m-HMPAO encapsulating VIP-SSL indicates the long-circulating nature of these liposomes. Moreover, various pharmacokinetic parameters calculated, were similar for both Tc-99m-HMPAO encapsulating SSL and Tc-99m-HMPAO encapsulating VIP-SSL, once again suggesting that the presence of VIP on the surface did not alter the pharmacokinetic characteristics of SSL.

This data clearly demonstrated that presence of VIP did not have any detrimental effect on the PK of SSL. This is most likely due to VIP being an endogenous peptide and the favorable interaction of VIP with lipids prevented removal from circulation by RES. The demonstration of long half-life of SSL-VIP is very important to ensure passive targeting with subsequent active targeting to breast tumors.

Pharmacokinetic Parameters	Formulation	
	Tc-99m-HMPAO encapsulating SSL	Tc-99m-HMPAO encapsulating VIP-SSL
K_{el} (h^{-1})	0.05 ± 0.01	0.05 ± 0.01
$T_{1/2\beta}$ (h)	15.76 ± 3.90	13.89 ± 1.61
CL (L/h)	0.72 ± 0.16	0.77 ± 0.16

Table 4: Pharmacokinetic Parameters of Tc-99m-HMPAO SSL and Tc-99m-HMPAO Classical Liposomes (CL) in normal rats and Tc-99m-HMPAO VIP-SSL in tumor bearing rats calculated using Win-Nonlin version 1.5. Values are expressed as mean ±SD, n = 3-5.

Status of Task 4: COMPLETED (Year 2)

Task 5: Image the Breast Tumors in Rats (Year 3 and 4)

The imaging studies were performed to evaluate the breast tumor image enhancement ability of Tc-99m-HMPAO VIP-SSL compared to Tc-99m-HMPAO SSL in tumor bearing rats. The rats were anesthetized with Ketamine/Xylazine (13.3/1.3 mg per 100g body weight, i.m.). They then were injected with the appropriate radioactive formulation (~300μCi / rat). The rats were imaged at 3hr and 27hr. For imaging the rats were again anesthetized and placed prone on one head of a triple headed Picker PRISM 3000 SPECT gamma camera equipped with low energy high-resolution collimator and a dedicated Odyssey computer. The images (100,000 counts/image) were acquired and stored in a 512X512 matrix.

Image Analysis: The Odyssey software program was used to analyze relative uptake in tumor tissues and the background tissue (calf muscles) in the same animal. The images were analyzed by drawing regions of interest (ROIs) over the breast tumors and calf muscles as background. The uptake was measured as counts per pixel. The uptake in the two calf muscles and the tumors, if more that one tumor per rat, were averaged. Counts per pixel values for five animals were calculated as mean ± SEM. Tumor tissue to background ratios were calculated.

Results: The breast tumor (arrow) was clearly visible in the whole body image of the rat taken using the gamma camera (Figure 8). The T-NT ratios about 3 h post injection were 4.30 ± 0.14 and 4.96 ± 0.32 (mean ± SEM; each group, n = at least 5) for Tc-99m-HMPAO encapsulated SSL and Tc-99m-HMPAO encapsulated VIP-SSL, respectively. The T-NT ratios at 27h post injection were 5.45 ± 0.15 and 6.30 ± 0.12 (mean ± SEM; each group, n= at least 5) for Tc-99m-HMPAO encapsulated SSL and Tc-99m-HMPAO encapsulated VIP-SSL, respectively (Figure 9). The T-NT ratios at both 3h and 27h post injection were significantly ($p<0.05$) more for Tc-99m-HMPAO encapsulated VIP-SSL than Tc-99m-HMPAO encapsulated SSL as determined by unpaired Students t-test.

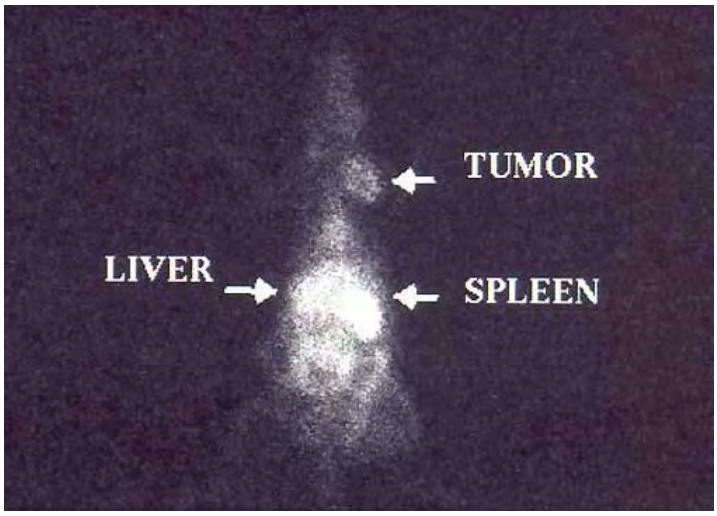

Figure 8: Gamma scintigraphic image of breast tumor bearing rat injected with Tc-99m-HMPAO encapsulating VIP-SSL about 27h post injection.

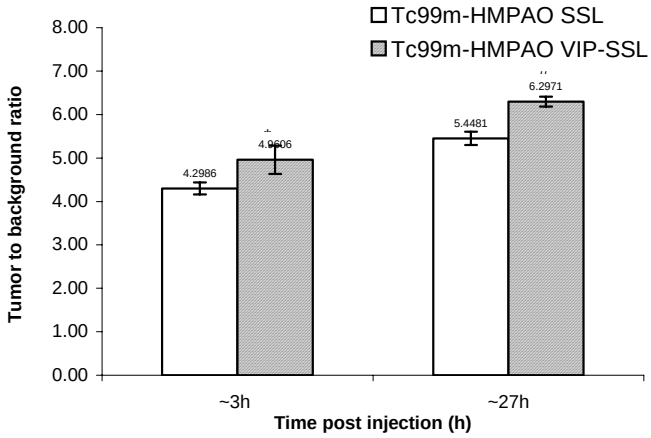

FIGURE 9: Tumor to background ratio of Tc-99m-HMPAO encapsulating SSL and VIP-SSL at ~3h and ~27h post injection. Data is expressed as Mean ± SEM, n = at least 5, * $p<0.05$ as compared to Tc99m-HMPAO at ~3h post injection and # $p<0.05$ as compared to Tc99m-HMPAO at ~27h post injection

Status of Task 5: Complete

KEY RESEARCH ACCOMPLISHMENTS

1. The Tc-99m-HMPAO labeled sterically stabilized liposomes were successfully prepared with a mean diameter of about 110 nm and a high Tc-99m labeling efficiency of about 85%. (Year 1)
2. Vasoactive intestinal peptide (VIP) was successfully conjugated to DSPE-PEG_{3400} at the N-terminal amine of the peptide. This DSPE-PEG_{3400} conjugated VIP retained the bioactivity of the native VIP. (Year 1)
3. The DSPE-PEG_{3400} conjugated VIP was used to form Tc-99m-HMPAO labeled sterically stabilized liposomes surface modified with VIP (VIP-SSL). No significant leakage of the encapsulated Tc-99m-HMPAO label and no significant change in size, phospholipid content and

labeling efficiency were observed due to the insertion process. This method was simple and ensured that all the VIP molecules are on the outer surface of the liposomes available for interaction with the receptors. (Year 1)

4. The *in vitro* targeting studies using breast cancer tissues and VIP-SSL with a non-exchangeable label, fluorescent cholesterol (BODIPY -Chol) incorporated in the bilayer, confirmed the successful binding of VIP-SSL to rat breast cancer *in vitro.* (Year 1)

5. Results of the biodistribution experiments demonstrated that there was significantly more accumulation of Tc-99m-HMPAO encapsulated SSL and Tc-99m-HMPAO encapsulated VIP-SSL in breast tumor as compared to normal breast tissue demonstrating passive targeting. (Year 2)

6. A significant increase in the accumulation of Tc-99m-HMPAO encapsulated VIP-SSL in comparison to Tc-99m-HMPAO encapsulated SSL in rat breast tumor demonstrated success in active targeting to breast tumors. (Year 2)

7. The prepared SSL had significantly slower clearance rate than classical liposomes resulting in increased circulation half-life. (Year 2)

8. The presence of VIP did not make a significant difference in the pharmacokinetic behavior of the SSL. Both SSL and VIP-SSL had similar blood profile and pharmacokinetic parameters demonstrating longevity in circulation. (Year 2)

9. Significantly improved T-NT (tumor to non-tumor) ratio at 3 hr and 27 hr post injection was obtained when Tc-99m-HMPAO encapsulated VIP-SSL was used for breast cancer scintigraphic imaging as compared to SSL. (Year 3-4)

REPORTABLE OUTCOMES

1) Onyuksel H, Dagar S, Krishnadas A, Blend M, Runbinstein I. VIP – Liposomes for active, cell specific targeted delivery of breast cancer in vivo, NCI and CRS *Second International Symposium on Tumor targeted delivery Systems*, Rockville, MD, 2002.
2) Dagar S, Krishandas A, Rubinstein I, Blend M, Onyuksel H. VIP grafted sterically stabilized liposomes for targeted imaging of breast cancer: in vivo studies. *Journal of Controlled Release* 91, 2003, 123-133.
3) Varun S, Onyuksel H, Rubinstein I. Liposomal Vasoactive Intestinal peptide. *Methods Enzymol.*391: 377-95, 2005.
4) Koo O, Rubinstein I and Onyuksel H. Camptothecin in sterically stabilized phospholipid micelles: A novel nanomedicine. *Nanomedicine: Nanotechnology, Biology and Medicine*1, 77-84, 2005.
5) Hayat Onyuksel, Summet Dagar, Aparna Krishnadas, Israel rubinstein, Marin Sekosan, Bao-Shiang Lee, Michel Blend. Tc-99m labeled and VIP receptor targeted liposomes for effective imaging of breast cancer. *Era of Hope 2005 Symposia, Department of defense breast cancer research program meeting*, Philadelphia, Pennsylvania 2005.
6) Koo O, Rubinstein I, Onyuksel H. Delivery of Camptothecin in Nanosized Pegylated Phospholipid Micelles to treat Murine Collagen Induced Arthritis. *PGSRM* 2005.

7) Onyuksel H, Koo O, Sethi V, Rubinstein I. Sterically stabilized Phospholipid micellar human vasoactive intestinal peptide: a novel disease-modifying drug for rheumatoid arthritis. *ACR* 2005.
8) Koo, O., Rubinstein I., Onyuksel, H. Camptothecin in sterically stabilized phospholipid micelles: a novel nanomedicine for rheumatoid arthritis. AAPS 2005.
9) Onyuksel H Targeted Drug Delivery using Nanotechnology, *Abstracts/ Chemical Biological Interactions* 2006.
10) Rubinstein I, Ikezaki H, Onyuksel H. Intratracheal and subcutaneous liposomal VIP normalizes arterial pressure in spontaneous hypertensive hamsters. *International Journal Of Pharmaceutics* 316 (2006) 144-147.
11) Pai A, Rubinstein I, Onyuksel H. PEGylated phospholipid nanomicelles interact with β-Amyloid and mitigate its β sheet formation, aggregation and neurotxicity in vitro*. Peptides* 27 (9) (2006) 2271-5
12) Jeon E. Rubinstein I, Onyuksel H. Interactions of peptide drugs with sterically stabilized phospholipid micelles at molecular level. *CRS* 2006.
13) Pai A, Rubinstein I, Onyuksel H. Nanosized sterically stabilized phospholipid micelles attenuate β-Amyloid aggregation and neurotoxicity in vitro. *CRS* 2006.
14) Soos I, Rubinstein I, Onyuksel H. Real time tracking of actively targeted phospholipid mixed micelles to human breast cancer cells using quantum dots. *CRS* 2006.
15) Koo, O., Rubinstein, I., Onyuksel, H. Camptothecin in sterically stabilized phospholipid nano-micelles: a novel solvent pH change solubilization method. J Nanoscience and Nanotechnology 6 (2006) 2996-3000.

CONCLUSIONS

In this study, we developed a novel liposomal imaging agent targeted to breast cancer and evaluated it by in vitro and in vivo studies. This targeted liposomal imaging agent was able to accumulate specifically at breast tumor tissues by passive and active targeting mechanisms, and provided significantly improved imaging due to sufficient T-NT (tumor to non-tumor) ratio which is required for clinical practice. The result obtained from this study shows the feasibility of this new targeted imaging technology to move towards its transition to the clinics and serve as a superior diagnostic tool for breast cancer.

REFRERENCES

1. Dagar, S., Stastny, J., Blend, M., Rubinstein, I. and Onyuksel, H.: Preparation of Tc-99m -HMPAO VIP-SSL for breast tumor detection. *Pharm.Sci.* 1 :S-294, 1998.

2. Dagar, S., Sekosan, M., Blend, M., Rubinstein, I. and Onyuksel, H.: Identification and Targeting of VIP Receptors in Rats with induced Breast Cancer. *Proceed. Intl. Symp. Control. Rel. Bioact. Mat.* 26:22-23, 1999.

3. Dagar, S., Sekosan, M., Rubinstein, I. and Onyuksel, H.: Detection of VIP receptors

in MNU-induced breast cancer in rats: Implications for breast cancer targeting. *Breast Cancer Research & Treatment* 65:49-54, 2001.

4. Sumeet Dagar, Israel Rubinstein, Hayat Onyuksel, Liposomes in Ultrasound and Gamma Scintigraphic Imaging, *Methods in Enzymology,* 373:198-214, 2003.

5. Sumeet Dagar, Aparna Krishnadas, Israel Rubinstein, Michael J Blend, Hayat Onyuksel, (2003), VIP grafted sterically stabilized liposomes for targeted imaging of breast cancer: in vivo studies. J *Control Release,* 91(1-2):123-33.

APPENDIX

1) Onyuksel H, Dagar S, Krishnadas A, Blend M, Runbinstein I. VIP – Liposomes for active, cell specific targeted delivery of breast cancer in vivo, NCI and CRS *Second International Symposium on Tumor targeted delivery Systems*, Rockville, MD, 2002.
2) Dagar S, Krishandas A, Rubinstein I, Blend M, Onyuksel H. VIP grafted sterically stabilized liposomes for targeted imaging of breast cancer: in vivo studies. *Journal of Controlled Release* 91, 2003, 123-133.
3) Varun S, Onyuksel H, Rubinstein I. Liposomal Vasoactive Intestinal peptide. *Methods Enzymol.*391: 377-95, 2005.
4) Koo O, Rubinstein I and Onyuksel H. Camptothecin in sterically stabilized phospholipid micelles: A novel nanomedicine. *Nanomedicine: Nanotechnology, Biology and Medicine*1, 77-84, 2005.
5) Hayat Onyuksel, Summet Dagar, Aparna Krishnadas, Israel rubinstein, Marin Sekosan, Bao-Shiang Lee, Michel Blend. Tc-99m labeled and VIP receptor targeted liposomes for effective imaging of breast cancer. *Era of Hope 2005 Symposia, Department of defense breast cancer research program meeting*, Philadelphia, Pennsylvania 2005.
6) Koo O, Rubinstein I, Onyuksel H. Delivery of Camptothecin in Nanosized Pegylated Phospholipid Micelles to treat Murine Collagen Induced Arthritis. *PGSRM* 2005.
7) Onyuksel H, Koo O, Sethi V, Rubinstein I. Sterically stabilized Phospholipid micellar human vasoactive intestinal peptide: a novel disease-modifying drug for rheumatoid arthritis. *ACR* 2005.
8) Koo, O., Rubinstein I., Onyuksel, H. Camptothecin in sterically stabilized phospholipid micelles: a novel nanomedicine for rheumatoid arthritis. AAPS 2005.
9) Onyuksel H Targeted Drug Delivery using Nanotechnology, *Abstracts/ Chemical Biological Interactions* 2006.
10) Rubinstein I, Ikezaki H, Onyuksel H. Intratracheal and subcutaneous liposomal VIP normalizes arterial pressure in spontaneous hypertensive hamsters. *International Journal Of Pharmaceutics* 316 (2006) 144-147.
11) Pai A, Rubinstein I, Onyuksel H. PEGylated phospholipid nanomicelles interact with β-Amyloid and mitigate its β sheet formation, aggregation and neurotxicity in vitro*. Peptides* 27 (9) (2006) 2271-5

12) Jeon E. Rubinstein I, Onyuksel H. Interactions of peptide drugs with sterically stabilized phospholipid micelles at molecular level. *CRS* 2006.
13) Pai A, Rubinstein I, Onyuksel H. Nanosized sterically stabilized phospholipid micelles attenuate β-Amyloid aggregation and neurotoxicity in vitro. *CRS* 2006.
14) Soos I, Rubinstein I, Onyuksel H. Real time tracking of actively targeted phospholipid mixed micelles to human breast cancer cells using quantum dots. *CRS* 2006.
15) Koo, O., Rubinstein, I., Onyuksel, H. Camptothecin in sterically stabilized phospholipid nano-micelles: a novel solvent pH change solubilization method. J Nanoscience and Nanotechnology 6 (2006) 2996-3000.

List of personnel who received payment from the research effort

Hayat Onyuksel, Ph.D.

Israel Rubinstein, M.D.

Michael Blend, Ph.D, D.O.

Kyonghee K. Son, Ph.D.

Imran Y. Saleem, Ph.D.

Jing Sun

Elena I. Vinokour

Varun Sethi

Beena Ashok

Imre H. Soos

Sumeet Dagar

Aparna Krishnadas

Maria E. Doukas

#29

VIP-LIPOSOMES FOR ACTIVE, CELL-SPECIFIC TARGETED DELIVERY TO BREAST CANCER IN VIVO

Hayat Onyuksel[1,3], Sumeet Dagar[1], Aparna Krishnadas[1], Michael J Blend[4], Israel Rubinstein[1,2]
Departments of [1]Pharmaceutics and Pharmacodynamics, [2]Medicine, [4]Nuclear Medicine and [3]Bioengineering, University of Illinois at Chicago, Chicago, IL 60612.
Hayat@uic.edu

ABSTRACT SUMMARY

Vasoactive intestinal peptide (VIP) receptors are overexpressed in breast cancer. This study investigated the targeting of labeled sterically stabilized liposomes with surface conjugated VIP to breast cancer in rats in vivo. VIP liposomes had significantly higher accumulation than liposomes without VIP indicating that passive and active targeting to breast cancer can be accomplished in vivo.

INTRODUCTION

Targeted delivery of radionuclides and therapeutic agents to tumors has important implications for detection, diagnosis and therapy of cancer. Biomarkers that differentiate cancerous tissue from normal tissues can be used as targets for this purpose. Since VIP receptors (VIP-R) are overexpressed in breast cancer (1), and these receptors do not express in the circulation they are promising targets. In order for VIP or its analog to interact with the VIP-R it needs to extravasate from the circulation. Particulate carriers such as liposomes with size of ~100nm can only extravasate at certain disease sites such as tumor or inflammation due to the presence of leaky vasculature. To this end, we aimed to develop a universal liposomal carrier system with active VIP on its surface for targeted delivery to breast cancer. In our previous studies we prepared sterically stabilized liposomes (SSL) encapsulating a radionuclide, technetium 99m-hexamethyl propylene amine oxide, (Tc99m-HMPAO) with non covalently associated VIP on their surface (2). When these liposomes were injected into breast tumor bearing rats and imaged by a gamma camera, no significant difference in image enhancement of the tumor was observed in the presence and absence of VIP (3). However, accumulation of liposomes in breast tissue with tumor was much higher than normal breast tissue (3). These results indicated that liposomes were passively targeted to breast cancer by extravasation but active targeting did not occur. We explained these results with the possibility of the VIP dissociating from liposomes at the receptor site. Recently we have developed a method to conjugate VIP on SSL covalently (4,5).

The purpose of this study was to prepare SSL encapsulating Tc99m-HMPAO with VIP covalently conjugated and test the tumor accumulation of these liposomes and compare it to SSL without VIP, in order to determine if any active targeting to breast tumor can be achieve by this novel carrier system.

EXPERIMENTAL METHODS

Preparation of Tc99m-HMPAO VIP-SSL

Tc99m-HMPAO VIP-SSL was prepared as previously described (5). Briefly, Tc99m-HMPAO SSL were first prepared by incubating lipophilic Tc99m-HMPAO complex with preformed glutathione-containing liposomes and separating the free label by gel filtration. Meanwhile VIP was conjugated to DSPE-PEG_{3400} as described before (5). DSPE-PEG_{3400}-VIP was incubated with Tc99m-HMPAO SSL at 37°C. The free DSPE-PEG_{3400}-VIP and the label were then removed by gel filtration to give Tc99m-HMPAO VIP-SSL. The size of both Tc99m-HMPAO SSL and Tc99m-HMPAO VIP-SSL was determined by quasi-elastic light scattering. The percent encapsulation of radiolabel was also determined for both SSL and VIP-SSL.

Breast tissue accumulation

Breast cancer was induced in female virgin rats with MNU as previously described (2,6).

Rats were anesthetized and were then given ~300 µCi of the assigned radiotracer (Tc99m-HMPAO encapsulating SSL or Tc99m-HMPAO encapsulating VIP-SSL) intravenously via the tail vein (minimum of 5 rats/group).

At 27 h post-injection, the rats were euthanized by overdose of ketamine/xylazine. Breast tissues (normal or tumor) were dissected out. They were washed with saline, dried between folds of paper towel and transferred to pre-weighed polypropylene tubes and capped. The tubes were then weighed and the weight of each of the tissue was determined. Their activity measured in a shielded well scintillation gamma counter. To correct for physical decay of Tc99m, and to permit calculation of the uptake of the radiolabeled liposomes, a 10µL aliquot of the injected dose was also counted. The results were expressed as percent injected dose per gram of tissue (% I.D. / g).

RESULTS AND DISCUSSION

The size and percent encapsulation of Tc99m-HMPAO SSL and Tc99m-HMPAO VIP-SSL were not significantly different from each other as shown in Table 1.

	Tc99m-HMPAO SSL	Tc99m-HMPAO VIP-SSL
SIZE, nm	109.81± 14.21	114.77± 13.72
LABELING EFFICIENCY	85.7 ± 4.46 %	83.8 ± 2.42 %

Table 1. Characteristics of Tc99m-HMPAO encapsulating SSL and VIP-SSL (each value, mean ± standard deviation, n = 6)

Both Tc99m-HMPAO SSL and Tc99m-HMPAO VIP-SSL showed significantly higher accumulation in breast tumor as compared to normal breast tissue, suggesting passive targeting of both liposomes to the tumor occurred most probably due to extravasation of the liposomes through leaky vasculature of the tumor (figure 1). However, the Tc99m-HMPAO SSL with VIP showed significantly higher accumulation in breast tumor as compared to liposomes without VIP. This demonstrates that active targeting of liposomes to breast cancer has been achieved by VIP and VIP-R (Figure 1).

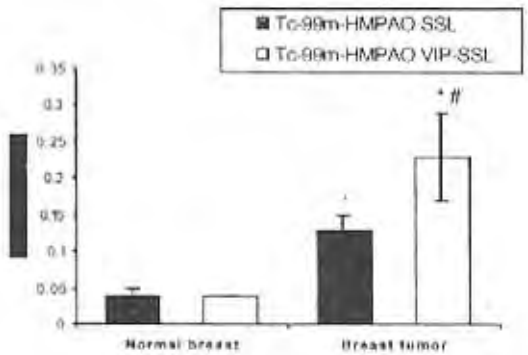

Figure 1. Accumulation of Tc-99m-HMPAO encapsulating SSL and Tc-99m-HMPAO encapsulating VIP-SSL in normal breast tissue and breast cancer (Each data, n=5, mean ± SEM).

* $p<0.05$ compared to Tc-99m-HMPAO encapsulating SSL in breast tumor

\# $p<0.05$ compared to Tc-99m-HMPAO encapsulating SSL and VIP-SSL in normal breast

^ $p<0.05$ compared to Tc-99m-HMPAO encapsulating SSL and VIP-SSL in normal breast

CONCLUSIONS

The results of this study indicate that the covalent conjugation of VIP on the surface of Tc99m-HMPAO SSL did not alter the characteristics of the liposomes, such as size and percent encapsulation. However, breast tumor accumulation of the Tc99m-HMPAO SSL was significantly higher in the presence of VIP due to active targeting. Hence, we have developed a novel carrier system, which is both passively and actively targeted to breast cancer. We are currently evaluating this targeted carrier system for the enhanced

imaging and effective therapy of breast cancer.

REFERENCES

1) J Reubi, J. Nucl. Med. 36: 1846-1853 (1995).
2) S Dagar *et al*, Pharm Sci. Suppl.1: S-294 (1998).
3) S. Dagar, *et al*, Proceed Int Symp Control Rel Bioact Mat 26: 22-23 (1999).
4) S Dagar *et al*, Pharm Sci. Suppl. 2: S-294 (2000).
5) S. Dagar, *et al*, J Control Rel. 74: 129-134 (2001).
6) S. Dagar, *et al*, Breast Cancer Res Treat: 49-54 (2001).

ACKNOWLEDGEMENTS

This work was supported in part by Susan G. Komen Breast Cancer Foundation, Grant # DISS 2000 353, the Department of Defense, BCRP, # BC 011268 and V A merit review.

Appendix (2)

Available online at www.sciencedirect.com
SCIENCE DIRECT®
Journal of Controlled Release 91 (2003) 123–133
journal of controlled release
www.elsevier.com/locate/jconrel

VIP grafted sterically stabilized liposomes for targeted imaging of breast cancer: in vivo studies

Sumeet Dagar[a], Aparna Krishnadas[a], Israel Rubinstein[a,b,c], Michael J. Blend[d], Hayat Önyüksel[a,e,*]

[a]*Department of Biopharmaceutical Sciences, University of Illinois at Chicago, 833 South Wood Street, Chicago, IL 60612-7231, USA*
[b]*Department of Medicine, University of Illinois at Chicago, 833 South Wood Street, Chicago, IL 60612-7231, USA*
[c]*VA Chicago Health Care System, West Side Division, Chicago, IL 60612, USA*
[d]*Department of Nuclear Medicine, University of Illinois at Chicago, 833 South Wood Street, Chicago, IL 60612-7231, USA*
[e]*Department of Bioengineering, University of Illinois at Chicago, 833 South Wood Street, Chicago, IL 60612-7231, USA*

Received 6 December 2002; accepted 22 January 2003

Abstract

Targeted delivery of radionuclides and therapeutic agents to specific biomarkers of breast cancer has important implications for the diagnosis and therapy of breast cancer. Vasoactive intestinal peptide receptors (VIP-R) are approximately five times more expressed in human breast cancer, compared to normal breast tissue. We have used VIP, a 28 amino acid mammalian neuropeptide, as a breast cancer targeting moiety for targeted imaging of breast cancer. VIP was covalently attached to the surface of sterically stabilized liposomes (SSL) that encapsulated a radionuclide, Tc99m-HMPAO. Rats with *n*-methyl nitrosourea (MNU)-induced in situ breast cancers were used to test this targeted liposomal imaging agent. Specifically, the pharmacokinetics and biodistribution of Tc99m-HMPAO encapsulating SSL with and without VIP were determined together with their ability to image breast cancer. The presence of VIP did not alter the size and Tc99m-HMPAO encapsulation ability of SSL. It also did not alter the pharmacokinetic profile of SSL. Long-circulating liposomes with and without VIP on their surface accumulated at significantly higher quantities in breast cancer when compared to normal breast, indicating passive targeting of these constructs to cancer tissues. Importantly, in breast cancer, Tc99m-HMPAO encapsulating SSL with VIP showed significantly more accumulation than SSL without VIP. The tumor to non-tumor ratio was also significantly higher for Tc99m-HMPAO encapsulating VIP–SSL than Tc99m-HMPAO encapsulating SSL without VIP, suggesting active targeting of VIP–SSL to breast cancer. Collectively, these data showed that Tc99m-HMPAO encapsulating VIP–SSL can be successfully used for the targeted imaging of breast cancer.

Keywords: Tc99m-HMPAO; VIP liposome pharmacokinetics; VIP liposome biodistribution; Tumor targeting; Breast cancer imaging

1. Introduction

Targeted delivery of radionuclides and therapeutic agents to cancer has important implications for detection, diagnosis and therapy of cancer. Bio-

*Corresponding author. Department of Biopharmaceutical Sciences (M/C 865), College of Pharmacy, University of Illinois at Chicago, 833 South Wood Street, Chicago, IL 60612-7231, USA. Tel.: +1-312-996-2097; fax: +1-312-996-0098.
E-mail address: hayat@uic.edu (H. Önyüksel).

0168-3659/03/$ – see front matter
doi:10.1016/S0168-3659(03)00242-6

markers that differentiate cancerous tissue from normal tissues can be used as targets for this purpose. One of these attractive molecular targets is vasoactive intestinal peptide receptors (VIP-R), which are overexpressed, about five times, in human breast cancer compared to normal breast tissue [1,2]. In vitro studies using human breast cancer tissues and cells have shown the presence of high densities of VIP receptors, with high affinity and specificity for VIP. Even though breast cancers are frequently known to be polyclonal, studies have shown that VIP receptors exist homogeneously in surgically resected human breast tumors and biopsies, both primaries and metastases. Therefore, VIP-R can be exploited to actively target carriers to breast cancer for effective diagnosis and therapy of breast cancer. In addition to active targeting, particulate carriers such as liposomes with mean size of about 100 nm are passively targeted by predominantly accumulating at certain disease sites such as cancer or inflammation due to the presence of leaky vasculature and liposomal extravasation.

The animal model we used in this study is an orthotropic model where the breast cancer is developed using a carcinogen, *n*-methyl nitrosourea (MNU). This model is more representative of human breast cancer than a xenograft model since the cancer develops in the breast without introduction of cancer cells exogenously. Recently, we have shown that VIP-R are approximately five times more overexpressed in rat breast cancer induced with MNU, similar to that observed in human breast cancer [3,4]. Previously, we have also developed a sterically stabilized liposomal carrier system with covalently attached active VIP on its surface and loaded with Tc99m-HMPAO [5]. The developed liposomal imaging agent encapsulates multiple molecules of Tc99m for high imaging sensitivity and its surface is modified with VIP for increased breast cancer specificity. The rationale behind our approach is depicted in Fig. 1.

Our long-term goal is to develop a targeted liposomal imaging agent for early detection of breast cancer. This study investigates the targeting ability of VIP grafted sterically stabilized liposomes (SSL) that encapsulates a radionuclide (Tc99m-HMPAO), in an animal model with fully developed breast cancer. The specific aim of this study was to determine the cancer tissue accumulation and cancer image enhancement ability of these liposomes in rats with MNU-induced breast cancer. The results are also compared to similar SSL without VIP, in order to evaluate the active targeting to breast cancer by this novel carrier system.

2. Materials and methods

2.1. Materials

L-α-Egg yolk phosphatidylcholine type V-E in chloroform–methanol (9:1, v/v), cholesterol, glutathione and HEPES buffer were obtained from Sigma (St. Louis, MO, USA), 1,2-dipalmitoyl-*sn*-glycero-3-phosphoglycerol from Sygena (Switzerland) and DSPE–PEG_{3400}-NHS {1,2-dioleoyl-*sn*-glycero-3-phosphoethanolamine-*n*-[poly(ethylene glycol)]-*N*-hydroxy succinamide, PEG mw 3400} and polyethylene glycol (mw 2000) conjugated distearoylphosphatidyl ethanolamine (DSPE–PEG_{2000}) were obtained from Shearwater Polymers (Huntsville, AL, USA). Vasoactive Intestinal Peptide (human/rat) was synthesized, using solid-phase synthesis, by the Protein Research Laboratory at the Research Resources Center, University of Illinois at Chicago. ELISA Kit for VIP was from Peninsula Laboratories (San Carlos, CA, USA). Chloroform HPLC grade and methanol HPLC grade were obtained from Fisher Scientific (Pittsburgh, PA, USA).

Freshly eluted Tc99m was obtained from the generator in the Section of Nuclear Medicine, University of Illinois Hospital. Hexamethyl propylene amine Oxime or Ceretec® was purchased from Amersham Healthcare (Arlington Heights, IL, USA). Virgin female Sprague–Dawley rats (~140 g, age 36 days old) were purchased from Harlan (Indianapolis, IN, USA).

2.2. Methods

2.2.1. Preparation of Tc99m-HMPAO encapsulating VIP–SSL and SSL

Tc99m-HMPAO encapsulating VIP–SSL were prepared as described previously [5]. First, Tc99m-HMPAO SSL were prepared by hydration of dried lipid film followed by extrusion, as described before

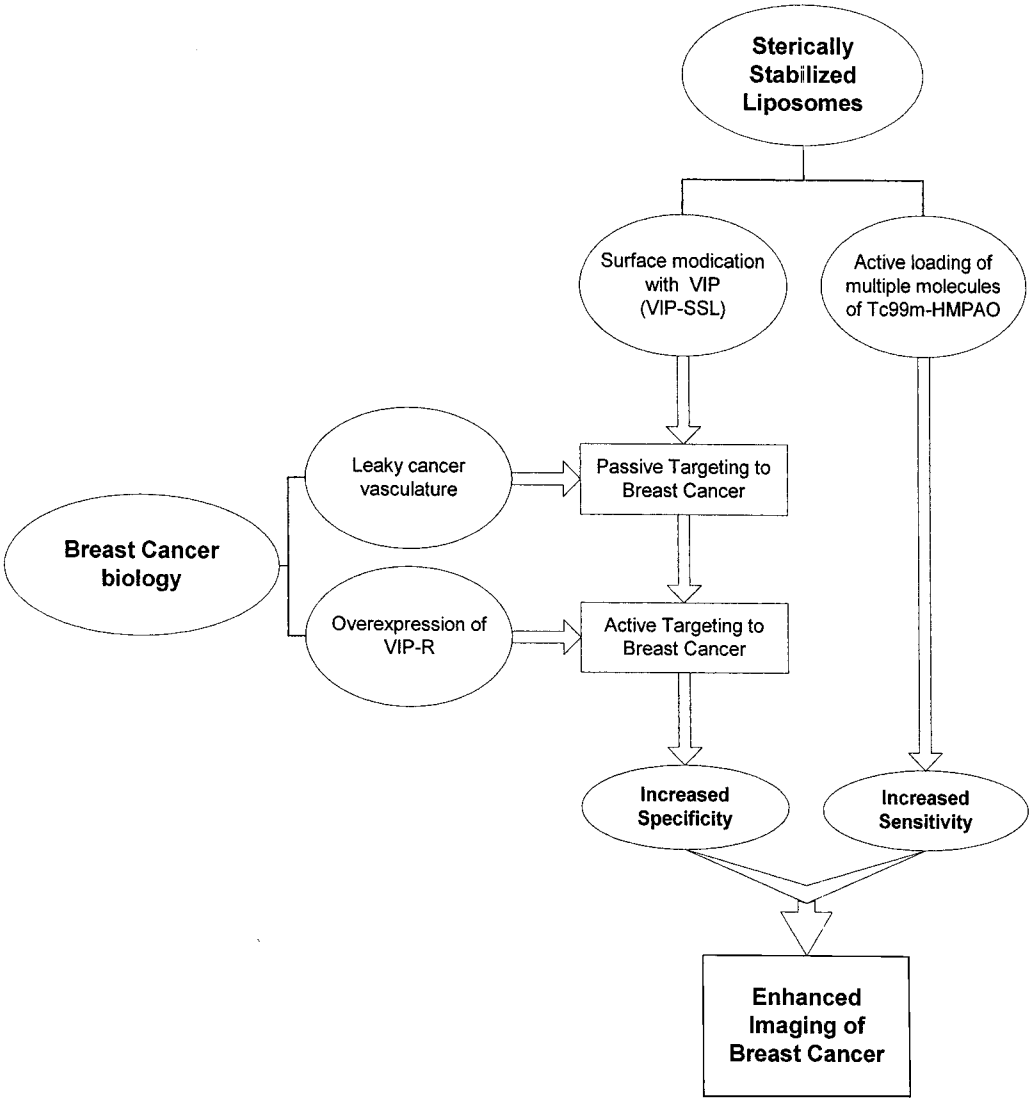

Fig. 1. Flow-chart depicting the novel approach for targeted breast cancer detection.

[6,7] with modifications. Briefly, egg-phosphatidylcholine (PC), cholesterol (CH), polyethylene glycol (molecular weight 2000) conjugated distearyl phosphatidylethanolamine (DSPE–PEG) and dipalmitoyl phosphatidylglycerol (DPPG) were dissolved in an organic solvent and solvent evaporated to form a dry film, which was hydrated with isotonic, 50 mM glutathione containing isotonic 0.01 M HEPES buffer (pH 7.4), and extruded through a polycarbonate filter to reduce the size. The unentrapped glutathione was removed by gel filtration and the liposomes immediately labeled with Tc-99m-HMPAO using an efficient Tc-99m loading procedure that we have adapted [8,9], with modifications [5,6]. DSPE–PEG_{3400}–VIP was inserted into Tc99m-HMPAO SSL by incubation at 37 °C. The free DSPE–PEG_{3400}–VIP and the label were then removed by gel filtration to give Tc99m-HMPAO VIP–SSL. The Tc99m-HMPAO encapsulating SSL were prepared in a similar manner, except 5 mol% of DSPE–PEG was

used instead of 3 mol% for Tc99m-HMPAO encapsulating VIP–SSL and the radiolabeled SSL were not incubated with DSPE–PEG_{3400}–VIP after separation of free Tc99m-HMPAO.

2.2.2. Characterization of Tc99m-HMPAO encapsulating VIP–SSL and SSL

The sizes of both Tc99m-HMPAO SSL and Tc99m-HMPAO VIP–SSL were determined by quasi-elastic light scattering using a NICOMP Particle Sizer Model 370 (Particle Sizing Systems, Menlo Park, CA, USA). The radioactivity content and the labeling efficiency were determined by counting the radioactivity of each fraction collected, along with radioactivity remaining in the column, using a dose calibrator, and calculating the percentage of radiolabel present in the liposomes versus the total radioactivity. The phospholipid content of the Tc-99m-HMPAO encapsulating liposomes was determined by the modified Bartlet phosphate assay [10]. The VIP content of Tc99m-HMPAO encapsulating VIP–SSL was determined by a commercial ELISA kit.

2.2.3. In vivo studies

Animal studies were carried out in accordance with the Institutional Animal Care Committee guidelines and the *Guide for the Care and Use of Laboratory Animals*, prepared by the Committee on Care and Use of Laboratory Animals of the Institute of Laboratory Animal Resources, National Research Council.

Female rats with MNU-induced mammary cancer were used as the animal model for the in vivo studies. Breast cancer was induced in virgin female Sprague–Dawley rats with MNU as previously described in the literature with some modification [4,5,11,12]. Briefly, virgin female Sprague–Dawley rats, 36 days old, weighing ~140 g, were anesthetized with ketamine/xylazine (13.3/1.3 mg per 100 g body weight, i.m.). Each animal received a single intravenous injection of MNU (50 mg/kg body weight) in acidified saline (pH 5.0), via the tail vein. The rats were weighed weekly. They were palpated every week, starting at 3 weeks post-MNU administration. Palpable mammary cancer was detected within 100–150 days after injection. The cancer-bearing rats, with an average tumor size of about 2 cm diameter, were divided into two groups of at least five rats each. Each group was assigned to receive one of the radiotracers: Tc99m-HMPAO VIP–SSL or Tc99m-HMPAO SSL. The same group of rats was used to perform the pharmacokinetic, biodistribution and imaging studies as detailed below.

2.2.4. Pharmacokinetic studies

These studies evaluated the behavior of labeled SSL with or without VIP on their surface in the blood. Rats were anesthetized with ketamine/xylazine (13.3/1.3 mg per 100 g body weight, i.p.). After anesthesia, the carotid artery was exposed and cannulated with a polyethylene cannula (PE-50) for blood sampling. The cannula was exteriorized near the back of the neck. It was then filled with Heparin solution to reduce the chance of blockage due to clotting. The incision used for exposure of the carotid artery was closed with wound clips. The cannulated rats were then given ~300 μCi of the assigned radiotracer (Tc99m-HMPAO encapsulating VIP–SSL or Tc99m-HMPAO encapsulating SSL) intravenously via the tail vein (at least five rats per group). 100 μl blood samples were then withdrawn from the chronic carotid artery cannula at 5 min and then at 0.5, 1, 2, 4, 8 and 27 h after injection. The radioactivity of each blood sample was measured in a gamma counter (Cobra 5005, Packard Instruments). The change in the amount of radioactivity in the blood at each sampling time point (compared with the 5 min sample) after intravenous injection of Tc-99m-HMPAO encapsulating VIP–SSL or SSL was calculated.

2.2.5. Imaging studies

These experiments evaluated the breast cancer image enhancement ability of Tc-99m-HMPAO encapsulating VIP–SSL or SSL using cancer-bearing rats. Imaging studies were performed as described before with appropriate adjustments [9] and on the same rats as those used for pharmacokinetic studies.

Briefly, the rats were anesthetized with ketamine/xylazine and then the appropriate radioactive formulation (~300 μCi/rat) was administered intravenously by tail vein. The rats were imaged at ~3 and ~27 h post-injection. For imaging the rats were again anesthetized and placed prone on one head of a

triple-headed Picker PRISM 3000 SPECT gamma camera equipped with a low-energy, high-resolution collimator and a dedicated Odyssey computer. The images (100,000 counts/image) were acquired and stored in a 512×512 matrix.

The Odyssey software program was used to analyze relative uptake in cancer tissues and the background tissue (calf muscles) in the same animal. The images were analyzed by drawing regions of interest (ROIs) over the breast tumors and calf muscles as background. The uptake was measured as counts per pixel. The uptake in the two calf muscles and the tumors, if more that one tumor per rat, were averaged. Counts per pixel values for five animals were calculated as mean±S.E.M. Tumor tissue to background (or tumor to non-tumor, T-NT) ratios were calculated. Statistical analysis was performed using unpaired Student's *t*-test to compare different formulations. The level of significance was set at $P<0.05$.

2.2.6. Biodistribution studies

These studies investigated the tissue distribution of Tc99m-HMPAO encapsulating SSL or VIP–SSL after systemic delivery to rats and the effect of the presence of VIP on the surface of SSL on their biodistribution.

The MNU-induced rats used were the same as those used for the pharmacokinetic studies described above. About 300 μCi of Tc99m-HMPAO encapsulating VIP–SSL or Tc99m-HMPAO encapsulating SSL was injected into the tail vein of the rat. At 27 h post-injection, the rats were euthanized by an overdose of ketamine/xylazine. A blood sample was obtained by cardiac puncture. Tissues (normal breast or breast cancer, liver, spleen, kidneys, calf muscle, heart and lungs) were dissected out. They were washed with saline, dried between folds of paper towel and transferred to pre-weighed polypropylene tubes and capped. The tubes were then weighed and the weight of each of the tissues was determined. Their activity was measured in a shielded well scintillation gamma counter (Cobra 5005, Packard Instruments). To correct for the physical decay of Tc99m, and to permit calculation of the uptake of the radiolabeled liposomes, a 10 μl aliquot of the injected dose was also counted. The results were expressed as percent injected dose per gram of tissue (% I.D./g).

The tissue radioactivity amounts, % I.D./g, were compared between formulations (Tc-99m-HMPAO encapsulating SSL or Tc-99m-HMPAO encapsulating VIP–SSL) as well as between normal and tumor-bearing rats for each of the formulations using unpaired Student's *t*-test. $P<0.05$ was considered significant.

3. Results

3.1. Characteristics of Tc99m-HMPAO encapsulating VIP–SSL and Tc99m-HMPAO encapsulating SSL

Tc99m-HMPAO encapsulating VIP–SSL with a high Tc-99m-HMPAO labeling efficiency were prepared in a reproducible manner. The characteristics of Tc99m-HMPAO encapsulating VIP–SSL and Tc99m-HMPAO encapsulating SSL were not significantly different from each other as shown in Table 1. The size of both Tc99m-HMPAO encapsulating VIP–SSL and SSL was around 110 nm. The phospholipid content of both Tc99m-HMPAO encapsulating VIP–SSL and SSL was about 3.0 μmol/

Table 1
Characteristics of Tc99m-HMPAO encapsulating VIP–SSL and SSL (each value is mean±standard deviation, n=at least 6)

Characteristic	Tc99m-HMPAO encapsulating SSL	Tc99m-HMPAO encapsulating VIP–SSL
Size (nm)	109.81±14.21	114.77±13.72
Phospholipid content (μmol/ml)	3.15±0.23	3.01±0.48
Radioactivity content (μCi/ml)	1008±160	800±113
Labeling efficiency (%)	85.7±4.46	83.8±2.42
VIP content (μg/μmol phospholipid)	N/A	10.5

ml. The radioactivity content of both Tc99m-HMPAO encapsulating VIP–SSL and SSL was about 900 μCi/ml. In addition, both the liposomes showed a high labeling efficiency of about 85%.

The VIP content of Tc-99m-HMPAO encapsulating VIP–SSL was found to be 10.5 μg/μmol phospholipid, which translates to approximately 225 VIP molecules per liposome.

3.2. Pharmacokinetic studies

The percent decrease in radioactivity with time was used to monitor the circulation time of liposomes. The radioactivity at 5 min was considered to be 100%. The decline of radioactivity in the blood with time in breast tumor-bearing rats was similar for both Tc99m-HMPAO encapsulating SSL with and without VIP, over a 27 h period, as seen in Fig. 2. The figure also shows that the decline of radioactivity for both formulations was largely monophasic. In addition, the pharmacokinetic parameters calculated from the blood radioactivity data using Win-Nonlin (data not shown) indicated that the half-lives (~16 h) of Tc99m-HMPAO encapsulating VIP–SSL and Tc99m-HMPAO encapsulating SSL were not significantly different from each other.

3.3. Imaging studies

The images acquired for both Tc-99m-HMPAO encapsulating VIP–SSL and Tc-99m-HMPAO encapsulating SSL injected into cancer-bearing rats at about 3 h and 27 h post-injection were analyzed using the counts per pixel on the stored images using commercial Odyssey software. As seen in Fig. 3, in all cases, the T-NT ratio was over 4 and for both SSL with and without VIP image enhancement (T-NT ratio) increased at the later imaging time. For both imaging times (3 and 27 h) SSL with VIP showed significantly higher image enhancement (higher T-NT ratio) than liposomes without VIP, as determined by unpaired Student's *t*-test.

3.4. Biodistribution studies

This study was conducted to determine the uptake of SSL and VIP–SSL by various tissues in tumor-bearing rats. In particular, breast cancer tissue was compared with normal breast tissue.

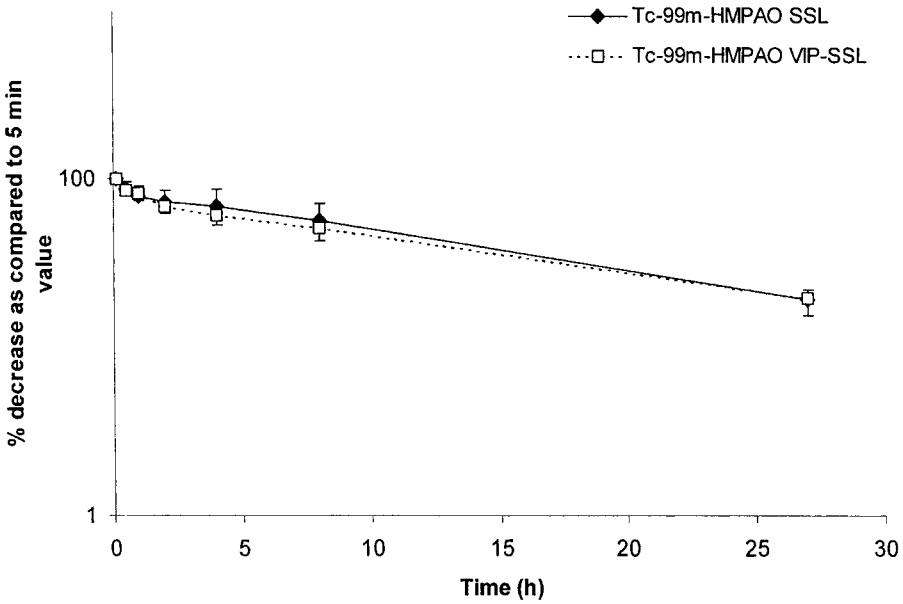

Fig. 2. Change in radioactivity in blood with time of Tc-99m-HMPAO VIP–SSL and Tc-99m-HMPAO SSL after injection in MNU-induced cancer-bearing rats. Each value is mean±S.D., n=at least 5.

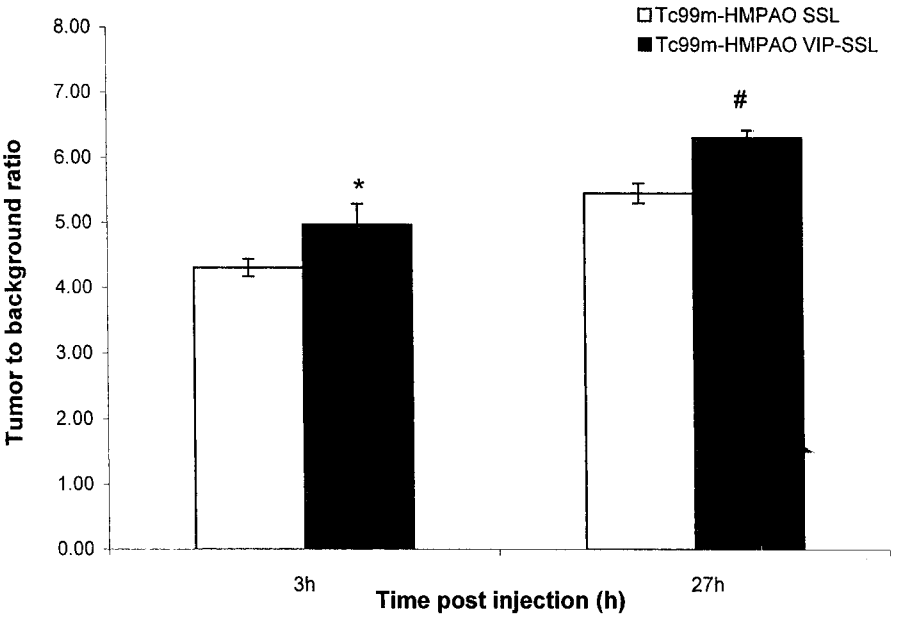

Fig. 3. Tumor to background ratio of Tc-99m-HMPAO encapsulating SSL with or without VIP at ~3 and ~27 h post-injection. Data are expressed as mean±S.E.M., n=at least 5. *$P<0.05$ as compared to Tc99m-HMPAO encapsulating SSL at ~3 h post-injection; #$P<0.05$ as compared to Tc99m-HMPAO encapsulating SSL at ~27 h post-injection.

The mean breast cancer uptake of Tc99m-HMPAO encapsulating VIP–SSL was about 1.8 times more compared to the cancer uptake of Tc99m-HMPAO encapsulating SSL (Fig. 4). In addition, there was significantly more uptake of VIP–SSL in kidneys as compared to SSL in tumor-bearing rats (Table 2). There was no significant difference in the accumulation of Tc99m-HMPAO encapsulating SSL and Tc99m-HMPAO encapsulating VIP–SSL in the other tissues analyzed (Table 2).

4. Discussion

The presence of DSPE–PEG on the surface and the mean diameter of ~110 nm ensured the long-circulating (half-life ~16 h) capability of our liposomal constructs and maximized their potential for passive targeting to breast tumors, most probably due to the ''Enhanced Permeability and Retention'' or EPR effect [13–15]. The loading efficiency of these liposomes was high (~85%). The label used, Tc99m, is the most preferable label for diagnostic applications [16,17] because of its relatively short half-life of 6.02 h, monoenergetic emission of 140 keV, lack of alpha or beta emission, low cost and widespread availability. Furthermore, the uniqueness of this system is that it is able to deliver multiple numbers of radionuclides to each target (VIP-R), hence increasing the sensitivity of detection. The covalent attachment of a peptide on the liposome surface without significant alteration of the labeled liposomes may indicate that similar liposomes carrying chemotherapeutic agents can be prepared to target the VIP receptors of breast or other cancers that overexpress VIP-R for targeted chemotherapy.

Both Tc99m-HMPAO encapsulating SSL and Tc99m-HMPAO encapsulating VIP–SSL showed a monophasic decline, characteristic of long-circulating liposomes, with no significant difference in half-lives (half-lives ~16 h). Similar to the in vitro characteristics, these data suggest that the presence of VIP on the SSL does not alter the long-circulating behavior of the liposomes. This finding is in good agreement with the literature. It has been shown that non-antibody ligands such as peptides when coupled to SSL do not significantly alter the circulation times of ligand-free SSL [18,19]. The long circulation

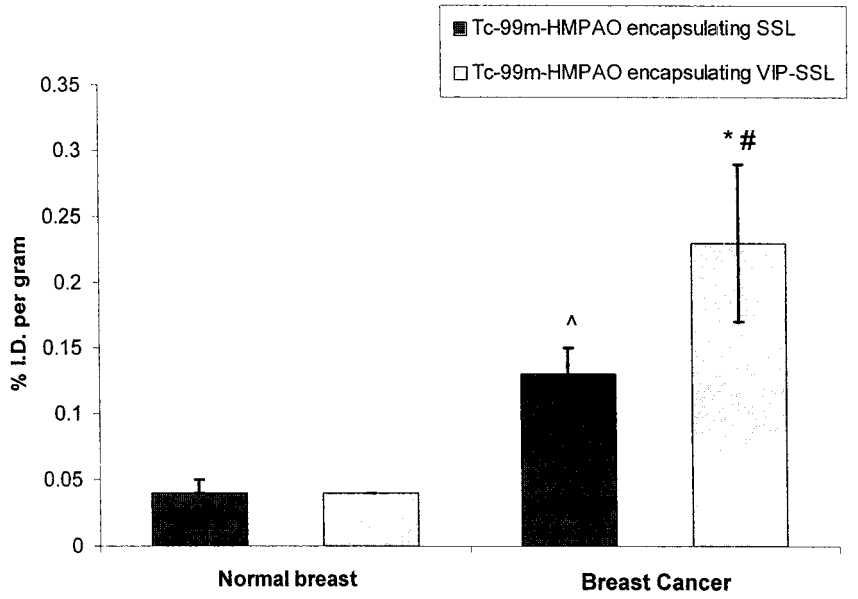

Fig. 4. Accumulation of Tc-99m-HMPAO encapsulating VIP–SSL and Tc-99m-HMPAO encapsulating SSL in normal breast tissue and breast cancer tissue (each data, $n=5$, mean±S.E.M.). *$P<0.05$ compared to Tc-99m-HMPAO encapsulating SSL in breast cancer; #$P<0.05$ compared to Tc-99m-HMPAO encapsulating SSL and VIP–SSL in normal breast; ×$P<0.05$ compared to Tc-99m-HMPAO encapsulating SSL and VIP–SSL in normal breast.

half-life of Tc-99m-labeled VIP–SSL along with their small size (~114 nm) make these liposomes suitable for accumulation in breast cancer due to the EPR effect.

The tumor to background (T-NT) ratio was better at 27 h post-injection than at 3 h post-injection for both formulations (Fig. 3), which can be explained by the EPR effect. It is known that, for particulate systems, more accumulation occurs into the areas of leaky vasculature with time and a more particulate imaging agent will sequester at the cancer site more than the background tissues, improving the tumor to non-tumor ratio and facilitating the detection of the cancer [14]. This increased T-NT ratio is indicative of long circulation in the blood and passive targeting of SSL to breast cancer. In addition, the tumor to non-tumor (T-NT) ratios for Tc99m-HMPAO encapsulating VIP–SSL were significantly ($P<0.05$) more than that for Tc99m-HMPAO encapsulating SSL, suggesting active targeting of VIP–SSL, most probably due to the interaction of liposomal VIP and VIP-R in the breast cancer. The T-NT ratio for Tc99m-HMPAO encapsulating VIP–SSL about 27 h post-injection was about 6:1, which is a clinically acceptable T-NT ratio for the tumor to be detected by planar gamma scintigraphy. This suggests that the targeted liposomes developed in this study can be successfully used to detect breast cancer in the clinic.

In agreement with imaging data, there was significantly more accumulation of both Tc99m-HMPAO encapsulating SSL and VIP–SSL in breast cancer as compared to normal breast tissue in rats,

Table 2
Biodistribution of Tc99m-HMPAO encapsulating VIP–SSL and Tc99m-HMPAO encapsulating SSL in MNU-induced cancer-bearing rats. Each value is the mean±S.E.M., $n=5$

Tissue	% I.D. per gram of tissue	
	SSL	VIP–SSL
Heart	0.09±0.02	0.07±0.02
Lungs	0.49±0.32	0.28±0.05
Spleen	10.36±1.60	13.37±1.19
Liver	0.83±0.16	0.90±0.19
Blood	1.44±0.11	1.17±0.26
Kidneys	1.02±0.11	1.57±0.24*
Muscle	0.03±0.01	0.01±0.01
Breast cancer	0.13±0.06	0.23±0.02#

*$P<0.05$ compared with Tc99m-HMPAO encapsulating SSL; #$P<0.05$ compared with Tc99m-HMPAO encapsulating SSL.

suggesting that the liposomes were passively targeted to the breast cancer, most probably due the presence of leaky vasculature in the tumor (Fig. 4). Similarly, in breast cancer, significantly more accumulation of Tc99m-HMPAO encapsulating VIP–SSL as compared to Tc99m-HMPAO encapsulating SSL confirms that the liposomes were indeed actively targeted to the breast tumor (Fig. 4). The variability in the data obtained for the accumulation of labeled VIP–SSL was more than for labeled SSL without VIP in breast cancer. Since VIP–SSL are both passively and actively targeted to breast cancer, the variability in actively targeted Tc99m-HMPAO encapsulating VIP–SSL may be related to the developmental stage of the cancer and the extent of VIP-R expression at that stage. There is some evidence in the literature that suggests the differential expression of genes that code for proteins during MNU-induced breast cancer growth [20]. The same differential expression may also be true for VIP-R in breast cancer. Hence, active targeting to VIP-R showed increased variability depending on the VIP-R expression level of the breast cancer stage at which the particular cancer-bearing rat was used for this study.

There was no significant difference in the accumulation of labeled SSL with and without VIP in all other tissues (heart, liver, spleen, blood and muscle), except for the kidneys. The higher uptake by the kidneys may be related to the reduced flexibility of the VIP–SSL membrane, due to the insertion of VIP in the SSL bilayer. This most likely causes the entrapment of these liposomes in the vascular bed of the kidneys. However, more studies are needed to elucidate this matter.

The spleen showed the most prominent uptake (~10% I.D./g) of all the tissues analyzed in both normal and tumor-bearing rats. These values fall in the range (8.53 to 16.25% I.D./g) reported in the literature for spleen uptake of Tc99m-HMPAO encapsulating SSL of about 100 nm in diameter [9,21,22]. In addition, this uptake was much less than the splenic uptake (~50% I.D./g) observed for Tc99m-HMPAO encapsulating classical liposomes of similar size [23], indicating the steric stabilization of these liposomes.

In this study the percent accumulation of injected dose of liposomes in breast cancer tissue (~0.2%) was several orders of magnitude less than those reported in the literature (2 to 20% per gram of tissue) [15,24–27]. The reasons for this discrepancy are unclear, but the data reported in the literature were obtained using xenograft tumors in nude mice, while values for this study were obtained from a MNU-induced in situ breast cancer rat model. Xenograft models do not represent the right environment that occurs in human tumors because, in xenograft models, the cells are already transformed when they are implanted in the mice, leading to shorter doubling times than observed in human cancer. Therefore, it is possible that less necrosis and a more aggressive blood supply exist within xenograft models [28]. This would lead to more extensive accumulation in the xenograft model when compared to human cancer [29]. MNU-induced breast cancer is a more representative model of human breast cancer, developing in the breast and not at the injection site and developing at a more realistic, slow rate. Therefore, due to the slow growth and the possibly larger areas of necrosis, the accumulation of liposomes in the cancer may be less with MNU-induced animals.

Active targeting to breast cancer can be further improved by taking into consideration the complex interplay of tumor biology (such as maximum VIP-R overexpression), product (such as optimum concentration of grafted VIP on SSL) and imaging procedure-related factors (such as optimum tumor imaging time post-injection).

5. Conclusion

Labeled, long-circulating, small liposomes with and without VIP accumulated significantly more in the tumor as compared to normal breast tissue, indicating passive targeting of SSL to breast cancer. There was significantly more accumulation of Tc99m-HMPAO labeled SSL surface grafted with VIP as compared to similar liposomes without VIP in breast tumors, indicating the successful use of VIP-R as molecular targets and the occurrence of active targeting of these liposomes to breast cancer in addition to passive targeting. Tumor accumulation of both the liposomes increased with time. Even though the image enhancement (T-NT ratio) observed in this study is considered sufficient for

tumors to be detected by planar scintigraphy in a clinical setting, the described novel targeted imaging technique can be further improved when images are taken at a tumor development stage with maximum VIP-R overexpression and tumor leakiness and by optimizing the product and imaging conditions. In addition, this targeted carrier system can be used for the imaging of other tumors that overexpress VIP-R such as prostate and endometrial cancers. This targeted carrier system is currently being evaluated in our laboratory for further improvement in imaging and also for targeted therapy of breast cancer with the use of VIP–SSL that encapsulate chemotherapeutic agents.

Acknowledgements

This work was supported, in part, by the Department of Defense, BCRP 011268, Susan G. Komen Breast Cancer Foundation, grant ≠DISS 2000 353 Veterans Affairs.

References

[1] J.C. Reubi, In vitro identification of vasoactive intestinal peptide receptors in human tumors: implications for tumor imaging, J. Nucl. Med. 36 (10) (1995) 1846–1853.
[2] J.C. Reubi, In vitro identification of VIP receptors in human tumors: potential clinical implications, Ann. N.Y. Acad. Sci. 805 (1996) 753–759.
[3] S. Dagar, M. Sekosan, M. Blend, I. Rubinstein, H. Onyuksel, Identification and targeting of VIP receptors in rats with induced breast cancer, in: Proceedings of an International Symposium on the Controlled Release of Bioactive Materials, Boston, MA, 1999, pp. 22–23, Vol. 26.
[4] S. Dagar, M. Sekosan, I. Rubinstein, H. Onyuksel, Detection of VIP receptors in MNU-induced breast cancer in rats: implications for breast cancer targeting, Breast Cancer Res. Treat. 65 (1) (2001) 49–54.
[5] S. Dagar, M. Sekosan, B.S. Lee, I. Rubinstein, H. Onyuksel, VIP receptors as molecular targets of breast cancer: implications for targeted imaging and drug delivery, J. Controlled Release 74 (1–3) (2001) 129–134.
[6] S. Dagar, J. Stastny, M. Blend, I. Rubinstein, H. Onyuksel, Preparation of Tc99m-HMPAO VIP–SSL for breast tumor detection, Pharm. Sci. 1 (1998) S294.
[7] M. Patel, I. Rubinstein, H. Ikezaki, H. Alkan-Onyuksel, Simplified preparation of vasoactive intestinal peptide in sterically stabilized liposomes, in: Proceedings of an International Symposium on the Controlled Release of Bioactive Materials, 1997, pp. 913–914, Vol. 24.
[8] W.T. Phillips, A.S. Rudolph, B. Goins, J.H. Timmons, R. Klipper, R. Blumhardt, A simple method for producing a technetium-99m-labeled liposome which is stable in vivo, Int. J. Radiat. Appl. Instr. B 19 (5) (1992) 539–547.
[9] O.C. Boerman, W.J. Oyen, L. van Bloois, E.B. Koenders, J.W. van der Meer, F.H. Corstens, G. Storm, Optimization of technetium-99m-labeled PEG liposomes to image focal infection: effects of particle size and circulation time, J. Nucl. Med. 38 (3) (1997) 489–493.
[10] M. Kates, Techniques in Lipidology, Elsevier, New York, 1972.
[11] R.C. Moon, G.J. Kelloff, C.J. Detrisac, V.E. Steele, C.F. Thomas, C.C. Sigman, Chemoprevention of MNU-induced mammary tumors in the mature rat by 4-HPR and tamoxifen, Anticancer Res. 12 (4) (1992) 1147–1153.
[12] G.O. Udeani, C. Gerhauser, C.F. Thomas, R.C. Moon, J.W. Kosmeder, A.D. Kinghorn, R.M. Moriarty, J.M. Pezzuto, Cancer chemopreventive activity mediated by deguelin, a naturally occurring rotenoid, Cancer Res. 57 (16) (1997) 3424–3428.
[13] Y. Matsumura, H. Maeda, A new concept for macromolecular therapeutics in cancer chemotherapy: mechanism of tumoritropic accumulation of proteins and the antitumor agent smancs, Cancer Res. 46 (12, Pt 1) (1986) 6387–6392.
[14] H. Maeda, The enhanced permeability and retention (EPR) effect in tumor vasculature: the key role of tumor-selective macromolecular drug targeting, Adv. Enzyme Regul. 41 (2001) 189–207.
[15] O. Ishida, K. Maruyama, K. Sasaki, M. Iwatsuru, Size-dependent extravasation and interstitial localization of polyethyleneglycol liposomes in solid tumor-bearing mice, Int. J. Pharm. 190 (1) (1999) 49–56.
[16] W.T. Phillips, Delivery of gamma-imaging agents by liposomes, Adv. Drug Deliv. Rev. 37 (1–3) (1999) 13–32.
[17] W.T. Phillips, in: G. Gregoriadas, X. McCormack (Eds.), Strategies for Stealth Therapeutic Systems, Targeting of Drugs, Vol. 6, Plenum Press, New York, 1998, pp. 109–129.
[18] T.M. Allen, D.D. Stuart, in: A. Janoff (Ed.), Liposomes: Rational Design, Marcel Dekker, New York, 1999, pp. 66–71.
[19] S. Zalipsky, N. Mullah, J.A. Harding, J. Gittelman, L. Guo, S.A. DeFrees, Poly(ethylene glycol)-grafted liposomes with oligopeptide or oligosaccharide ligands appended to the termini of the polymer chains, Bioconjug. Chem. 8 (2) (1997) 111–118.
[20] X. Yang, L.H. Young, J.M. Voigt, Expression of a vitamin D-regulated gene (VDUP-1) in untreated- and MNU-treated rat mammary tissue, Breast Cancer Res. Treat. 48 (1) (1998) 33–44.
[21] W.J. Oyen, O.C. Boerman, G. Storm, L. van Bloois, E.B. Koenders, R.A. Claessens, R.M. Perenboom, D.J. Crommelin, J.W. van der Meer, F.H. Corstens, Detecting infection and inflammation with technetium-99m-labeled Stealth liposomes, J. Nucl. Med. 37 (8) (1996) 1392–1397.
[22] P. Laverman, E.T. Dams, W.J. Oyen, G. Storm, E.B. Koenders, R. Prevost, J.W. van der Meer, F.H. Corstens, O.C.

Boerman, A novel method to label liposomes with 99mTc by the hydrazino nicotinyl derivative, J. Nucl. Med. 40 (1) (1999) 192–197.
[23] B. Goins, R. Klipper, A.S. Rudolph, W.T. Phillips, Use of technetium-99m-liposomes in tumor imaging, J. Nucl. Med. 35 (9) (1994) 1491–1498.
[24] D.B. Kirpotin, J.W. Park, K. Hong, Y. Shao, G.T. Colbern, W.-w. Zheng, O. Meyer, C.C. Benz, D. Papahadjopoulos, in: D. Lasic, D. Papahadjopoulos (Eds.), Medical Applications of Liposomes, Elsevier, Amsterdam, 1998.
[25] M.S. Newman, G.T. Colbern, P.K. Working, C. Engbers, M.A. Amantea, Comparative pharmacokinetics, tissue distribution, and therapeutic effectiveness of cisplatin encapsulated in long-circulating, pegylated liposomes (SPI-077) in tumor-bearing mice, Cancer Chemother. Pharmacol. 43 (1) (1999) 1–7.
[26] K.J. Harrington, G. Rowlinson-Busza, K.N. Syrigos, P.S. Uster, R.M. Abra, J.S. Stewart, Biodistribution and pharmacokinetics of 111In-DTPA-labelled pegylated liposomes in a human tumour xenograft model: implications for novel targeting strategies, Br. J. Cancer 83 (2) (2000) 232–238.
[27] J.W. Park, D.B. Kirpotin, K. Hong, R. Shalaby, Y. Shao, U.B. Nielsen, J.D. Marks, D. Papahadjopoulos, C.C. Benz, Tumor targeting using anti-her2 immunoliposomes, J Controlled Release 74 (1–3) (2001) 95–113.
[28] S.N. Khleif, G.A. Curt, in: X. Holland (Ed.), Cancer Medicine, Williams and Wilkins, Baltimore, 1997.
[29] H.J. Kuh, S.H. Jang, M.G. Wientjes, J.R. Weaver, J.L. Au, Determinants of paclitaxel penetration and accumulation in human solid tumor, J. Pharmacol. Exp. Ther. 290 (2) (1999) 871–880.

[21] Liposomal Vasoactive Intestinal Peptide

By VARUN SETHI, HAYAT ÖNYÜKSEL, and ISRAEL RUBINSTEIN

Abstract

Liposomes have been investigated as drug carriers since first discovered in the 1960s. However, the first-generation, so-called classic liposomes found relatively limited therapeutic utility. Nonetheless, the advent in the 1980s of the second-generation sterically stabilized liposomes (SSL) that evade uptake by the host's reticuloendothelial system greatly enhanced their utility as drug carriers because of their prolonged circulation half-life and passive targeting to injured and cancerous tissues. Over the past decade, our work focused on exploiting the bioactivity of vasoactive intestinal peptide (VIP), a ubiquitous 28-amino acid, amphipathic and pleiotropic mammalian neuropeptide, as a drug. To this end, the peptide expresses distinct and unique innate bioactivity that could be harnessed to treat several human diseases that represent unmet medical needs, such as pulmonary hypertension, stroke, Alzheimer's disease, sepsis, female sexual arousal dysfunction, acute lung injury, and arthritis. Unfortunately, the bioactive effects of VIP last only a few minutes due to its rapid degradation and inactivation by enzymes, catalytic antibodies, and spontaneous hydrolysis in biological fluids. Hence, our goal was to develop and test stable, long-acting formulations of VIP using both classic and SSL as platform technologies. We found that spontaneous association of VIP with phospholipid bilayers leads to a transition in the conformation of the peptide from random coil in an aqueous environment to α-helix, the preferred conformation for ligand–receptor interactions, in the presence of lipids. This process, in turn, protects VIP from degradation and inactivation and amplifies its bioactivity *in vivo*. Importantly, we discovered that the film rehydration and extrusion technique is the most suitable to passively load VIP onto SSL at room temperature and yields the most consistent results. Collectively, these attributes indicate that VIP on SSL represents a suitable formulation that could be tested in human disease.

Introduction

Since the discovery of classic liposomes (CL) or first-generation liposomes in the 1960s (Bangham *et al.*, 1965), CL have been extensively investigated as potential carriers for biologically active molecules and drugs *in vivo* (Düzgüneş *et al.*, 1988; Heath *et al.*, 1986; Huang and Rorstad,

0076-6879/05 $35.00

1987; Matthay *et al*., 1986; Mayhew and Rustum, 1985; Papahadjopoulos *et al*., 1985; Straubinger *et al*., 1985). However, their short half-life in the circulation due to rapid uptake by the reticuloendothelial system (RES) has limited their potential use as drug carrier systems. In the 1990s, development of second-generation sterically stabilized liposomes (SSL) greatly advanced the ability to utilize liposomes as drug carrier systems (Klibanov *et al*., 1990, 1991; Maruyama *et al*., 1991a). SSL were found to have increased circulation half-life because of decreased RES uptake through ''steric hindrance'' of opsonins that would otherwise adsorb on their surface, thereby tagging them for RES uptake.

Over the past few years, our laboratory has been investigating the delivery of vasoactive intestinal peptide (VIP) using various formulations of liposomes. VIP is a 28-amino acid ubiquitous amphipathic neuropeptide that displays a broad range of biological activities (Gomariz *et al*., 2001; Said, 1986). It is widely distributed in the central and peripheral nervous systems, where it functions as a nonadrenergic, noncholinergic neurotransmitter and neuromodulator (Gao *et al*., 1994). VIP is localized in the gastrointestinal tract, heart, lung, thyroid, kidney, urinary bladder, genital organs, and brain (Gozes *et al*., 1994, 1996). It is also localized in perivascular nerves and upon its release elicits a potent, though short-lived, endothelium-dependent and -independent vasodilation (Brizzolara and Burnstock, 1991; Gao *et al*., 1994; Gaw *et al*., 1991; Huang and Rorstad, 1987; Ignarro *et al*., 1987; Suzuki *et al*., 1995, 1996a). VIP has important actions on the respiratory tract, including relaxation of airway smooth muscle and attenuation of inflammation (Said, 1992). Recently, VIP has been shown to have several immunomodulatory functions and is secreted by several immune-competent cells in response to various immune signals (Gomariz *et al*., 2001). Deficiency in the release and/or degradation of VIP has been implicated in the pathogenesis of several diseases, such as cystic fibrosis, impotence, congenital megacolon in Hirschsprung's disease, and achalasia of the esophagus (Gozes *et al*., 1994, 1996; Ollerenshaw *et al*., 1989). The bioactive effects of VIP are mediated via high-affinity transmembrane receptors on target cells (Harmar *et al*., 1998). These receptors are overexpressed in various cancer cells and thus can be actively targeted for tumor imaging and therapeutics using VIP as the ligand (Dagar *et al*., 2001; Thakur *et al*., 2000). VIP could be used to treat essential and pulmonary hypertension, congestive heart failure, bronchial asthma, erectile dysfunction, acute food impaction in the esophagus, acute lung injury, and arthritis (Davis *et al*., 1981; Delgado *et al*., 2001; Refai *et al*., 1999).

However, as seen with other peptides, the bioactive effects of VIP are short-lived, lasting only a few minutes after intravenous administration

(Domschke *et al*., 1978; Hassan *et al*., 1994). This short-term efficacy of VIP is most likely due to its degradation by enzymes, catalytic antibodies, and by spontaneous hydrolysis. Several attempts have been made to synthesize more stable and potent analogues of VIP for the treatment of asthma (Bolin *et al*., 1995), impotence (Gozes *et al*., 1994), neurodegenerative diseases (Gozes *et al*., 1996), and inadequate regional blood flow (Refai *et al*., 1999). However, none of these analogues has reached the clinic. In fact, a recent clinical study using a cyclic VIP analogue in patients with asthma has been terminated prematurely. This often implies that high concentrations of VIP are required to observe significant physiological effects, thus causing severe side effects such as reduced systemic arterial pressure (Thakur *et al*., 2000).

Clearly, for VIP to be considered in therapeutics, its half-life in biological fluid should be prolonged appreciably. To this end, this chapter describes work in our laboratories using liposomes as a novel delivery system for VIP.

VIP on Classical Liposomes

Preparation

Synthetic VIP can either be purified by successive reverse-phase high-performance liquid chromatography (HPLC) on a preparative C_{18} column in triethylamine phosphate/acetonitrile and trifluoacetic acid (TFA)/acetonitrile solvent systems or purchased from commercial sources such as American Peptide Company (Sunnyvale, CA). Radioiodination and purification of VIP can be performed as previously described (Paul *et al*., 1989). Classic liposomes can be prepared by several well-established procedures.

Reverse-Phase Evaporation. In this method, a mixture of egg yolk phosphatidylcholine (ePC), egg yolk phosphatidylglycerol (ePG), and cholesterol in a molar ratio of 1:4:5 is used (Sigma Chemical Co., St. Louis, MO) (Gao *et al*., 1994). The phospholipid solution (12 m*M* each) is mixed with 3 ml diethyl ether containing 3 m*M* synthetic VIP, a mixture of 0.2 m*M* labeled VIP and 3 m*M* unlabeled VIP, or 0.2 m*M* radioactive peptide alone with 1 ml of 50 m*M* HEPES buffer, pH 7.3. Sonication of the mixture and subsequent evaporation of the ether *in vacuo* form vesicles. The resulting dispersion is diluted with 10 ml 50 m*M* HEPES buffer and centrifuged (12,500*g*, 7 min). The supernatant is discarded, and the pellet is washed three times with buffer containing 0.15 *M* NaCl. The larger vesicles are removed by passing the dispersion through 1-μm polycarbonate filters (Nuclepore, Pleasonton, CA). The inorganic phosphate content

of the liposomes is measured by a microtiter Bartlett assay (Gao *et al.*, 1994; Suzuki *et al.*, 1995). This method of preparation yields liposomes of ~600 nm. The amount of VIP encapsulated in these liposomes is estimated by using radioimmuno assay (RIA) specific toward VIP (Gao *et al.*, 1994; Suzuki *et al.*, 1995). A VIP/lipid mole ratio of ~0.008 is anticipated using this method of preparation.

Film Rehydration and Extrusion Method. This method provides a more controlled method to prepare CL of the desired size compared with reverse-phase evaporation. For the film rehydration and extrusion method, the phospholipids are dissolved in chloroform, and the solution is dried to a film. The dried lipid film is hydrated with 100 μl of 0.15 *M* NaCl containing 0.7 mg VIP by vortex mixing followed by sonication of the dispersion. The dispersion obtained is frozen and thawed five times using a dry ice–acetone bath. The resulting liposomes are extruded nine times through two polycarbonate filters (3 μm) using a Liposofast apparatus (Avestin Inc., Ottawa, Canada). The liposomes are passed through a gel filtration column to separate free VIP from liposome-encapsulated VIP. The liposomes are recovered in the void volume and stored at 4° prior to use. Size of liposomes is determined by dynamic laser light scattering. A liposome size of ~600 nm is obtained for liposomes prepared by this method. The phosphate content is estimated by modified Bartlett assay as previously mentioned. The VIP/lipid mole ratio is assessed by an enzyme-linked immunosorbent assay (ELISA) specific for VIP. A VIP/lipid mole ratio of ~0.008 is anticipated using this preparation method as well (Gao *et al.*, 1994; Suzuki *et al.*, 1995). Both these methods have been successful in forming liposome-encapsulating VIP that showed improved *in vitro* and *in vivo* activities compared with aqueous VIP (Gao *et al.*, 1994; Gozes *et al.*, 1996).

Classic liposomes are also prepared in the gel state to study the interaction between VIP and phospholipid bilayers (Ikezaki *et al.*, 1999; Önyüksel *et al.*, 2003). Phospholipids with a higher transition temperature such as dipalmitoylphosphatidyl choline (DPPC) and ePG in a molar ratio of 9:1 are used to prepare gel state CL using the film rehydration and extrusion method. Different sizes of liposomes (30 and 100 nm) having the same composition as above are used to study the effects of rigidity and curvature of the bilayer on their interaction with VIP (Ikezaki *et al.*, 1999; Önyüksel *et al.*, 2003).

In Vitro *Effects*

Encapsulation of VIP on CL using either the reverse-phase evaporation or film rehydration/extrusion method was successful in preventing the trypsin-catalyzed degradation of the peptide over 60 min (Gao *et al.*,

1994; Gololobov *et al.*, 1998). This was clearly evident as liposomal VIP was three to four orders of magnitude less susceptible to the trypsin-catalyzed reaction than was aqueous VIP (Gololobov *et al.*, 1998). Moreover, in an autoantibody-catalyzed reaction for VIP hydrolysis, VIP encapsulated in CL showed a 5-fold increase in the K_m values without any significant increase in the V_{max} values compared with aqueous VIP. This suggested that the change in K_m was due to poor recognition of the substrate by antibodies and not to a change in the enzyme rate constant (Gololobov *et al.*, 1998). Stability experiments conducted in the presence of human plasma showed that only 10% of VIP encapsulated in CL was released after incubation for 8 days at 37°, thereby improving the stability of the peptide *in vitro* (Fig. 1).

Secondary structure of liposomal VIP evaluated using circular dichroism (CD) showed that the enhanced *in vitro* activity of the VIP encapsulated in CL was due to change in the conformation of the peptide from predominantly random coil in aqueous solution to α-helix in the presence of phospholipids (Gololobov *et al.*, 1998). These data corroborated the results obtained from other groups, demonstrating the increase in the α-helicity of the peptide in the presence of phospholipids compared with VIP in aqueous solution (Robinson *et al.*, 1982; Rubinstein *et al.*, 2000). The increase in the α-helicity of VIP can be attributed to the interaction and subsequent partitioning of the VIP into the phospholipid bilayer (Noda *et al.*, 1994). However, recent data from our laboratory have

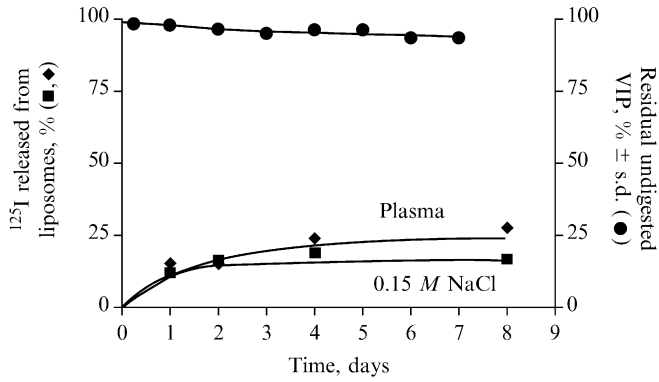

FIG. 1. VIP release from and stability in liposomes. [Tyr$^{10-125}$I] VIP-containing liposomes (4 nmol VIP/1.4/μmol Pi) were incubated for 8 days at 37° in the absence and presence of 25% human plasma in 0.15 *M* NaCl. Total available [Tyr$^{10-125}$I]VIP per assay tube was 10^4 cpm. Released VIP was separated from liposomal VIP by passage through Sepharose 4B columns. Residual undigested VIP in the liposome fractions was estimated by the TCA precipitation method. Reproduced with permission from Gololobov *et al.* (1998).

shown that the interaction of VIP with the phospholipid bilayer is dependent on the biophysical state of the bilayer. A change in the bilayer from liquid-crystalline to the gel state was associated with a marked decrease in α-helicity of the peptide (Önyüksel *et al*., 2003).

In Vivo *Effects*

To study the effect of the peptide *in situ*, a well-established hamster cheek pouch model to assess the vasoactive effects of neuropeptides was used (Davis *et al*., 1981; Gao *et al*., 1994; Rubinstein and Mayhan, 1995; Suzuki *et al*., 1995). The check pouch microcirculation can be visualized using a method previously described in our laboratory (Suzuki *et al*., 1995, 1996a). The effect of VIP either as aqueous solution or liposomal formulation on arteriolar diameter and its duration of action are summarized in

TABLE I
EFFECTS OF VASOACTIVE INTESTINAL PEPTIDE (VIP) AND LIPOSOMAL VIP ON ARTERIOLAR DIAMETER IN THE INTACT HAMSTER CHEEK POUCH

Formulation	Observed effects			Reference
	Size of liposomes (nm)	Arteriolar diameter (% change from baseline)	Duration of effect (min)	
VIP in saline[a]	N/A	13	4	Gao *et al*., 1994
VIP on classical liposomes[a]				
Reverse-phase evaporation	600	35	16	Gao *et al*., 1994
Film rehydration and extrusion	600	38	13	Suzuki *et al*., 1995
VIP on sterically stabilized liposomes[a]				
Freeze–thaw extrusion	224	10	5	Séjourné *et al*., 1997a
Extrusion/dehydration–rehydration	250	38	16	Séjourné *et al*., 1997a
Optimized extrusion/dehydration–rehydration method[b]	89	22	15	Patel *et al*., 1999
VIP in gel-state classic liposomes[a]	100	10	5	Ikezaki *et al*., 1999

[a] VIP 1.0 nmol was used in all experiments.
[b] VIP 0.1 nmol was used in this group only.

Table I. These data show that encapsulation of VIP in CL prolongs both the duration of action and magnitude of vasodilation compared with VIP in aqueous solution (Suzuki *et al*., 1995). Importantly, encapsulation of VIP in CL restored vasoreactivity in spontaneously hypertensive hamsters and rats (Gao *et al*., 1994; Suzuki *et al*., 1996b) (Fig. 2). However, no prolongation in duration of vasodilation was observed in these animals due to possible elaboration of vasoconstrictory substances in the microcirculation.

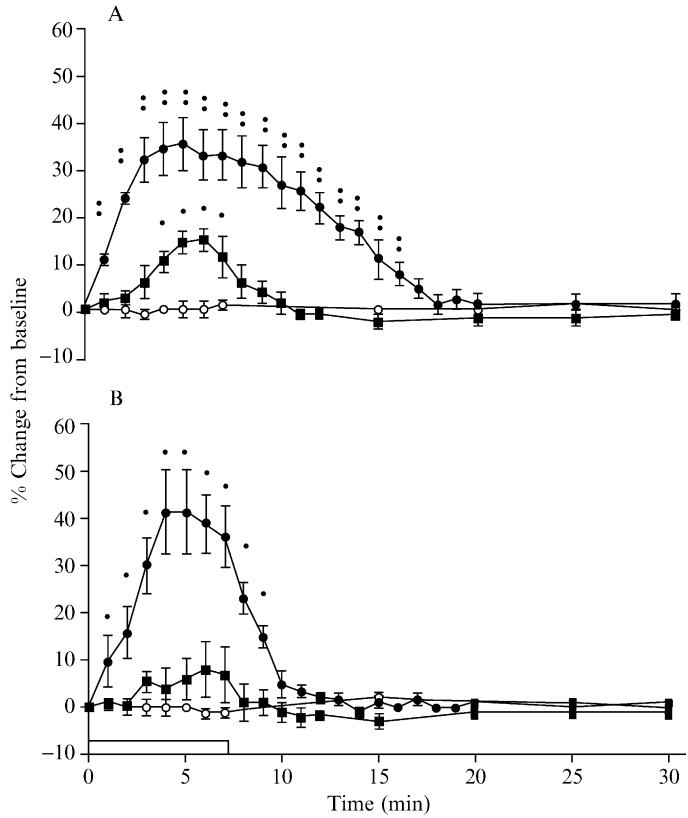

FIG. 2. Time course of changes in arteriolar diameter during suffusion of VIP alone (0.1 nmol; ■), empty liposomes (○), and VIP (0.1 nmol) encapsulated into liposomes (●) in normotensive (A) and hypertensive (B) hamsters. Values are means ± SE; each group, n = four animals. *$p < 0.05$ in comparison with baseline. **$p < 0.05$ in comparison with VIP alone. Open bar indicates duration of suffusion. Reproduced with permission from Suzuki *et al*. (1996a).

In vivo studies using mice (Gololobov *et al*., 1998) and rats (Refai *et al*., 1999) have shown a prolonged half-life for VIP encapsulated in CL. Encapsulation of VIP in liposomes increases the half-life of the peptide by ~8-fold (Refai *et al*., 1999). This is a marked improvement from the previous estimated half-life of 1.0 min in humans and 0.4 min in rats (Domschke *et al*., 1978; Hassan *et al*., 1994). Although the half-life of VIP encapsulated in CL was markedly improved relative to VIP in aqueous solution, the use of VIP encapsulated in CL for therapeutic purposes is limited due to rapid uptake of CL by the RES. This problem was overcome by using SSL as an improved delivery system for VIP.

VIP in Sterically Stabilized Liposomes

Preparation

Three successive methods of preparing SSL encapsulating/incorporating VIP were developed in our laboratory. These are the (1) freeze–thaw extrusion, (2) extrusion/dehydration–rehydration, and (3) optimized extrusion/dehydration–rehydration methods (Patel *et al*., 1999; Séjourné *et al*., 1997a). All three methods use the same composition of phospholipids, distearoylphosphatidylethanolamine-poly(ethylene glycol) $(DSPE–PEG)_{2000}$, ePC, ePG, and cholesterol, at a molar ratio of 0.5:5:1:3.5 with total phospholipid content of 17 μmol. Phospholipids are dissolved in chloroform in a round-bottom flask. The chloroform is evaporated in a rotary evaporator (Labconco, Kansas City, MO) at 45°. The film is used to prepare SSL using the various methods outlined later.

Freeze–Thaw Extrusion. The dried lipid film is hydrated with 250 μl 0.15 *M* saline containing 0.4 mg VIP. The dispersion is vortexed and then sonicated for 5 min in a waterbath sonicator (Fisher Scientific, Itasca, IL). Finally, the dispersion is frozen and thawed five times in an acetone–dry ice bath. Following freeze–thaw, the dispersion is extruded through stacked polycarbonate filters (200 nm) using the Liposofast apparatus (Avestin Inc., Ottawa, Canada). Liposomes with an average diameter of 224 nm are obtained with this method. The VIP-associated liposomes are separated from the free VIP by passing the extruded dispersion through a gel filtration column (Bio-Rad, A-5m, Bio-Rad Labs, Richmond, CA). The separated fraction, which is normally eluted in the void volume of the column at 4°, is stored for further *in vitro* testing (Séjourné *et al*., 1997a). The problem with this method is the high stress associated with extrusion of the SSL in the presence of the peptide leading to partial sloughing of the peptide, and some loss in bioactivity (Séjourné *et al*., 1997a).

Extrusion/Dehydration–Rehydration. The dried lipid film is hydrated with 250 μl of 0.15 *M* NaCl. The dispersion is vortexed rigorously and sonicated for 5 min. The dispersion is extruded through stacked polycarbonate filters of pore size 200, 100, and 50 nm to form liposomes (Séjourné *et al.*, 1997a). Then 0.4 mg VIP and 30 mg of trehalose (cryoprotectant) in powder form, are added to the extruded dispersion. The mixture is frozen in an acetone–dry ice bath and lyophilized at -46° under $\sim 5 \times 10^{-3}$ mBar pressure overnight using the Lab-Scale freeze-dryer (Labconco, Kansas City, MO). The freeze-dried cake is resuspended in 250 μl deionized water. Liposomes of $\sim$250 nm in size are anticipated after resuspending the freeze-dried cake. The dispersion is subsequently separated as in method 1 and stored at 4° until use (Séjourné *et al.*, 1997a). This method avoids extrusion of SSL after incubation with the peptide. However, freeze drying the formulation following extrusion changes the liposome size following rehydration of the freeze-dried cake due to the fusion of the preformed liposomes (Szucs and Tilcock, 1995). This problem is avoided by optimizing the formulation, such that the freeze-dry step is eliminated from the preparation method.

Optimized Extrusion/Dehydration–Rehydration Method. This new and optimized method to prepare VIP-SSL avoids the freeze-drying step in method 2, thereby decreasing the preparation time, and conserves liposome size. In this optimized preparation, the dried phospholipid film (same composition as in methods 1 and 2) is hydrated with 250 μl 0.15 *M* NaCl. The dispersion is vortexed thoroughly and sonicated for 5 min in a bath sonicator. The dispersion is extruded through stacked polycarbonate filters to yield an average size of 80 nm liposomes (using sequential filters of size 200, 100, and 50 nm). VIP (0.3 mg) is added to the extruded suspension, and the mixture is incubated at room temperature (25°) for 2 h. Free VIP is separated from liposome-associated VIP by gel filtration chromatography as described above. The final amount of VIP associated with liposomes is quantified by ELISA (Peninsula Laboratories, Santa Clara, CA). Liposome size is measured by quasielastic light scattering to confirm the size (Nicomp 270, Particle Sizing System, Santa Barbara, CA). The inorganic phosphate content of the liposomes is measured using a modified Bartlett assay, as mentioned above. A phospholipid yield of $\sim$50% is anticipated using this method. The VIP-SSL are stored at 4° until use (Patel *et al.*, 1999). All three methods outlined above yield a VIP/phospholipid molar ratio of $\sim$0.004.

VIP on SSL prepared by method 3 was evaluated as a passively targeted system for breast cancer (Dagar *et al.*, 1999). The results suggested that VIP dissociates from the surface of liposomes in the vicinity of VIP

receptors, due to stronger affinity of VIP for its cognate receptors compared with SSL (Dagar *et al*., 1999). To overcome this problem, VIP was actively conjugated to the distal end of an activated DSPE–PEG_{3400}–NHS moiety (Dagar *et al*., 2001). The reaction mixture needs to be maintained at pH 6.6 such that the histidine (pK_a = 7–8) group of the peptide will be involved in the formation of the conjugate. This is important because using a different pH exposes multiple lysine groups in the peptide, which are a critical component of the α-helical domain, involved in VIP receptor recognition. SSL are prepared as previously described in method 3, without adding VIP. These preformed SSL are incubated with the conjugated mixture (DSPE–PEG_{3400}–VIP) overnight at 4° to insert them into the liposomes (Dagar *et al*., 2001). VIP-SSL prepared by this method are more stable, and VIP does not dissociate from the SSL upon interaction with its receptors (Dagar *et al*., 2001).

In Vitro *Studies*

As shown above, VIP on liposomes overcomes trypsin-, autoantibody-, and plasma-induced inactivation of VIP *in vitro* (Gao *et al*., 1994; Gololobov *et al*., 1998). Studies conducted using VIP on SSL significantly potentiated DNA synthesis in oral keratinocytes *in vitro* compared with synthesis in the presence of VIP alone (Fig. 3) (Rubinstein *et al*., 2001). The effect on DNA synthesis was not dependent on empty SSL thus indicating that the increase in activity was due to the marked improvement in stability and activity of VIP on SSL. Conformation studies conducted in the presence of PEGylated phospholipid aggregates (sterically stabilized micelles, SSM) have shown an increase in α-helicity of VIP associated with SSM (Rubinstein *et al*., 2000). We have used SSM instead of SSL to study the change in conformation of VIP in the presence of phospholipids, because experiments conducted with SSL expressed a large signal-to-noise ratio, thereby rendering data analysis impractical. Moreover, α-helicity of VIP associated with SSM is potentiated in the presence of low concentrations (10^{-11}–10^{-10} *M*) of calmodulin (CaM), a ubiquitous extracellular membrane-bound and intracellular protein (Table II; Rubinstein *et al*., 2000). This interaction requires the presence of preformed α-helix VIP, i.e., phospholipid-associated VIP. This strategy could be used to amplify the effect of other therapeutic amphipathic peptides with limited bioavailability.

VIP (alone or on SSL) did not modulate the chemotactic response of human neutrophils to *N*-formyl-methionylleucyl-phenylalanine (FMLP) and zymosan, two potent chemotaxis agents, *in vitro* (Hatipoğlu *et al*., 1998). On the contrary, chemotaxis was attenuated by DSPE–PEG_{2000}

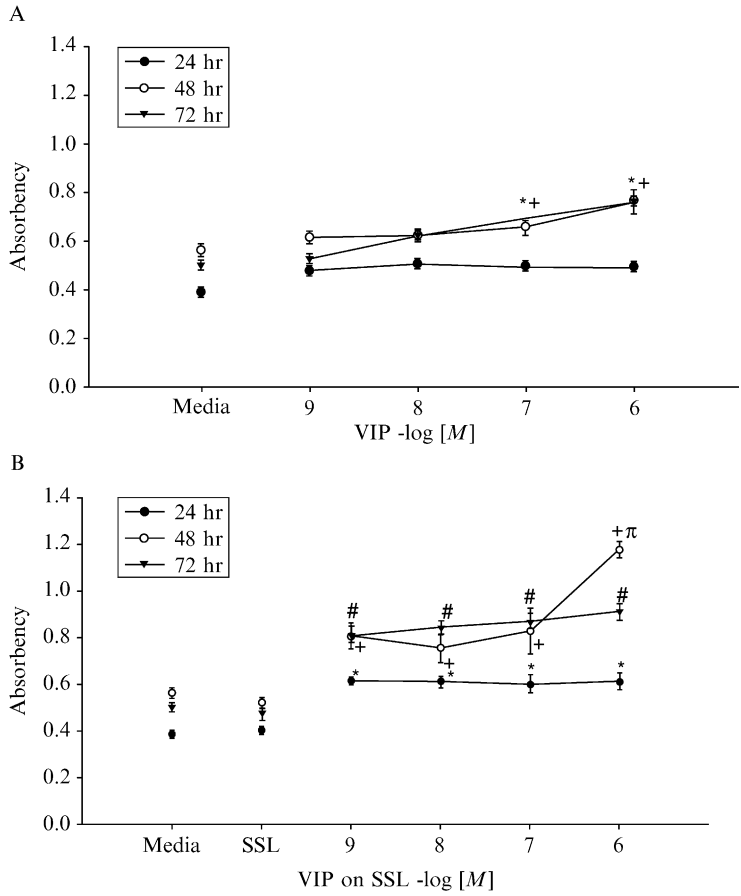

FIG. 3. (A) Incorporation of bromodeoxyuridine (BrdU) into DNA of HCPC-1 cells incubated in the absence and presence of vasoactive intestinal peptide (VIP) for 24, 48, and 72 h. Values are means ± SEM; each group, n = four experiments in triplicate. $^{*}p < 0.05$ in comparison to media. $^{+}p < 0.05$ in comparison to 24 h. (B) BrdU incorporation into DNA of HCPC-1 cells incubated in the absence and presence of vasoactive intestinal peptide on sterically stabilized liposomes (VIP on SSL) and empty SSL for 24, 48, and 72 h. Values are means ± SEM; each group, n = four experiments in triplicate. $^{*}p < 0.05$ in comparison to media. $^{+}p < 0.05$ in comparison to 24 h. $^{\#}p < 0.05$ in comparison to 24 h. $^{\pi}p < 0.05$ in comparison to 72 h. Reproduced with permission from Rubinstein *et al.* (2000).

and empty SSL (Hatipoğlu *et al.*, 1998). Stability studies of VIP on SSL showed ~80% peptide activity even after storage for 30 days at 4°. Although studies detailing stability of the peptide in SSL in the presence of serum and trypsin were not conducted, we anticipate its stability to be

TABLE II
EFFECT OF PHOSPHOLIPIDS ON α-HELICITY OF VASOACTIVE INTESTINAL PEPTIDE (VIP) AT 25° AND 37°[a]

	α-Helix (%)	
	Saline	Micelles[b]
VIP at room temperature	5 ± 1	27 ± 2*, **
VIP at 37°	2 ± 1	67 ± 3***
Calmodulin at room temperature	0	0
VIP and calmodulin at room temperature	1 ± 1	42 ± 2*, **, ****
Arginine^z-vasopressin at room temperature	8 ± 1	16 ± 2*
Arginine^z-vasopressin and calmodulin at room temperature	8 ± 1	16 ± 2*

[a] α-Helix conformation of VIP and arginine^z-vasopressin in saline and sterically stabilized micelles by circular dichroism.
[b] Values are means ± SEM of four experiments (each experiment is an average of nine continuous scans).
*$p < 0.05$ in comparison to saline.
**$p < 0.05$ in comparison to arginine^z-vasopressin.
***$p < 0.05$ in comparison to VIP in micelles at room temperature.
****$p < 0.05$ in comparison to VIP in micelles at room temperature.
Reproduced with permission from Rubinstein *et al.* (2000).

similar or even better than what is observed for VIP encapsulated in CL (Gololobov *et al.*, 1998).

In Vivo *Studies*

The bioactivity of VIP are in either in CL or SSL using the *in situ* cheek pouch model hamster summarized in Table I. The effects on both arteriolar diameter and duration of action of both formulations are very similar, suggesting no change in the *in situ* bioactivity of the peptide. However, the effect of VIP on SSL on mean arterial pressure following intravenous administration in hamsters is markedly different from that observed with aqueous VIP (Fig. 4) (Séjourné *et al.*, 1997a). Intravenous administration of VIP on SSL to normotensive hamsters has no significant effect on systemic arterial pressure, as SSL cannot extravasate through normal blood vessel wall (Fig. 5). Moreover, it has been previously shown that VIP receptors are expressed on the abluminal side of blood vessel wall (Fahrenkrug *et al.*, 2000); thus VIP would need to extravasate across the luminal cavity to exert its action. VIP on SSL extravasates preferentially in areas with damaged endothelium, as evident in hypertensive animals (Rubinstein and Mayhan, 1995; Thomas *et al.*, 1997). Figure 5 shows preferential

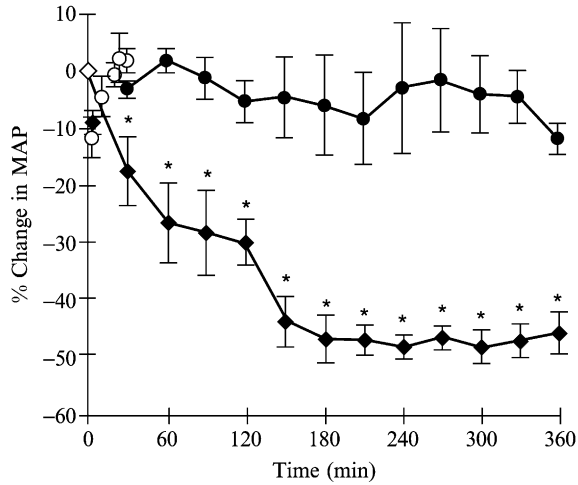

FIG. 4. Percentage change in mean arterial pressure after bolus intravenous injection of 0.1 nmol VIP on SSL (method B, ◆), native VIP (○), and empty SSL (●) in hamsters with spontaneous hypertension. Values are mean ± SEM; each group $n =$ four animals. *$p < 0.05$ compared to baseline. Reproduced with permission from Séjourné *et al.* (1997a).

lowering of systemic arterial pressure after intravenous administration of a low concentration of VIP on SSL in hypertensive animals. Moreover, clinical studies from other laboratories have previously shown that free VIP express adverse effects, most likely due to extravasation of the free peptide followed by subsequent intraction with VIP receptors (Thakur *et al.*, 2000). Collectively, these data show that VIP on SSL can be used selectively in systemic hypertension circumventing adverse effects seen when using higher concentrations of aqueous VIP.

We have previously shown that VIP on SSL activates VIP receptors in the peripheral microcirculation (Séjourné *et al.*, 1997b). However, receptor-independent pathways are also involved (Ikezaki *et al.*, 1998; Séjourné *et al.*, 1997b).

Formulations of VIP on SSL elicit a significant concentration-dependent increase in arteriolar diameter in the intact hamster cheek pouch. Suffusion of anti-VIP antibody had no significant effects on VIP on SSL-induced responses. Arteriolar diameter increased by 22% from baseline during VIP-SSL (0.1 nmol) suffusion alone and by 21% and 19% during suffusion of 0.1 nmol VIP-SSL together with 0.02 and 0.04 mg anti-VIP antibody, respectively, whereas suffusion of VIP alone (1.0 nmol) in the presence of anti-VIP antibody (0.02 and 0.04 mg) shows significantly attenuated vasodilation (Ikezaki *et al.*, 1998). These results confirm the

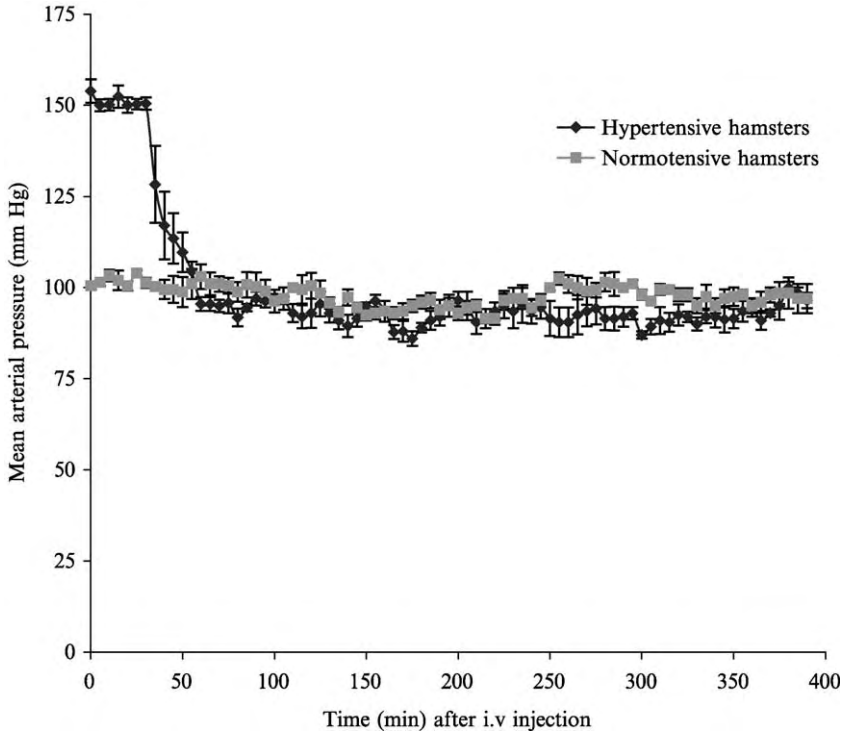

FIG. 5. Effects of intravenous VIP on SSC (0.1 nmol; bolus) on mean arterial pressure in normotensive and spontaneously hypertensive hamsters (data are means ± SEM; each n = four animals).

in vitro stability improvement of VIP in either CL or SSL formulations. Collectively, interaction of VIP with these liposomes significantly increases biological activity, *in vivo* half-life, stability, and targetability of the peptide.

Conclusions and Future Directions

Several methods to prepare liposomal VIP have been described. However, SSL prepared by method 3 (optimized film rehydration and extrusion) are the most practical for preparation of liposomal VIP. There are several reasons for this conclusion; first, method 3 involves the incorporation of the peptide on preformed SSL, thereby avoiding possible loss of VIP by extrusion during liposome preparation in the presence of the peptide (method 1). Second, method 3 provides control over the size of the liposomes, unlike freeze-drying the formulation and then rehydrating

(method 2), where the size of liposomes cannot be controlled. Third, the formulation according to method 3 is simple to prepare, as the peptide needs only to be incubated for only 2 h at room temperature with preformed liposomes before use. These factors favor the use of method 3 in preparation of liposomal VIP.

Association of VIP with liposomes, either CL or SSL, stabilizes the peptide and improves its bioactivity. Liposomal VIP elicits significant potentiation and prolongation of the vasoactive effects of VIP, when VIP is either encapsulated in liposomes (CL) or associated with SSL. VIP interactions with liposomes prevent VIP degradation by trypsin and autocatalytic antibodies, thus prolonging the molecular half-life of the peptide. Moreover, association of VIP with liposomes converts the conformation of the peptide from predominantly random coil in aqueous solution to α-helix in the presence of phospholipids. These factors contribute to a longer half-life of VIP when associated with liposomes. Although the *in vivo* half-life of VIP encapsulated in CL is $\sim$8-fold higher than that of aqueous VIP, preliminary experiments from our laboratory indicate that the half-life of VIP on SSL would be much longer due to their longer circulation time. This is in agreement with other groups that have shown longer circulation half-lives for other proteins and peptides using SSL (Liu *et al*., 1992; Maruyama *et al*., 1991b; Oku *et al*., 1994). Development of second-generation liposomal VIP using SSL is a major breakthrough, because VIP is now associated with SSL and its RES uptake is reduced, resulting in a longer circulation half-life of the peptide *in vivo*. Evidently, association of VIP with either CL or SSL also significantly increases peptide stability of the VIP *in vitro* to almost $\sim$15 days when stored at 4° compared with a few hours for aqueous (Gololobov *et al*., 1998; Patel *et al*., 1999).

Recent work in our laboratory involving conjugation of VIP to the distal end of phospholipids has expanded the use of the liposomal VIP formulation. This third-generation VIP on SSL could be used for active targeted delivery of compounds, either therapeutic or diagnostic/imaging, to specific sites where VIP receptors are overexpressed, thereby circumventing systemic adverse reactions (Dagar *et al*., 2001). In this regard, SSL have been shown to extravasate preferentially in tumors and inflamed tissues due to the leakiness of the local microvasculature (Carr *et al*., 2001; Dvorak *et al*., 1991; Ezaki *et al*., 2001; Gabizon and Martin, 1997; Oku and Namba, 1994; Yuan *et al*., 1994). These disease states thus provide a suitable opportunity to use VIP-SSL as a delivery system for both passive and active targeting.

In summary, developments in pharmaceutical technologies have made it possible to bring liposomal formulations to the clinic. Various methods have been designed to produce liposomes on a large scale, making it possible to

move this field from the bench to the market. This trend is evident as more liposome-based drugs have been made available to patients. We propose that liposomal-VIP is an appropriate candidate for such a product.

Acknowledgments

Supported, in part, by VA Merit Review grant, NIH Grants R01A G024026 and R01 HL72323, and Department of Defense Grant DAMD17-02-1-0415. We thank the students, research associates, and postdoctoral fellows who contributed to this research.

References

Bangham, A. D., Standish, M. M., and Watkins, J. C. (1965). Diffusion of univalent ions across the lamellae of swollen phospholipids. *J. Mol. Biol.* **13,** 238–252.

Bolin, D. R., Michalewsky, J., Wasserman, M. A., and O'Donnell, M. (1995). Design and development of a vasoactive intestinal peptide analog as a novel therapeutic for bronchial asthma. *Biopolymers* **37,** 57–66.

Brizzolara, A. L., and Burnstock, G. (1991). Endothelium-dependent and endothelium-independent vasodilatation of the hepatic artery of the rabbit. *Br. J. Pharmacol.* **103,** 1206–1212.

Carr, D. B., McDonald, G. B., Brateng, D., Desai, M., Thach, C. T., and Easterling, T. R. (2001). The relationship between hemodynamics and inflammatory activation in women at risk for preeclampsia. *Obstet. Gynecol.* **98,** 1109–1116.

Dagar, S., Sekosan, M., Blend, M., Rubinstein, I., and Önyüksel, H. (1999). Optimized formulation of vasoactive intestinal peptide on sterically stabilized liposome. *In Proc. 26th Int. Symp. Control. Rel. Bioactive Mater.*, pp. 22–23.

Dagar, S., Sekosan, M., Lee, B. S., Rubinstein, I., and Önyüksel, H. (2001). VIP receptors as molecular targets of breast cancer: Implications for targeted imaging and drug delivery. *J. Control. Rel.* **74,** 129–134.

Davis, M. J., Joyner, W. L., and Gilmore, J. P. (1981). Responses of pulmonary allograft and cheek pouch arterioles in the hamster to alterations in extravascular pressure in different oxygen environments. *Circ. Res.* **49,** 125–132.

Delgado, M., Abad, C., Martinez, C., Leceta, J., and Gomariz, R. P. (2001). Vasoactive intestinal peptide prevents experimental arthritis by downregulating both autoimmune and inflammatory components of the disease. *Nat. Med.* **7,** 563–568.

Domschke, S., Domschke, W., Bloom, S. R., Mitznegg, P., Mitchell, S. J., Lux, G., and Strunz, U. (1978). Vasoactive intestinal peptide in man: Pharmacokinetics, metabolic and circulatory effects. *Gut* **19,** 1049–1053.

Düzgüneş, N., Perumal, V. K., Kesavalu, L., Goldstein, J. H., Debs, R. J., and Gangadharam, P. R. J. (1988). Enhanced effect of liposome-encapsulated amileacin on *Mycobacterium avium-intraccellulare* complex in beige mice. *Antimicrob. Agents Chemother.* **27,** 1404–1411.

Dvorak, H. F., Nagy, J. A., and Dvorak, A. M. (1991). Structure of solid tumors and their vasculature: Implications for therapy with monoclonal antibodies. *Cancer Cells* **3,** 77–85.

Ezaki, T., Baluk, P., Thurston, G., La Barbara, A., Woo, C., and McDonald, D. M. (2001). Time course of endothelial cell proliferation and microvascular remodeling in chronic inflammation. *Am. J. Pathol.* **158,** 2043–2055.

Fahrenkrug, J., Hannibal, J., Tams, J., and Georg, B. (2000). Immunohistochemical localization of the VIP1 receptor (VPAC1R) in rat cerebral blood vessels: Relation to PACAP and VIP containing nerves. *J. Cereb. Blood Flow Metab.* **20,** 1205–1214.

Gabizon, A., and Martin, F. (1997). Polyethylene glycol-coated (pegylated) liposomal doxorubicin. Rationale for use in solid tumours. *Drugs* **54**(Suppl. 4), 15–21.

Gao, X.-P., Noda, Y., Rubinstein, I., and Paul, S. (1994). Vasoactive intestinal peptide encapsulated in liposomes: Effects on systemic arterial blood pressure. *Life Sci.* **54,** 247–252.

Gaw, A. J., Aberdeen, J., Humphrey, P. P., Wadsworth, R. M., and Burnstock, G. (1991). Relaxation of sheep cerebral arteries by vasoactive intestinal polypeptide and neurogenic stimulation: Inhibition by L-N^G-monomethyl arginine in endothelium-denuded vessels. *Br. J. Pharmacol.* **102,** 567–572.

Gololobov, G., Noda, Y., Sherman, S., Rubinstein, I., Baranowska-Kortylewicz, J., and Paul, S. (1998). Stabilization of vasoactive intestinal peptide by lipids. *J. Pharmacol. Exp. Ther.* **285,** 753–758.

Gomariz, R. P., Martinez, C., Abad, C., Leceta, J., and Delgado, M. (2001). Immunology of VIP: A review and therapeutical perspectives. *Curr. Pharm. Des.* **7,** 89–111.

Gozes, I., Reshef, A., Salah, D., Rubinraut, S., and Fridkin, M. (1994). Stearylnorleucine-vasoactive intestinal peptide (VIP): A novel VIP analog for noninvasive impotence treatment. *Endocrinology* **134,** 2121–2125.

Gozes, I., Bardea, A., Reshef, A., Zamostiano, R., Zhukovsky, S., Rubinraut, S., Fridkin, M., and Brenneman, D. E. (1996). Neuroprotective strategy for Alzheimer disease: Intranasal administration of a fatty neuropeptide. *Proc. Natl. Acad. Sci. USA* **93,** 427–432.

Harmar, A. J., Arimura, A., Gozes, I., Journot, L., Laburthe, M., Pisegna, J. R., Rawlings, S. R., Robberecht, P., Said, S. I., Sreedharan, S. P., Wank, S. A., and Waschek, J. A. (1998). International Union of Pharmacology. XVIII. Nomenclature of receptors for vasoactive intestinal peptide and pituitary adenylate cyclase-activating polypeptide. *Pharmacol. Rev.* **50,** 265–270.

Hassan, M., Refai, E., Andersson, M., Schnell, P. O., and Jacobsson, H. (1994). *In vivo* dynamical distribution of 131I-VIP in the rat studied by gamma-camera. *Nucl. Med. Biol.* **21,** 865–872.

Hatipoğlu, U., Gao, X., Verral, S., Séjourné, F., Pitrak, D., Alkan-Önyüksel, H., and Rubinstein, I. (1998). Sterically stabilized phospholipids attenuate human neutrophils chemotaxis *in vitro*. *Life Sci.* **63,** 693–699.

Heath, T. D., Lopez, N. G., Piper, J. R., Montgomery, J. A., Stern, W. H., and Papahadjopoulos, D. (1986). Liposome-mediated delivery of pteridine antifolates to cells *in vitro*: Potency of methotrexate, and its alpha and gamma substituents. *Biochim. Biophys. Acta* **862,** 72–80.

Huang, M., and Rorstad, O. P. (1987). VIP receptors in mesenteric and coronary arteries: A radioligand binding study. *Peptides* **8,** 477–485.

Ignarro, L. J., Byrns, R. E., Buga, G. M., and Wood, K. S. (1987). Mechanisms of endothelium-dependent vascular smooth muscle relaxation elicited by bradykinin and VIP. *Am. J. Physiol.* **253,** H1074–H1082.

Ikezaki, H., Paul, S., Alkan-Önyüksel, H., Patel, M., Gao, X. P., and Rubinstein, I. (1998). Vasodilation elicited by liposomal VIP is unimpeded by anti-VIP antibody in hamster cheek pouch. *Am. J. Physiol.* **275,** R56–R62.

Ikezaki, H., Patel, M., Önyüksel, H., Akhter, S. R. A., Gao, X. P., and Rubinstein, I. (1999). Exogenous calmodulin potentiates vasodilation elicited by phospholipid-associated VIP *in vivo*. *Am. J. Physiol.* **276,** R1359–R1365.

Klibanov, A. L., Maruyama, K., Torchilin, V. P., and Huang, L. (1990). Amphipathic polyethyleneglycols effectively prolong the circulation time of liposomes. *FEBS Lett.* **268,** 235–237.

Klibanov, A. L., Maruyama, K., Beckerleg, A. M., Torchilin, V. P., and Huang, L. (1991). Activity of amphipathic poly(ethylene glycol) 5000 to prolong the circulation time of

liposomes depends on the liposome size and is unfavorable for immunoliposome binding to target. *Biochim. Biophys. Acta* **1062,** 142–148.

Liu, D., Mori, A., and Huang, L. (1992). Role of liposome size and RES blockade in controlling biodistribution and tumor uptake of GM1-containing liposomes. *Biochim. Biophys. Acta* **1104,** 95–101.

Maruyama, K., Yuda, T., Okamoto, A., Ishikura, C., Kojima, S., and Iwatsuru, M. (1991a). Effect of molecular weight in amphipathic polyethyleneglycol on prolonging the circulation time of large unilamellar liposomes. *Chem. Pharm. Bull.* **39,** 1620–1622.

Maruyama, K., Mori, A., Bhadra, S., Subbiah, M. T., and Huang, L. (1991b). Proteins and peptides bound to long-circulating liposomes. *Biochim. Biophys. Acta* **1070,** 246–252.

Matthay, K. K., Heath, T. D., Badger, C. C., Bernstein, I. D., and Papahadjopoulos, D. (1986). Antibody-directed liposomes: Comparison of various ligands for association, endocytosis, and drug delivery. *Cancer Res.* **46,** 4904–4910.

Mayhew, E., and Rustum, Y. M. (1985). The use of liposomes as carriers of therapeutic agents. *Prog. Clin. Biol. Res.* **172B,** 301–310.

Noda, Y., Rodriguez-Sierra, J., Liu, J., Landers, D., Mori, A., and Paul, S. (1994). Partitioning of vasoactive intestinal polypeptide into lipid bilayers. *Biochim. Biophys. Acta* **1191,** 324–330.

Oku, N., and Namba, Y. (1994). Long-circulating liposomes. *Crit. Rev. Ther. Drug Carrier Syst.* **11,** 231–270.

Oku, N., Naruse, R., Doi, K., and Okada, S. (1994). Potential usage of thermosensitive liposomes for macromolecule delivery. *Biochim. Biophys. Acta* **1191,** 389–391.

Ollerenshaw, S., Jarvis, D., Woolcock, A., Sullivan, C., and Scheibner, T. (1989). Absence of immunoreactive vasoactive intestinal polypeptide in tissue from the lungs of patients with asthma. *N. Engl. J. Med.* **320,** 1244–1248.

Önyüksel, H., Ashok, B., Dagar, S., Sethi, V., and Rubinstein, I. (2003). Interactions of VIP with rigid phospholipid bilayers: Implications for vasoreactivity. *Peptides* **24,** 281–286.

Papahadjopoulos, D., Heath, T., Bragman, K., and Matthay, K. (1985). New methodology for liposome targeting to specific cells. *Ann. N.Y. Acad. Sci.* **446,** 341–348.

Patel, M., Önyüksel, H., Ikezaki, H., Dagar, S., Akhter, S. R., and Rubinstein, I. (1999). *Proc. Int. Symp. Control. Rel. Bioactive Mater* **26,** #6238.

Paul, S., Said, S. I., Thompson, A. B., Volle, D. J., Agrawal, D. K., Foda, H., and de la Rocha, S. (1989). Characterization of autoantibodies to vasoactive intestinal peptide in asthma. *J. Neuroimmunol.* **23,** 133–142.

Refai, E., Jonsson, C., Andersson, M., Jacobsson, H., Larsson, S., Kogner, P., and Hassan, M. (1999). Biodistribution of liposomal 131I-VIP in rat using gamma camera. *Nucl. Med. Biol.* **26,** 931–936.

Robinson, R. M., Blakeney, E. W., Jr., and Mattice, W. L. (1982). Lipid-induced conformational changes in glucagon, secretin, and vasoactive intestinal peptide. *Biopolymers* **21,** 1271–1274.

Rubinstein, I., and Mayhan, W. G. (1995). L-arginine dilates cheek pouch arterioles in hamsters with hereditary cardiomyopathy but not in controls. *J. Lab. Clin. Med.* **125,** 313–318.

Rubinstein, I., Patel, M., Ikezaki, H., Dagar, S., and Önyüksel, H. (2000). Conformation and vasoreactivity of VIP in phospholipids: Effects of calmodulin. *Peptides* **20,** 1497–1501.

Rubinstein, I., Dagar, S., Sethi, V., Krishnadas, A., and Önyüksel, H. (2001). Surface-active properties of vasoactive intestinal peptide*. *Peptides* **22,** 671–675.

Said, S. I. (1986). Vasoactive intestinal peptide. *J. Endocrinol. Invest.* **9,** 191–200.

Said, S. I. (1992). Vasoactive intestinal polypeptide (VIP) in lung function and disease. *Biomed. Res.* **13,** 257–268.

Séjourné, F., Rubinstein, I., Suzuki, H., and Alkan-Önyüksel, H. (1997a). Development of a novel bioactive formulation of vasoactive intestinal peptide in sterically stabilized liposomes. *Pharm. Res.* **14,** 362–365.

Séjourné, F., Suzuki, H., Alkan-Önyüksel, H., Gao, X. P., Ikezaki, H., and Rubinstein, I. (1997b). Mechanisms of vasodilation elicited by VIP in sterically stabilized liposomes *in vivo*. *Am. J. Physiol.* **273,** R287–292.

Straubinger, R. M., Düzgüneş, N., and Papahadjopoulos, D. (1985). pH-sensitive liposomes mediate cytoplasmic delivery of encapsulated macromolecules. *FEBS Lett.* **179,** 148–154.

Suzuki, H., Noda, Y., Paul, S., Gao, X. P., and Rubinstein, I. (1995). Encapsulation of vasoactive intestinal peptide into liposomes: Effects on vasodilation *in vivo*. *Life Sci.* **57,** 1451–1457.

Suzuki, H., Noda, Y., Gao, X. P., Séjourné, F., Alkan-Önyüksel, H., Paul, S., and Rubinstein, I. (1996a). Encapsulation of VIP into liposomes restores vasorelaxation in hypertension *in situ*. *Am. J. Physiol.* **271,** H282–287.

Suzuki, H., Gao, X. P., Olopade, C. O., and Rubinstein, I. (1996b). Aqueous smokeless tobacco extract impairs endothelium-dependent vasodilation in the oral mucosa. *J. Appl. Physiol.* **81,** 225–231.

Szucs, M., and Tilcock, C. (1995). Lyophilization and rehydration of polymer-coated lipid vesicles containing a lipophilic chelator in the presence of sucrose: Labeling with 99mTc and biodistribution studies. *Nucl. Med. Biol.* **22,** 263–268.

Thakur, M. L., Marcus, C. S., Saeed, S., Pallela, V., Minami, C., Diggles, L., Pham, H. L., Ahdoot, R., Kalinowski, E. A., and Moody, T. (2000). 99mTc-labeled vasoactive intestinal peptide analog for rapid localization of tumors in humans. *Ann. N.Y. Acad. Sci.* **921,** 37–44.

Thomas, C. L., Artwohl, J. E., Suzuki, H., Gao, X., White, E., Saroli, A., Bunte, R. M., and Rubinstein, I. (1997). Initial characterization of hamsters with spontaneous hypertension. *Hypertension* **30,** 301–304.

Yuan, F., Salehi, H. A., Boucher, Y., Vasthare, U. S., Tuma, R. F., and Jain, R. K. (1994). Vascular permeability and microcirculation of gliomas and mammary carcinomas transplanted in rat and mouse cranial windows. *Cancer Res.* **54,** 4564–4568.

[22] Liposomal Superoxide Dismutases and Their Use in the Treatment of Experimental Arthritis

By M. Eugénia M. Cruz, M. Manuela Gaspar, M. Bárbara F. Martins, and M. Luísa Corvo

Abstract

It has long been suggested that superoxide dismutase (SOD) be used for antioxidant therapy on the basis of its ability to catalyze the dismutation of superoxide radicals involved in the pathogenesis of several inflammatory disorders such as rheumatoid arthritis. However, the administration of SOD in free form has some disadvantages, most importantly, the low accumulation of SOD in inflamed areas due to its reduced half-life in the

0076-6879/05 $35.00

Appendix (4)

Available online at www.sciencedirect.com

SCIENCE DIRECT®

nanomedicine

Nanomedicine: Nanotechnology, Biology, and Medicine 1 (2005) 77–84

www.nanomedjournal.com

Oncology

Camptothecin in sterically stabilized phospholipid micelles: A novel nanomedicine

Otilia M. Koo, MD,[a] Israel Rubinstein, MD,[a,b,d] Hayat Onyuksel, PhD[a,c,*]

[a]*Department of Biopharmaceutical Sciences, University of Illinois, Chicago, Illinois*
[b]*Department of Medicine, University of Illinois, Chicago, Illinois*
[c]*Department of Bioengineering, University of Illinois, Chicago, Illinois*
[d]*Jesse Brown Veterans Affairs Medical Center, Chicago, Illinois*

Received 24 September 2004; accepted 18 November 2004

Abstract

Background: Camptothecin (CPT) is a well-established topoisomerase I inhibitor against a broad spectrum of cancers. However, poor aqueous solubility, instability, and toxic effects to normal tissues have limited CPT clinical development. Recently, sterically stabilized micelles (SSM) composed of polyethylene glycol (PEGylated) phospholipids have been introduced as safe, biocompatible nanocarriers for the delivery of poorly water-soluble drugs. It was the aim of this study to develop and evaluate in vitro camptothecin-containing SSM (CPT-SSM) as a novel nanomedicine for parenteral administration.

Methods: The solubilization potential, stability, and in vitro cytotoxicity of CPT in SSM were studied. Lyophilization of CPT-SSM under controlled conditions was also studied.

Results: The mean size of CPT-SSM was found to be ~14 nm with a narrow size distribution. CPT-SSM were prepared by coprecipitation reconstitution. At a concentration of 15 mmol/L of PEGylated phospholipids where no micelle–micelle interaction was observed, CPT solubilization in SSM was 25-fold higher than CPT in buffer. We determined that CPT can be solubilized in SSM up to molar ratios of CPT/lipid = 0.0063:1. Above this critical molar ratio, heterogeneous systems of CPT-SSM and CPT self-aggregated particles were formed. CPT in SSM was at least 3 times more stable and 3-fold more cytotoxic to MCF-7 cells than CPT alone. Furthermore, CPT-SSM alone was lyophilized without additional lyoprotectants and cryoprotectants and reconstituted without any significant change in properties.

Conclusion: We have shown that CPT in SSM is a promising nanomedicine with improved drug solubility, stability, freeze-drying properties, and anticancer activity. It is anticipated that, because of the nanosize and steric stability of the micelles, CPT-SSM will be passively targeted to solid cancers in vivo, resulting in high drug concentration in tumors and reduced drug toxicity to the normal tissues.

Key words: Camptothecin; Phospholipid; Micelles; Formulation; Lyophilization

Camptothecin (CPT) is a potent anticancer agent that has been found to be active against a broad spectrum of cancers, such as colon, breast, ovarian, and lung cancers [1-4]. DNA relaxation by the enzyme DNA topoisomerase I is required for replication and transcription [5]. CPT and its analogs inhibit DNA topoisomerase I, subsequently stabilizing the DNA-topoisomerase complex resulting in apoptosis of cancer cells. However, clinical application of CPT against cancer has been limited by its formulation and delivery problems. Parenteral administration of CPT is hampered largely by poor water solubility of its active lactone form [6,7]. CPT lactone is also unstable under physiologic conditions and converts to the inactive carboxylate form [8]. Finally, CPT can cause a number of toxic side effects to normal tissues, such as hemorrhagic cystitis and myelosuppression [6,9,10]. The purpose of this study was to begin to address these problems by formulating and evaluating in

* Corresponding author. University of Illinois at Chicago, College of Pharmacy, Department of Biopharmaceutical Sciences (M/C 865), 833 South Wood St, Chicago, IL 60612-7231.

E-mail address: hayat@uic.edu (H. Onyuksel).

1549-9634/$ – see front matter © 2005 Elsevier Inc. All rights reserved.
doi:10.1016/j.nano.2004.11.002

vitro CPT in a safe nanocarrier that can increase the drug solubility and stability and that also has the right size to increase CPT accumulation in the tumors as well as minimize CPT exposure to normal tissues.

Recently, our laboratory and others have reported on the novel nanotechnology of sterically stabilized micelles (SSM) as targeted drug carriers for the delivery of poorly water-soluble drugs and peptides [11-13]. SSM form spontaneously in an aqueous environment when diacyllipid-polyethylene glycol (PEG) phospholipids exist at concentrations above their critical micelle concentrations (CMC). Thus, SSM can be formed reproducibly with a narrow size distribution and in a simpler manner than other carriers such as liposomes and other nanoparticles. PEGylated phospholipid micelles are also advantageous as nanocarriers because they are formed from biocompatible, biodegradable, and relatively nontoxic molecules [11,14]. SSM are superior to conventional detergent micelles, because they have extremely low CMCs, at micromolar range, resulting in greater thermodynamic stability toward dilution on in vivo administration [11].

The long-term aim of this study is to develop CPT-SSM as a novel nanomedicine. We chose to formulate CPT in SSM because of its potential to self-associate with the hydrophobic regions of SSM to improve its aqueous solubility. Also, the stability of CPT in active lactone form should be increased because of decreased water content and hence decreased hydrolytic inactivation in the micelles. Maximal aqueous stability of CPT in SSM when stored under ambient conditions was evaluated in this study. We also studied the lyophilization and reconstitution of CPT micellar dispersions without any formulation modifications. We anticipated that drug-containing SSM can be freeze-dried because of PEG, a hydrophilic polymer, in their outer corona that can act as both cryoprotectant and lyoprotectant. Outer corona of PEG chains on SSM also have the potential to increase CPT circulation times in vivo by avoiding reticuloendothelial system (RES) uptake [15]. Importantly, unlike free CPT and other water-soluble CPT analogs that distribute freely to normal and tumor tissues, CPT associated with SSM, as a result of the nanosize of the construct, passively accumulates to a greater extent in tissues with leaky vasculature, such as tumors, and decrease normal tissue distribution [16]. This should improve the therapeutic index of CPT.

Material and methods

Chemicals

Camptothecin (99% purity, molecular weight 348.3) was a gift from Boehringer Ingelheim Fine Chemicals (Germany). Poly(ethylene glycol 2000)-conjugated distearoyl phosphatidylethanolamine (DSPE-PEG2000) was purchased from Northern Lipids Inc (Vancouver, Canada). HPLC-grade methanol and acetonitrile were obtained from Fisher Scientific (Hanover Park, Ill). Buffer and all other reagents used were analytic grade and purchased from Sigma-Aldrich (St Louis, Mo). Water was deionized at 18 megaohms/cm, and sterile filtered before use.

Preparation of CPT-SSM

Aqueous dispersions of CPT-SSM were prepared by the coprecipitation and reconstitution method. Various molar ratios of CPT:DSPE-PEG2000 (0.001:1 to 0.057:1) were dissolved in methanol in a 100-mL round-bottom flask. The methanol was removed by vacuum rotary evaporation (45°C, 150 revolutions/min, and 600 mm Hg vacuum) under a stream of argon to form a dry film. This film was further dried under vacuum overnight to remove any traces of methanol. The film was then rehydrated by vortexing (Thermolyne Maxi Mix II) for 5 minutes, and sonicating (Fisher Scientific bath sonicator B2200R-1) for 5 minutes with 0.01 mol/L acetate buffer (pH 5). The resulting aqueous dispersion was equilibrated in the dark for 2 hours at 25°C. Any excess precipitated drug was removed by centrifugation (13,000*g*) before characterization. All dispersions were prepared in triplicate.

Size analysis and morphologic features

Particle size was measured by quasielastic light scattering (QELS) with a NICOMP 380 particle-size analyzer (Santa Barbara, Calif), equipped with a 5 mW helium-neon laser at 632.8 nm. Mean diameters ($\bar{d}_h$) of the particles in the aqueous dispersions were calculated using the Stokes–Einstein equation as described previously [11].

The CPT aqueous dispersions were observed under transmission electron microscope (TEM) (Jeol JEM-1220, Jeol USA Inc, Peabody, Mass) at 100 kV for morphology. A 0.05-mL drop of sample was placed on the formvar carbon support film (grid mesh 200), and stained with 1% uranylacetate (pH 4.5) for 1 minute. Excess stain was removed, and the sample was air dried at room temperature. TEM images were recorded by a multiscan camera (Gatan Inc, Pleasonton, Calif) using the Gatan Digital Micrograph version 2.5 software. For comparison, TEM images of CPT powder as raw material were also taken.

HPLC analysis for CPT concentration

The concentration of solubilized CPT in the aqueous dispersions was measured by reversed-phase HPLC using conditions modified from the literature [17]. Experiments were performed at ambient temperature at a flow rate of 1 mL/min with use of a HPLC setup that consisted of the following: ThermoFinnigan Spectra System P2000 pump, Spectra System AS3500 Autosampler, and Spectra Focus Forward Optical Scanning Detector. Injection volumes of 20 μl were used, and the mobile phase was acetonitrile-10 nmol/L potassium phosphate (45:55 vol/vol, pH 7). Separations were achieved on an Agilent Zorbax SB-C18 reverse-phase column (250 × 4.6 mm, 5 mm). Ultraviolet detection was achieved at a wavelength of 365 nm. A

calibration curve was produced based on the average peak area of standard injections. All injections were performed in triplicate.

Fluorescence emission spectroscopy

A shift in CPT peak fluorescence emission toward a lower wavelength is indicative of CPT movement from the aqueous medium into the more hydrophobic environment [8]. Because SSM provided a more hydrophobic environment, fluorescence emission experiments demonstrated the association of CPT with SSM. Fluorescence emission spectra of CPT were recorded at a scan rate of 1 nm per second with an SLM-Aminco 8000 spectroflourimeter (Edison, NJ) at an excitation wavelength of 360 nm [18]. Samples were measured in cuvets of 1-cm path length at ambient temperature. Fluorescence emission spectra for each sample were obtained in duplicate.

Aqueous stability of CPT-SSM

CPT-SSM aqueous dispersions were stored at 25°C in the dark with air in the headspace and characterized for micelle size, CPT concentration and fluorescence emission spectra as described above, at fixed time intervals from 2 hours up to 7 days after preparation.

In vitro cytotoxic activity

MCF-7 breast cancer cells were used to evaluate CPT in vitro antitumor activity. The cells were cultured in Eagle's minimal essential medium (EMEM) containing 2 mmol/L L-glutamine and Earle's BSS adjusted to contain 1.5 g/L sodium bicarbonate, 0.1 mmol/L nonessential amino acids, and 1 mm sodium pyruvate and supplemented with 0.01 mg/mL bovine insulin fetal bovine serum = 90%:10%.

The optimum solution of CPT-SSM (composed of 15 mmol/L DSPE-PEG2000, 20 μg/mL CPT) chosen from the solubilization studies was used as the test solutions. Corresponding concentrations of CPT in 10% dimethyl sulfoxide (DMSO) solutions were also tested for comparison. Drug-free SSM in 0.01 mol/L acetate buffer (pH 5) were prepared at the same concentrations as the test solution and used as controls. In vitro cytotoxicity was assessed using the sulforhodamine B assay adopted for routine use in the National Cancer Institute in vitro antitumor screen [19,20]. Briefly, serial dilutions were made to obtain CPT concentrations (0.001 to 1 μg/mL) using the respective solvent, that is, either acetate buffer or 10% DMSO. MCF-7 cells (190 μL) were trypsinized and plated at a density of 1000 cells per well in a 96-well plate. A total of 10 μL/well of the test solutions and controls were added to the microtiter plates. Control groups with 10 μL of the solvents were also added. Each sample was tested at n = 4. The plates were then incubated for 24 hours or 96 hours in a 5% carbon dioxide–humidified atmosphere at 37°C. After the incubation period, the cells were fixed to the plates by adding 100 μL/well of cold 20% trichloroacetic acid and incubating for 1 hour at 4°C. The plates were then washed, air-dried, and stained with 100 μL/well of 0.4% sulforhodamine B in 1% acetic acid for 30 minutes. Then the plates were washed with 1% acetic acid and rinsed, and 10 mmol/L TRIS (tris-[hydroxymethyl]-aminomethane) buffer (200 μL/well) was added. The optical density was then read at 560 nm, and the readings obtained for the solvent controls were used to define 100% growth after correcting for the value obtained for the zero-day control. These values were then expressed as survival percentage, and ED_{50} values calculated using nonlinear regression analysis (survival percentage vs concentration).

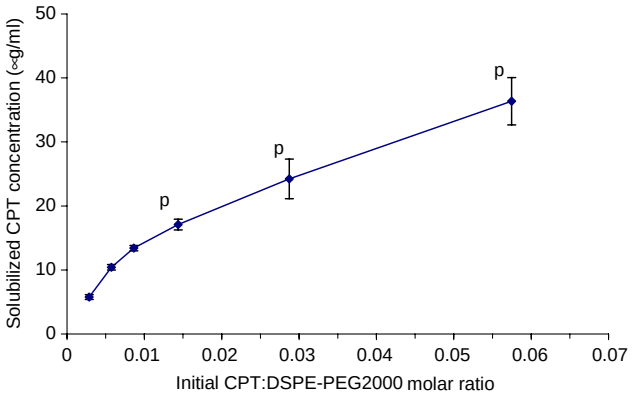

Fig 1. Solubilized camptothecin (CPT) concentrations as CPT-SSM with increasing initial CPT:DSPE-PEG2000 (fixed DSPE-PEG2000 concentration = 5 mmol/L). The p's indicate the presence of an additional population of CPT self-aggregated particles besides CPT-SSM. Values are n = 3; error bars represent SD.

Freeze-drying of CPT-SSM

The optimal CPT-SSM formulation (composed of 15 mmol/L DSPE-PEG2000, 20 μg/mL CPT) based on CPT solubilization experiments, without addition of a cryoprotectant and lyoprotectant, was placed into 2-mL vials at fill volumes of 1 mL and subjected to a controlled lyophilization cycle by the Virtis Genesis 25 EL freeze dryer as described in the literature [21]. Briefly, slow freezing of the samples was achieved by decreasing the temperature at 0.25°C/min to −40°C. In the first step of the freeze-drying process, the shelf temperature was maintained at −0°C for 3.5 hours, followed by an additional drying step of 7 hours at 0°C. During this additional drying step, the chamber pressure was maintained at -55×10^{-3} mm Hg. The condenser temperature ranged from −77.5°C to −83.6°C. Phospholipid concentrations before and after freeze-drying were determined by Bartlett's analysis as described previously [22]. CPT-SSM was characterized for size, CPT concentration, and fluorescence emission as described above after reconstitution.

Data and statistical analyses

Formulation and characterization data are averages of triplicates, and in vitro cytotoxicity data are average of

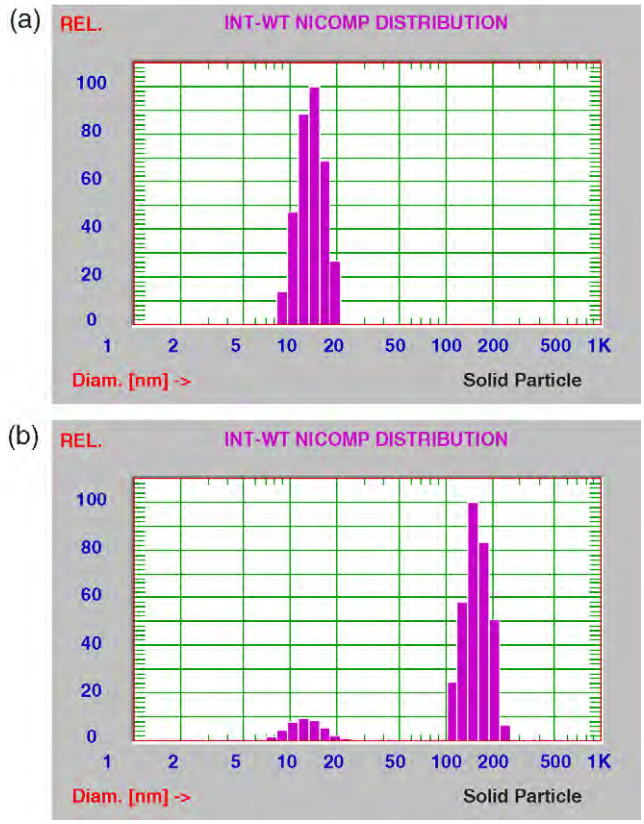

Fig 2. Representative quasi-elastic light-scattering plots to illustrate mean hydrodynamic diameter ($\bar{d}_h$) and size distribution of **(a)** CPT-SSM and **(b)** CPT-SSM in the presence of a second population of CPT particles. Fixed DSPE-PEG2000 concentration = 5 mmol/L.

quadruplicates, expressed as means with ± SDs. The relationship between CPT solubilization with increasing phospholipid concentration was analyzed by linear least-squares regression. ED_{50} values of the cytotoxicity assay were determined by linear least-squares regression. Differences between groups were compared statistically with use of 1-way analysis of variance, followed by Scheffe post-hoc test. All statistical analyses were performed using SPSS version 10.0 (Chicago, Ill). A P value of $<.05$ was considered statistically significant.

Results and discussion

Solubilization of CPT in SSM

At a fixed DSPE-PEG2000 phospholipid concentration of 5 mmol/L, CPT solubilization increased with increasing initial CPT/DSPE-PEG2000 molar ratio (Figure 1), as more CPT was available for solubilization in SSM. CPT-SSM mean diameters ($\bar{d}_h$) were 13.8 ± 0.4 nm, and of a narrow size distribution as shown in Figure 2, *a.* When observed under TEM, CPT-SSM were spherical (Figure 3, *a*). When CPT solubilization in SSM was exceeded, a second and larger population of CPT self-aggregated particles ($\bar{d}_h$ = 100 to 300 nm) besides CPT-SSM were observed, as depicted in Figure 2, *b.* The CPT particles were morphologically different from CPT-SSM and CPT starting powder (Figure 3). Similar to the observations made by Zhang et al [23], CPT-SSM and CPT self-aggregated particles observed under the TEM were smaller than the sizes measured by quasielastic light scattering (Figure 2 vs Figure 3). This can be attributed to differences in the methods. TEM measures the size from the projected area where the outer PEG chains are not visible. QELS, on the other hand, measures the size of the particles based on hydrodynamic principles and movement of particles, which is dependent on their mass. Therefore, the effect of the PEG chains is considered in the size determinations in QELS. CPT has been reported to undergo self-aggregation by stereospecific stacking interaction between quinoline rings of CPT chromophores with the inverse position of the nitrogen atoms [24]. We believe that these CPT self-aggregated particles were sufficiently stabilized by PEGylated phospholipids on their surface against further precipitation and remain in the nanosize range, suspended in the clear aqueous dispersions. PEGylated lipid-coated particles also have a promising future to be used as nanomedicine, as indicated in a recent review [25]. However, we have limited the scope of this study to only micellar CPT formulation due to its reproducible and easy preparation.

Fluorescence emission of CPT associated with SSM had peak emission wavelengths of 430.1 ± 0.7 nm that were significantly shifted ($P < .05$) compared with CPT in buffer alone (peak emission wavelength = 434.0 ± 1.0 nm). This indicated association of CPT with SSM as CPT moved from the aqueous medium into the more hydrophobic environment of SSM [8]. There was no difference in peak emission wavelength ($P > .05$) for aqueous dispersions prepared with varying initial molar ratios of CPT:DSPE-PEG2000, even for 0.014:1 and above, where CPT particles coexisted with CPT-SSM.

Our purpose was to prepare a nanocarrier system of homogeneous CPT-SSM without CPT-aggregated particles. Therefore, we first determined the concentration of maximum CPT solubilized without the formation of CPT aggregates in a given DSPE-PEG2000 concentration. Then we varied DSPE-PEG2000 concentration and plotted the maximum CPT concentrations versus the corresponding lipid concentration, as shown in Figure 4. As PEGylated phospholipid concentration increased, more SSM were formed in the system; thus, more CPT was incorporated in the SSM before CPT self-aggregation occurred. At least up to 15 mmol/L DSPE-PEG2000 concentration where no micelle-micelle interaction was observed, and a linear relationship existed between maximum solubilized CPT concentration and lipid concentration (Figure 4). Taking into account the molar ratios of CPT:DSPE-PEG2000 for maximum CPT solubilization at each corresponding phospholipid concentration, maximal solubilization of CPT in SSM can be achieved with an average critical molar ratio of CPT:DSPE2000 = 0.0063:1 ± 0.0013:1 for the entire concentration range of DSPE-PEG2000 studied. Therefore,

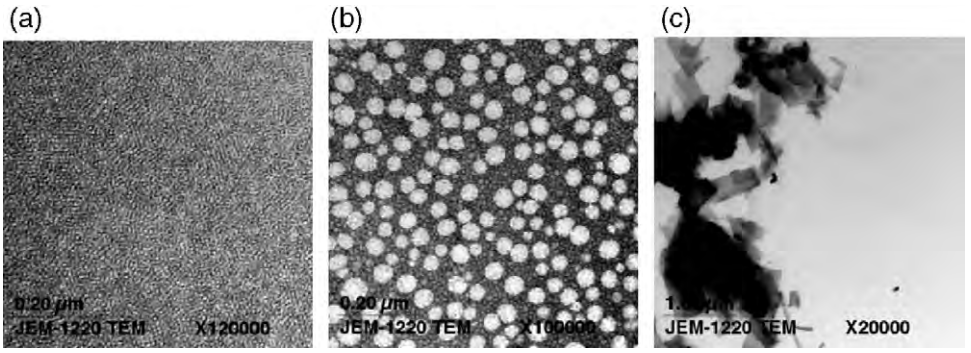

Fig 3. Transmission electron microscopy images of **(a)** CPT-SSM, **(b)** CPT-SSM and CPT particles, and **(c)** CPT powder as starting material.

for any given DSPE-PEG2000 concentration, molar ratios of CPT:DSPE-PEG2000 below this critical molar ratio should be used to avoid exclusion of CPT from the micelle and formation of CPT particles in the final systems.

Using a concentration of 15 mmol/L DSPE-PEG2000, an almost 25-fold increase in CPT solubilization in SSM, compared with CPT alone in buffer, was achieved. DSPE-PEG2000 has a much lower critical micelle concentration (0.5 to 1 μmol/L) than did Pluronic surfactants (0.3 to 0.55 mmol/L) [26] and Tween surfactants (0.01 to 0.025 mmol/L) [27]. This gives two important advantages of SSM over classical detergent micelles. Firstly, because of a lower concentration of monomers, PEGylated phospholipid monomers will interact significantly less with biologic membranes compared with the other surfactant monomers, resulting in lower toxicity. Second, on aqueous dilution, which is inevitable after intravenous injection, significantly lower numbers of micelles will be breaking to release the solubilized drug. Previous work in our laboratory using vasoactive intestinal peptide (5-μmol/L) associated SSM (DSPE-PEG2000 = 5 mmol/L) has shown that more than 90% of the peptide remained associated with SSM after 100-fold dilution [28]. If drug precipitation is still significant upon in vivo dilution after injection, then we propose to supplement CPT-SSM formulation with empty SSM based on our previous dilution work, so that these micelles can break first and reduce drug precipitation. Furthermore, SSM are composed of PEGylated phospholipids that have a proven favorable safety profile [14]. When the solubilizations of CPT in different surfactant micelles are compared at their safe concentrations for in vivo administration, it is seen that CPT aqueous solubility increased by 25-fold using SSM, 4-fold using Pluronic micelles [26], and 5-fold using Tween micelles [17]. Classical liposomes have been found to solubilize CPT to a greater extent in terms of drug-to-phospholipid molar ratio (CPT/total phospholipids = 0.025:1) [29]; however, they require more preparation steps compared with SSM [8,29,30]. Although the stability of CPT in liposomes has not been investigated, it is likely that CPT in bilayers may aggregate and precipitate upon storage, as demonstrated with another hydrophobic anticancer drug—paclitaxel—when associated with liposomes [31,32]. Phospholipid micelles do not show this phenomenon, most probably as a result of a lower number of drug molecules per micelle. Furthermore, the smaller size of micelles (in our study, CPT-SSM were ~14 nm) compared with liposomes (usually =50 nm) [33] allow more efficient extravasation from circulation and distribution of drugs throughout the tumor mass [30]. In contrast to liposomal incorporation of hydrophobic drugs that result in destabilization of the liposomal structure [34], micellar incorporation of poor water-soluble drugs do not cause any disruption of the micellar structure.

Aqueous stability of CPT-SSM

CPT lactone associated with SSM was more stable in the aqueous environment than CPT alone. CPT lactone concentration, expressed as a fraction to the initial concentration obtained 2 hours after preparation, was significantly reduced after 1 day (Figure 5, *a*). In contrast, there was stabilization of CPT lactone concentration when CPT was associated with SSM for at least 3 days after preparation. No significant fractional reduction in CPT concentration ($P > .05$) in the CPT-SSM aqueous systems was observed until 7 days after preparation. Greater chemical stability of CPT lactone when associated with SSM was attributed to the reduced tendency of CPT lactone to undergo hydrolytic conversion to its carboxylate form in the hydrophobic environment of the SSM. After 7 days, the fraction of CPT concentration remaining in the system was similar for CPT-SSM and free CPT. This can be attributed to phospholipid degradation after 7 days when stored at 25°C, resulting in fewer SSM for CPT solubilization, as well as CPT degradation. We confirmed by thin-layer chromatography that there was significant phospholipid degradation after 7 days in similar storage conditions (data not shown). There was no significant change in diameter, $\bar{d}_h$ of remaining CPT-SSM in the system up to 7 days after preparation (Figure 5, *b*). These results demonstrated that SSM had the potential to improve CPT aqueous stability for clinical application.

In vitro cytotoxicity

In vitro cytotoxicity of free CPT in 10% DMSO and CPT-SSM against MCF-7 cells was compared and illustrat-

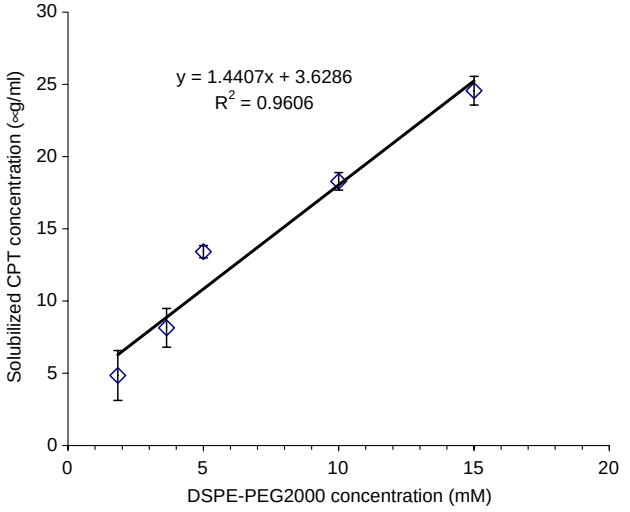

Fig 4. Effect of increasing DSPE-PEG2000 concentration on solubilized CPT concentration as CPT-SSM. Values are n = 3; error bars represent SD.

ed in Figure 6. There was no significant difference in ED_{50} values between free CPT and CPT-SSM after 24 hours of incubation ($P > .05$). CPT prolongs the lifetime of the DNA-topoisomerase I complex formed during DNA replication, and cells in the S-phase of the cell cycle with ongoing DNA synthesis have been reported to be more susceptible to the cytotoxic action of CPT [6]. After 24 hours of incubation, there was no difference in cytotoxicity between free CPT and CPT-SSM because the same fraction of cells in the S-phase were exposed to CPT. However, there was a significant 3-fold increase in CPT-SSM cytotoxicity against MCF-7 cells compared with free CPT after 96 hours of incubation ($P < .05$). This was attributed to greater CPT stability when associated with SSM than free CPT for cytotoxic action on the cells, as more cells entered the S-phase with incubation time. Optimal therapeutic efficacy of S-phase–specific drugs such as CPT generally requires prolonged exposure of the tumor cells to CPT concentrations exceeding a minimum cytotoxic threshold [6]. This conclusion is also supported by our aqueous stability data that CPT associated with SSM was more stable than free CPT, thus exerting greater in vitro cytotoxicity over time. Another possible explanation of the data can be greater cellular uptake of CPT by phagocytosis or by fusion processes of drug-containing phospholipid micelles. More work is being conducted in our laboratory to investigate the various mechanisms of cellular uptake of drug-containing SSM. The enhanced potency of CPT in SSM resulting from greater stability and cellular uptake confers greater advantages to applying CPT-SSM as a novel nanomedicine entity compared with free CPT.

Freeze-drying of CPT-SSM

The optimal CPT-SSM formulation was prepared using the initial CPT-DSPE-PEG2000 = 0.004:1 (DSPE-PEG2000 concentration = 15 mmol/L, CPT concentration =

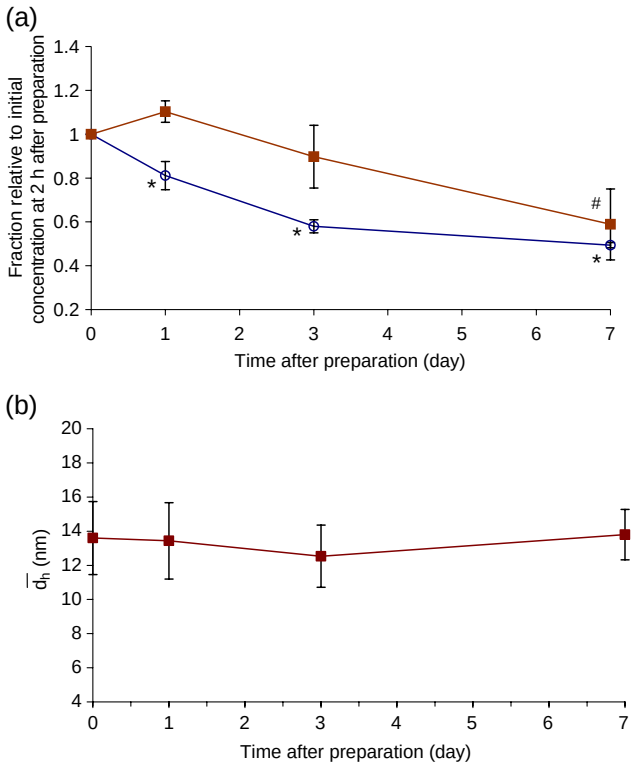

Fig 5. **a,** Fractional decrease in CPT lactone concentration with time, expressed relative to initial concentration achieved 2 hours after preparation. **b,** Mean hydrodynamic diameter ($\bar{d}_h$) of CPT-SSM with time. *Open circle,* CPT alone in buffer; *closed square,* CPT:DSPE-PEG2000 = 0.006:1; DSPE-PEG2000 concentration = 5 mmol/L. *Asterisk* and *pound sign* indicate significant difference from 2 hours after preparation (analysis of variance, $P < .05$). Values are n = 3; error bars represent SD.

20 μg/mL). This formulation solubilized a therapeutically relevant CPT concentration for future in vivo administration and was below the critical molar ratio of CPT/DSPE2000 = 0.0063:1 ± 0.0013:1, so that only a homogeneous population of CPT-SSM existed. Although we have shown here that short-term stability of CPT-SSM in aqueous media was satisfactory, because of the instability of lipids in aqueous media during long-term storage, we tested the lyophilization of this formulation. CPT-SSM formulation was lyophilized without any modification and no addition of lyoprotectants and cryoprotectants. CPT-SSM lyophilized cakes were elegant in appearance and of excellent bulk. The properties of CPT-SSM in terms of solubilized CPT concentrations, peak fluorescence emission wavelength, micelle size, and phospholipid concentration did not change significantly after freeze-drying and reconstitution (Table 1). These data indicated that CPT was incorporated or stayed in the same region of the micelles after freeze-drying and reconstitution. This can be attributed to PEGylated phospholipids playing the roles of lyoprotectant and cryoprotectant during freeze-drying as a result of their protective PEG chains. Polyethylene glycols (PEG) have been used as excipients to stabilize labile proteins during lyophilization [35]. Furthermore, PEGylated proteins exhibit greater

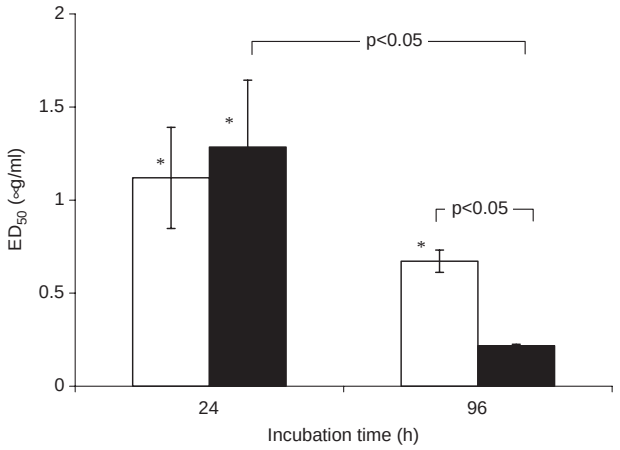

Fig 6. In vitro cytotoxicity of CPT in 10% DMSO *(open squares)* and CPT-SSM *(closed squares)* to MCF-7 cells after 24 and 96 hours of incubation. ED_{50} of empty SSM controls were >2 mg/mL. Values are means ± SDs; each group n = 4, experiments in triplicate. *Asterisk,* No significant difference ($P > .05$) was found between these groups.

stabilization during lyophilization [36]. To date, there has been no report on the controlled freeze-drying of PEGylated phospholipid nanomicelles. Therefore, our data on the successful lyophilization of CPT-SSM without any modification and additional excipients has important implications in the clinical development of these micellar delivery systems as novel nanomedicines.

Conclusions

We have prepared CPT in SSM to initiate the development of CPT-SSM as a novel nanomedicine entity. CPT was solubilized up to 25-fold more in SSM composed of PEGylated phospholipids than in buffer. The critical molar ratio of CPT/PEGylated lipid for CPT solubilization as a single, homogeneous CPT-SSM population of ~14 nm in diameter, without coexistence of lipid-coated, CPT self-aggregated particles, was 0.0063:1. CPT associated with SSM exhibited greater aqueous stability up to 3 days after preparation because of a reduced hydrolytic conversion of its active lactone to inactive carboxylate in the more hydrophobic environment of SSM. Similarly, CPT-SSM was 3-fold more cytotoxic than free CPT, which was attributed to the enhanced stability of CPT associated with SSM to act on the cells as they enter the S-phase of the cell cycle and/or another possible lipid-based delivery mechanism. CPT-SSM were successfully freeze-dried and reconstituted without drug modification or addition of lyoprotectants and cryoprotectants. Therefore, CPT-SSM could be stored with greater stability as lyophilized powder form and reconstituted before use. This has important implications in the clinical development of CPT-SSM. CPT-SSM has advantages as a nanomedicine because, unlike free CPT and other water-soluble CPT analogs that do not discriminate in their distribution to tumor and normal tissues, nanosized CPT-SSM is too big to pass through

Table 1
Properties of CPT-SSM (CPT:DSPE-PEG2000 = 0.004:1, 15 mmol/L DSPE-PEG2000) before and after freeze-drying/reconstitution[a]

Properties	Before freeze-drying Mean ± SD	After freeze-drying Mean ± SD
Solubilized CPT concentration (μg/ml)	21.1 ± 0.9	21.0 ± 0.4
Peak fluorescence emission wavelength (nm)	429.0 ± 1.0	429.3 ± 0.6
Micelle diameter (nm)	12.3 ± 0.3	11.7 ± 0.5
Phospholipid concentration (mm)	14.5 ± 0.4	14.6 ± 0.3

SD, standard deviation.
[a] For each group, n = 4 experiments; $p > 0.05$ for all comparisons.

normal vasculature. On the other hand, CPT-SSM is sufficiently small to extravasate in tumors because of tumor leaky microvasculature. This will result in accumulation of micelle solubilized drug in the tumor, avoiding the normal cells. Future studies will evaluate CPT-SSM for its in vivo performance. These include biodistribution, pharmacokinetics, efficacy, and safety studies in animal models.

Acknowledgments

Supported in part by a VA Merit Review grant, Department of Defense grant BCRP, No. DAMD 17-02-1-0415, and National Institutes of Health grants No. RO1 AG024026-01 and RO1 HI 72323-01. O. T. K. is a recipient of the UIC University Fellowship.

References

[1] Clements MK, Wasi S, Daoud SS. Camptothecin exhibits selective cytotoxicity towards human breast carcinoma as compared to normal bovine endothelial cells in vitro. Anticancer Drugs 1996; 7:851-7.
[2] Natelson EA, Giovanella BC, Verschragen CF, Fehir KM, De Ipolyi PD, Harris N, et al. Phase I clinical and pharmacological studies of 20-(S)-camptothecin and 20-(S)-9-nitrocamptothecin as anticancer agents. Ann N Y Acad Sci 1996;803:224-30.
[3] Gupta M, et al. Inactivation of p53 increases the cytotoxicity of camptothecin in human colon HCT116 and breast MCF-7 cancer cells. Clin Cancer Res 1997;3:1653-60.
[4] Oberlies NH, Kroll DJ. Camptothecin and taxol: historic achievements in natural products research. J Nat Products 2004;67:129-35.
[5] Redinbo MR, et al. Crystal structures of human topoisomerase I in covalent and noncovalent complexes with DNA. Science 1998;279: 1504-13.
[6] Garcia-Carbonero R, Supko JG. Current perspectives on the clinical experience, pharmacology, and continued development of the camptothecins. Clin Cancer Res 2002;8:641-61.
[7] Kehrer DF, et al. Modulation of camptothecin analogs in the treatment of cancer: a review. Anticancer Drugs 2001;12:89-105.
[8] Burke TG, et al. Lipid bilayer partitioning and stability of camptothecin drugs. Biochemistry 1993;32:5352-64.
[9] Schaeppi U, Fleischman RW, Cooney DA. Toxicity of camptothecin (NSC-100880). Cancer Chemother Rep 3 1974;5:25-36.
[10] Erickson-Miller CL, et al. Differential toxicity of camptothecin, topotecan and 9-aminocamptothecin to human, canine, and murine myeloid progenitors (CFU-GM) in vitro. Cancer Chemother Pharmacol 1997;39:467-72.

[11] Ashok B, et al. In vitro characterization of pegylated phospholipid micelles for improved drug solubilization: effects of peg chain length and PC incorporation. J Pharm Sci 2004;93:2476-87.
[12] Krishnadas A, Rubinstein I, Onyuksel H. Sterically stabilized phospholipid mixed micelles: in vitro evaluation as a novel carrier for water-insoluble drugs. Pharm Res 2003;20:297-302.
[13] Onyuksel H, et al. A novel formulation of VIP in sterically stabilized micelles amplifies vasodilation in vivo. Pharm Res 1999;16:155-60.
[14] Working PK, Dayan AD. Pharmacological-toxicological expert report—CAELYX (Stealth liposomal doxorubicin HCl). Hum Exp Toxicol 1996;15:751-85.
[15] Allen C, et al. Controlling the physical behavior and biological performance of liposome formulations through use of surface grafted poly(ethylene glycol). Biosci Rep 2002;22:225-50.
[16] Maeda H, et al. Vascular permeability enhancement in solid tumor: various factors, mechanisms involved and its implications. Int Immunopharmacol 2003;3:319-28.
[17] Cortesi R, et al. Formulation study for the antitumor drug camptothecin: liposomes, micellar solutions and a microemulsion. Int J Pharm 1997;159:95-103.
[18] Ertl B, et al. Poly(D,L-lactic-co-glycolic acid) microspheres for sustained delivery and stabilization of camptothecin. J Control Release 1999;61:305-17.
[19] Skehan P, et al. New colorimetric cytotoxicity assay for anticancer-drug screening. J Natl Cancer Inst 1990;82:1107-12.
[20] Papazisis KT, et al. Optimization of the sulforhodamine B colorimetric assay. J Immunol Methods 1997;208:151-8.
[21] Johnson RE, Kirchhoff CF, Gaud HT. Mannitol-sucrose mixtures — versatile formulations for protein lyophilization. J Pharmaceutical Sci 2002;91:914-22.
[22] Onyuksel H, et al. Interactions of VIP with rigid phospholipid bilayers: implications for vasoreactivity. Peptides 2003;24:281-6.
[23] Zhang L, et al. Camptothecin derivative-loaded poly(caprolactone-co-lactide)-b-PEG-b-poly(caprolactone-co-lactide) nanoparticles and their biodistribution in mice. J Control Release 2004;96:135-48.
[24] Nabiev I, et al. Spectroscopic and biochemical characterisation of self-aggregates formed by antitumor drugs of the camptothecin family: their possible role in the unique mode of drug action. Biochem. Pharmacol 1998;55:1163-74.
[25] Rabinow BE. Nanosuspensions in drug delivery. Nat Rev Drug Discovery 2004;3:785-96.
[26] Barreiro-Iglesias R, et al. Solubilization and stabilization of camptothecin in micellar solutions of pluronic-g-poly(acrylic acid) copolymers. J Control Release 2004;97:537-49.
[27] Mukerjee P, Mysels KJ. Critical Micelle Concentrations of Aqueous Surfactant Systems, vol. 36. Washington (DC): US National Bureau of Standards; 1971.
[28] Sethi V. Delivery of phospholipid-associated VIP for the effective treatment of rheumatoid arthritis [dissertation]. Chicago: University of Illinois; 2003. p. 81-5.
[29] Daoud SS, Fetouh MI, Giovanella BC. Antitumor effect of liposome-incorporated camptothecin in human malignant xenografts. Anticancer Drugs 1995;6:83-93.
[30] Tsukioka Y, et al. Pharmaceutical and biomedical differences between micellar doxorubicin (NK911) and liposomal doxorubicin (Doxil). Jpn J Cancer Res 2002;93:1145-53.
[31] Campbell RB, Balasubramanian SV, Straubinger RM. Influence of cationic lipids on the stability and membrane properties of paclitaxel-containing liposomes. J Pharmaceutical Sci 2001;90:1091-105.
[32] Zhao L, Feng SS, Go ML. Investigation of molecular interactions between paclitaxel and DPPC by Langmuir film balance and differential scanning calorimetry. J Pharmaceutical Sci 2004;93:86-98.
[33] Torchilin VP. PEG-based micelles as carriers of contrast agents for different imaging modalities. Adv Drug Deliv Rev 2002;54:235-52.
[34] Bernsdorff C, Reszka R, Winter R. Interaction of the anticancer agent Taxol (paclitaxel) with phospholipid bilayers. J Biomed Mater Res 1999;46:141-9.
[35] Mi Y, et al. Effects of polyethylene glycol molecular weight and concentration on lactate dehydrogenase activity in solution and after freeze-thawing. PDA J Pharm Sci Technol 2002;56:115-23.
[36] Heller MC, Carpenter JF, Randolph TW. Conformational stability of lyophilized PEGylated proteins in a phase-separating system. J Pharmaceutical Sci 1999;88:58-64.

Era of Hope 2005 Abstract

TC-99M LABELED AND VIP-RECEPTOR TARGETED LIPOSOMES FOR EFFECTIVE IMAGING OF BREAST CANCER

Hayat Onyuksel, Sumeet Dagar, Aparna Krishnadas, Israel Rubinstein, Marin Sekosan, Bao-Shiang Lee, Michael Blend
Affiliations: University of Illinois at Chicago, Chicago, IL 60612
primary author's e-mail address: hayat@uic.edu

Breast cancer is the second leading cause of death among women in USA. Early detection can significantly increase the chances of breast cancer survival. The goal of this research was to develop a targeted carrier system, incorporating a gamma emitting radiolabel, Tc-99m for enhanced imaging of breast cancer.

We developed long-circulating sterically-stabilized liposomes (SSL, diameter ~100nm), surface grafted with a peptide, vasoactive intestinal peptide (VIP, whose receptors are overexpressed in breast tumors), and incorporating a radiolabel, Tc99m, for gamma scintigraphic detection of breast tumors. The conjugation of VIP to pegylated phospholipid was confirmed by gel electrophoresis and bioactivity of conjugated-VIP confirmed by a hamster cheek-pouch model before insertion into preformed SSL to form SSL-VIP. Influence of VIP on the physical properties of Tc99m-SSL, such as size, radioactivity content and labeling efficiency, were also determined in the presence and absence of VIP. A carcinogen (MNU) induced rat breast cancer model was used for animal studies. The targetability of the developed targeted system (Tc99m-VIP-SSL) was tested in vitro on rat breast cancer tissues. In vivo experiments using this animal model were performed including, pharmacokinetics, biodistribution and imaging studies.

As demonstrated by gel electrophoresis, the conjugation reaction yielded predominantly the desired product (1:1 VIP: pegylated phospholipid conjugate). VIP retained its bioactivity post conjugation. Insertion of VIP-conjugate into Tc99m-SSL did not interfere with its physical properties. VIP-SSL bound significantly more to MNU-induced rat breast cancer tissue sections compared to SSL without VIP on the surface, indicating the targeting ability of VIP-SSL to breast cancer. Moreover this targeting was specific to VIP receptors as indicated by lack of binding in the presence of excess VIP. Pharmacokinetic (PK) data demonstrated that presence of VIP on SSL does not alter PK profile of SSL. In addition, VIP-SSL were long circulating with half-life of ~14 -16 h. Biodistribution data indicated that Tc99m-VIP-SSL accumulated significantly more in breast tumors (~6 times) by both passive and active targeting mechanisms. This increased accumulation with Tc99m-VIP-SSL resulted in significantly higher breast tumor image enhancement (tumor: background ratio ~6) as compared to Tc99m-SSL.

In conclusion, VIP was covalently attached to sterically stabilized liposomes for targeted delivery to breast cancer. VIP-SSL loaded with radionuclide, Tc-99m, was effectively used for the enhanced imaging of breast cancer. Conceivably, this research should lead to an improved modality for the detection of breast cancer with enhanced specificity and sensitivity. Clinical application of this novel detection mode should result in increased prognosis and survival rates amongst women with breast cancer.

The U.S. Army Medical Research and Material Command under DAMD17-02-1-0415 supported this work.

PGSRM2005

DELIVERY OF CAMPTOTHECIN IN NANOSIZED PEGYLATED PHOSPHOLIPID MICELLES TO TREAT MURINE COLLAGEN-INDUCED ARTHRITIS

Purpose: Camptothecin (CPT) causes cellular apoptosis by inhibiting the DNA-topoisomerase I complex. However, its clinical application is limited by poor solubility and instability in vivo. Previously, we have developed a novel formulation of CPT in PEGylated phospholipid-based sterically stabilized micelles (CPT-SSM) that increased drug solubilization and stability by 25-fold and 3-fold, respectively[1]. Rheumatoid arthritis (RA), a chronic debilitating autoimmune disorder, leads to disability and eventual death. Disease-modifying drugs (DMD) for RA are few and may cause serious adverse events. Hence, there is a need to develop new DMDs for RA. In the RA synovium, apoptosis of inflammatory cells is diminished appreciably, therefore, drugs promoting apoptosis of these cells could be beneficial in RA. In this study, we aim to deliver and test the *in vivo* efficacy as well as safety of CPT-SSM against RA using an established collagen-induced arthritis (CIA) mouse model.

Methods: CIA was induced in DBA/1 mice by 2 collagen injections (0.2 mg) given on Day 0 and 21. CPT-SSM (0.3 mg/kg) was administered *i.v.* or *s.c.* on Day 28 at the onset of arthritic symptoms. Efficacy was monitored by paw thickness, clinical arthritic score and histological analysis of hind limb joints. Toxicity was measured by loss in body weight, complete blood count and histological analysis of major organs at the end of the study (Day 60).

Results: A single 10-fold lower dose of CPT-SSM than that used for chemotherapy, reduced paw thickness (up to 20 %) and clinical arthritic score (up to 48 %) significantly, when compared to untreated mice regardless of injection route ($p>0.05$). Free CPT and methotrexate was not as effective in reversing CIA symptoms. This can be attributed to targeting of CPT to the inflamed joints when delivered in SSM. Paw histology indicated no joint damage in CPT-SSM treated mice. Normal blood counts and tissue histology, as well as no significant weight loss indicated that CPT-SSM treated mice did not experience toxicity.

Conclusions: CPT delivered in SSM was efficacious and safe in mice with CIA. We suggest that CPT-SSM can be a novel DMD for RA

[1]Koo et al, *Nanomedicine* 1:77-84 (2005). Supported by UIC Fellowship, NIHR01AG024026-01, NIHR01HI72323-01, DMAD17-02-1-0415, VA Merit Grant.

ACR 2005

Sterically stabilized phospholipid micellar human vasoactive intestinal peptide: a novel disease-modifying drug for rheumatoid arthritis

Category: 18 RA treatment – biologics and gene therapy: treatment of human rheumatoid arthritis including biologics and gene therapy approaches

Hayat Önyüksel, Otilia M. Koo, Varun Sethi, Israel Rubinstein
University of Illinois at Chicago

Statement of Purpose: Few disease-modifying drugs (DMDs) are presently available to treat rheumatoid arthritis (RA) and their prolonged use is associated with serious adverse events. Hence, there is an urgent need to develop and test new DMDs for RA. To this end, human vasoactive intestinal peptide (VIP), a pleiotropic 28-amino acid biological response modifier, expresses potent immunomodulatory and anti-inflammatory effects in mice with collagen-induced arthritis (CIA). However, relatively high doses of naked VIP are required because of the short half-life (<5 min) of the peptide. This, in turn, elicits a precipitous reduction in systemic arterial pressure thereby hampering the use of VIP in clinical practice. We have shown that spontaneous association of VIP with biocompatible and biodegradable sterically stabilized phospholipid micelles (SSM) prolongs the half-life of the peptide in the systemic circulation for several hours and amplifies its bioactivity. The purpose of this study was to harness these unique properties of micellar VIP to clinical practice by determining its effects in mice with CIA.

Methods: Micellar VIP, naked VIP (each, 0.5&5 nmol) and empty micelles were administered *i.v.* to mice with CIA 22 days after primary immunization. Untreated mice served as controls. Hind paw joint inflammation was determined histologically and radiographically by a blinded investigator. Histopathological changes were scored on a scale of 0–30. Radiolographical changes were graded from 0 to 3. Serum levels of TNF-α, IL-1, IL-4, IL-10, MMP-2 and MMP-9 were determined by ELISA 60 days post-immunization.

Summary of results: Micellar VIP, but not naked VIP, abrogated CIA in mice. Hind paw histopathology and radiolographical scores of mice treated with micellar VIP (0.5 nmol) were 8.6 ± 1.1 and 2.0 ± 0.4, respectively (means ± SEM), and were similar to those in normal mice (10.6 ± 2.2 and 1.4 ± 0.5, respectively)(each group, n=4 animals; $p>0.5$). Only a 10-fold higher dose of naked VIP (5 nmol) evoked similar responses. Levels of circulating TNF-α, IL-1, MMP-2 and MMP-9 were significantly reduced in mice with CIA treated with 0.5 nmol micellar VIP in comparison to naked VIP ($p<0.05$). Importantly, IL-10 and IL-4 levels were significantly increased in mice with CIA treated with micellar VIP in comparison to naked VIP (each, 0.5 nmol; $p<0.05$). Empty micelles had no significant effects on arthritis endpoints and circulating mediators.

Conclusions: Biocompatible and biodegradable sterically stabilized phospholipid micellar human VIP abrogates CIA in mice. These salutary effects are observed at a 10-fold lower dose than that of naked VIP and are related, in part, to downregulation of pro-inflammatory mediators and up-regulation of anti-inflammatory cytokines. We suggest that micellar VIP is a novel DMD for RA.

Supported by R01AG024026, R01HL72323, DMAD17-02-1-0415 & VA Merit Review

Appendix (8) 2005 AAPS Annual Meeting and Exposition, Nashville, Tennessee

Camptothecin in Sterically Stabilized Phospholipid Micelles: A Novel Nanomedicine for Rheumatoid Arthritis

O. Koo, I. Rubinstein, H. Onyuksel

Biopharmaceutical Sciences, University of Illinois at Chicago

Purpose: Rheumatoid arthritis (RA), a chronic debilitating autoimmune disorder, leads to disability and eventual death. Disease-modifying drugs (DMD) for RA are few and may cause serious adverse events. Hence, there is a need to develop new DMDs for RA. In the RA synovium, apoptosis of inflammatory cells is diminished appreciably. Therefore, drugs promoting apoptosis of these cells could be beneficial in RA. Previously, we have developed a novel formulation of a proapoptotic drug, camptothecin (CPT) in PEGylated phospholipid-based sterically stabilized micelles (CPT-SSM) that increased drug solubilization and stability by 25-fold and 3-fold, respectively[1]. The aim of this study was to test the efficacy and safety of CPT-SSM in mice with collagen-induced arthritis (CIA). Methods: CPT-SSM was prepared by co-precipitation/reconstitution[1]. CIA was induced in DBA/1 mice by collagen (0.2 mg) injections on Day 0 and 21. Treatment was given on Day 28. Efficacy was monitored by paw thickness, clinical arthritis score and joint histology. Toxicity was measured by body weight, complete blood count and tissue histology. Results: CPT-SSM ($\geq$ 0.3 mg/kg) reduced paw thickness and clinical score to normal values within 4 days. A 3-fold greater free CPT dose was required for the same efficacy, and the action was delayed (after 10 days) and shorter lasting. Methotrexate (10 mg/kg) was only effective in preventing further deterioration of symptoms but did not reverse CIA. Unlike CPT-SSM treated animals with normal bone marrow and liver histologies, free CPT caused damage to these tissues. This was most probably due to selective extravasation of nanosized CPT-SSM through leaky vasculature of inflamed sites, avoiding normal tissues. Conclusions: CPT-SSM was more efficacious and safer than free CPT and methotrexate in CIA. We suggest that CPT-SSM is a novel DMD in RA.

Supported by UIC Fellowship, NIHR01AG024026-01, NIHR01HI72323-01, DMAD17-02-1-0415, VA Merit Grant.

[1]Koo et al, *Nanomedicine* 1:77-84 (2005)

Appendix (9)

S51
Targeted drug delivery using nanotechnology

H. Onyuksel

Director of Lipid Based Drug Delivery Laboratory, Department of Biopharmaceutical Sciences, University of Illinois, College of Pharmacy, Chicago, IL, USA

Delivery of drugs directly to the site of action is very desirable due to decreased side effects, increased efficiency and cost-effectiveness. Recently, we have developed an innovative technology that can deliver drugs to specifically diseased tissues with the use of a targeted nanocarrier. The nanocarrier is the self-assembly of biocompatible/biodegradable, polyethylene glycol conjugated phospholipid which we call as sterically stabilized micelle (SSM). Targeting agent, vasoactive intestinal peptide (VIP), is attached on the surface of the carrier to make it specific to VIP-receptors overexpressed in cancer and inflamed tissues. The size of the targeted drug carrier is 15 nm, which is too big to extravasate at the normal vasculature, but small enough to extravasate easily at the leaky vasculature of cancerous or inflamed tissues. Therefore drugs, encapsulated in SSM can accumulate at the diseased tissue by passive targeting due to nanotechnology and can interact with cells expressing VIP-R for active targeting. Since VIP-Rs do not express in the vasculature, VIP-SSM can only deliver its load to the diseased tissues after extravasating and interacting *in vivo* with VIP-R. Using a carcinogen induced rat breast cancer model, we have shown that paclitaxel (P) loaded sterically stabilized mixed micelles (SSMM) both with and without VIP on their surface, showed significantly higher anti-cancer activity than Taxol, the commercial product of paclitaxel currently used in the clinics. Our biodistribution data showed that paclitaxel accumulated significantly more in breast tumors and less in bone marrow and liver when administered as P-VIP-SSMM compared to Taxol, indicating significant decrease in drug toxicity to healthy organs. In another study using collagen induced mice rheumatoid arthritis model, we have shown that camptothecin (C) encapsulated in VIP-SSM is targeted to inflamed tissues of the joints and showed the same extent of anti-arthritic effect as free camptothecin at one tenth of the dose. We conclude that P-VIP-SSMM and C-VIP-SMM are promising nanomedicines of the future to treat breast cancer and rheumatoid arthritis. Funding: DAMD 17-02-1-0415, R01AG024026-01, VA Merit Review grant.

S52
Nanoconjugate based on polymalic acid for tumor treatment

M. Fujita[a], E. Holler[b,c], N. Khazenzon[a], K. Black[a,c], J. Ljubimova[a,c]

[a]*Cedar-Cinai Medical Center, Los Angeles, USA*
[b]*Universitat Regensburg, Regensburg, Germany*
[c]*Arrogene, Inc., Tarzana, CA*

A new prototype of drug delivery system, the nanoconjugate Polycefin, was tested for its ability to show tumor accumulation due to enhanced permeability and retention (EPR) effect and receptor mediated endocytosis. Polycefin was synthesized for targeted delivery of Morpholino oligonucleotides and antibodies into certain tumors, and consists of modules active in endosomal uptake, disruption of endosomal membranes, oligonucleotide release in the cytoplasm and protection against enzymatic degradation in the vascular system. These are covalently conjugated with polymalic acid (M_w 50,000, M_w/M_n 1.3) highly purified from cultures of myxomycete *Physarum polycephalum*. The polymer is biodegradable, non-immunogenic and non-toxic. Alexa Fluor 680 C2-maleimide was coupled to the polymer for the drug *in vivo* detection. MDA-MB 468 human breast cancer cells were injected subcutaneously into the left posterior mid-dorsum and human glioma cell line U87 MG intracranially inoculated into nude mice. Polycefin at concentration of 2.5 mg/kg was injected via the tail vein. *In vivo* fluorescence tumor imaging was performed at different time points, 0–180 min up to 48 h after the drug injection. The macro-illumination (MISTY) and Xenogen 200 imaging systems were used to study the drug accumulation *in vivo* in breast and brain tumor bearing animals. In breast tumors the fluorescence signal in large blood vessels and in the tumor increased rapidly until 60 min and remained at a level six times higher in the tumor, than in surrounding tissue (180 min) ($p < 0.003$). In brain tumors the drug accumulated selectively in the tumor in 24 h with the signal undetectable in the non-tumor surrounding area. The results of imaging were corroborated histologically by fluorescence microscopy, examining of various organs and only the tumor, kidney and liver were positive for fluorescent signals. Drug treatment significantly reduced the tumor angiogenesis and prolonged the survival of tumor-bearing animals. In the toxicity study, no animals showed clinical abnormalities after multiple administration of drugs.

Appendix (10)

Available online at www.sciencedirect.com
SCIENCE DIRECT®
ELSEVIER
International Journal of Pharmaceutics 316 (2006) 144–147
INTERNATIONAL JOURNAL OF PHARMACEUTICS
www.elsevier.com/locate/ijpharm

Pharmaceutical Nanotechnology

Intratracheal and subcutaneous liposomal VIP normalizes arterial pressure in spontaneously hypertensive hamsters

Israel Rubinstein [a,b,d,*], Hiroyuki Ikezaki [a,d], Hayat Önyüksel [b,c]

[a] *Department of Medicine (M/C 719), University of Illinois at Chicago, 840 South Wood Street, Chicago, IL 60612-7323, United States*
[b] *Department of Biopharmaceutical Sciences, University of Illinois at Chicago, Chicago, IL 60612, United States*
[c] *Department of Bioengineering, University of Illinois at Chicago, Chicago, IL 60612, United States*
[d] *Jesse Brown VA Medical Center, Chicago, IL 60612, United States*

Received 14 October 2005; received in revised form 14 February 2006; accepted 15 February 2006
Available online 6 March 2006

Abstract

We determined whether a single intratracheal and subcutaneous administration of biocompatible and biodegradable vasoactive intestinal peptide self-associated with sterically stabilized liposomes (VIP-SSL) normalizes mean arterial pressure (MAP) in spontaneously hypertensive hamsters (SHH). We found that VIP-SSL (0.1 nmol) administered by either routes normalizes MAP ($p < 0.05$). Maximal effect was observed within 10–20 min and lasted for 6 h. VIP-SSL had no significant effects on heart rate. VIP alone (0.1 nmol) and empty SSL had no significant effects on MAP. VIP-SSL (0.1 nmol) had no significant effects on MAP and heart rate in age/genetically-matched control hamsters. Given these data, we suggest that pulmonary and subcutaneous delivery of VIP-SSL should be further developed as peptide nanomedicine for essential hypertension.

Keywords: Formulation; Drug delivery; DSPE-PEG; Sterically stabilized liposomes

Despite recent advances in medical therapeutics, essential hypertension still represents an unmet medical need (Cosentino and Volpe, 2005). Hence, there is an ongoing need to develop and test new drugs to treat this condition (Henning and Sawmiller, 2001). To this end, we sought to determine whether a single intratracheal and subcutaneous administration of self-associated VIP with biocompatible and biodegradable sterically stabilized liposomes (VIP-SSL) normalizes systemic arterial pressure in spontaneously hypertensive hamsters.

Egg yolk phosphatidylcholine, egg yolk phosphatidylglycerol, cholesterol and polyethylene glycol (molecular mass, 1,900) grafted to distearoyl-phosphatidylethanolamine (molar ratio, 5:1:3.5:0.5; total phospholipid content, 17 mmol) were mixed and dissolved in chloroform as previously described in our laboratory (Séjourné et al., 1997). The solvent was evaporated at 45 °C in a rotary evaporator followed by vacuum drying overnight. The dry lipid film was then hydrated in 250 μl saline, vortexed, bath-sonicated for 5 min and extruded through stacked polycarbonate filters (pore size, 200, 100, 50 nm). Human VIP (0.4 mg) was added to the extruded suspension which was then frozen in acetone-dry ice bath and lyophilized overnight at −46 °C under constant pressure. Thereafter, the lyophilized "cake" was resuspended in 250 μl deionized water. VIP associated with SSL was separated from free VIP by column chromatography and stored at 4 °C for up to 15 days. Size of SSL was 250 ± 10 nm (mean ± S.D.). VIP/phospholipids mole ratio in the formulation was 0.004.

Adult male hamsters with spontaneous hypertension and age/genetically-matched normotensive hamsters (120–140 g body weight) were anesthetized with pentobarbital sodium (6 mg/100 g body weight, i.p.) (Séjourné et al., 1997). A tracheostomy was performed to facilitate spontaneous breathing and for drug administration. A femoral vein was cannulated to inject supplemental anesthesia during the experiment (2–4 mg/100 g body weight/h) and saline. A femoral artery was cannulated to record systemic arterial blood pressure and heart rate. Body temperature was monitored and kept constant (37–38 °C) throughout the experiment using a heating pad. Arterial blood pressure and heart rate were recorded continuously during the experiment using a pressure transducer and a strip-chart recorder. Mean arterial pressure (MAP) was calculated as diastolic pressure plus one-third pulse pressure.

* Corresponding author. Tel.: +1 312 996 8039; fax: +1 312 996 4665.
E-mail address: IRubinst@uic.edu (I. Rubinstein).

0378-5173/$ – see front matter © 2006 Elsevier B.V. All rights reserved.
doi:10.1016/j.ijpharm.2006.02.028

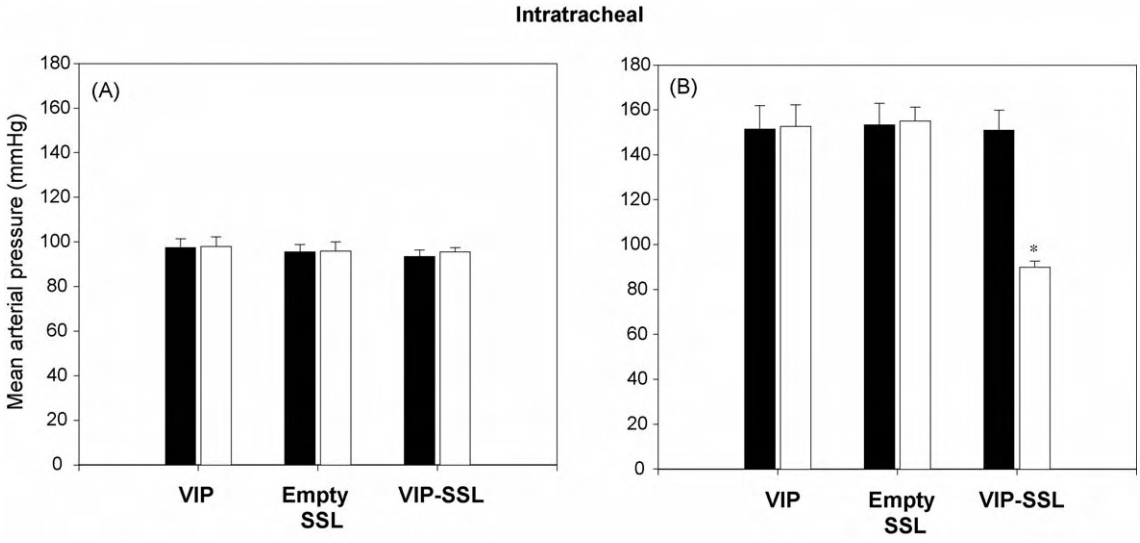

Fig. 1. Effects of a single intratracheal administration of self-associated VIP with sterically stabilized liposomes (VIP-SSL), VIP alone (each, 0.1 nmol) and empty SSL on mean arterial pressure in control hamsters (A) and spontaneously hypertensive hamsters (B). Closed bars, baseline; open bars, conclusion of the 6-h observation period. Data are means ± S.D. Each group, $n = 4$ animals; $p < 0.05$ in comparison to baseline.

VIP-SSL, VIP alone (each, 0.1 nmol) or empty SSL diluted in phosphate-buffered saline (final volume, 1.0 ml) was injected intratracheally through a PE-90 tubing inserted into the tracheostomy tube of hamsters followed by 1.0 ml room air at a rate of 1.0 ml/min using an infusion pump. MAP and heart rate were recorded before and for 6 h after administration of drugs. This time point was chosen because it conforms to rodent welfare guidelines during general anesthesia.

VIP-SSL, VIP alone (each, 0.1 nmol) or empty SSL diluted in phosphate-buffered saline (final volume, 0.25 ml) was injected subcutaneously at the inter-scapular region of hamsters over 1 min using an infusion pump. MAP and heart rate were recorded in before and for 6 h after administration of drugs as outlined above.

Data are expressed as means ± S.D. Statistical analysis was performed using ANOVA and Neuman–Keuls test. A $p < 0.05$ was considered statistically significant.

Intratracheal VIP-SSL, VIP alone (each, 0.1 nmol) and empty SSL had no significant effects on MAP and heart rate in normotensive hamsters (Figs. 1A and 2A; $p > 0.5$). By contrast, intratracheal VIP-SSL elicited a significant decrease in MAP in hypertensive hamsters that was observed within 10 min and lasted for 6 h (Fig. 1B; $p < 0.05$). Intratracheal VIP-SSL (0.1 nmol) had no significant effects on heart rate (Fig. 2B; $p > 0.5$). Intratracheal VIP alone (0.1 nmol) and empty SSL had no significant effects on MAP and heart rate in hypertensive hamsters (Figs. 1B and 2B; $p > 0.5$).

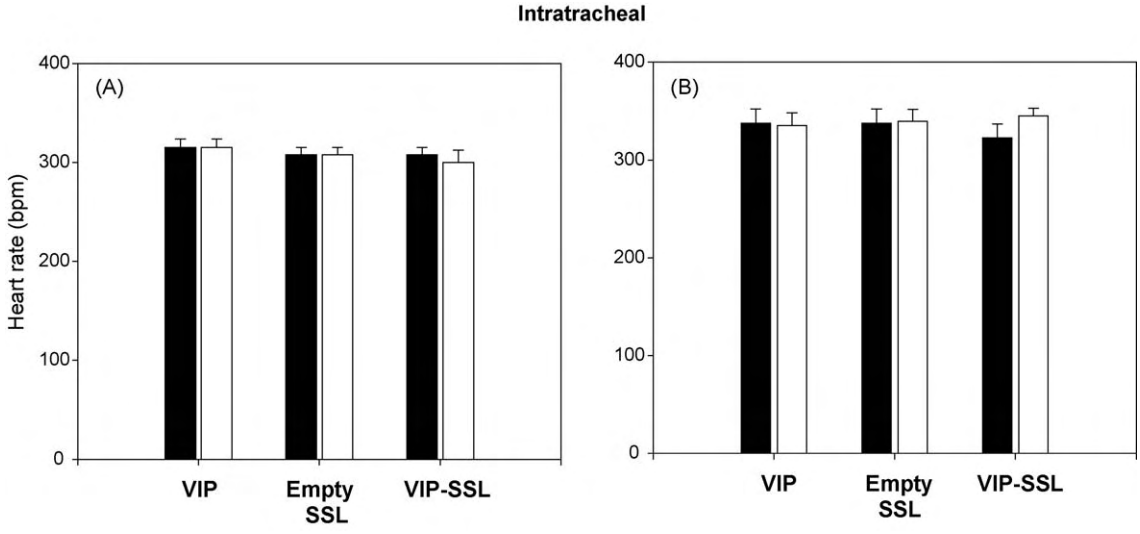

Fig. 2. Effects of a single intratracheal administration of self-associated VIP with sterically stabilized liposomes (VIP-SSL), VIP alone (each, 0.1 nmol) and empty SSL on heart rate in control hamsters (A) and spontaneously hypertensive hamsters (B). Closed bars, baseline; open bars, conclusion of the 6-h observation period. Data are means ± S.D. Each group, $n = 4$ animals.

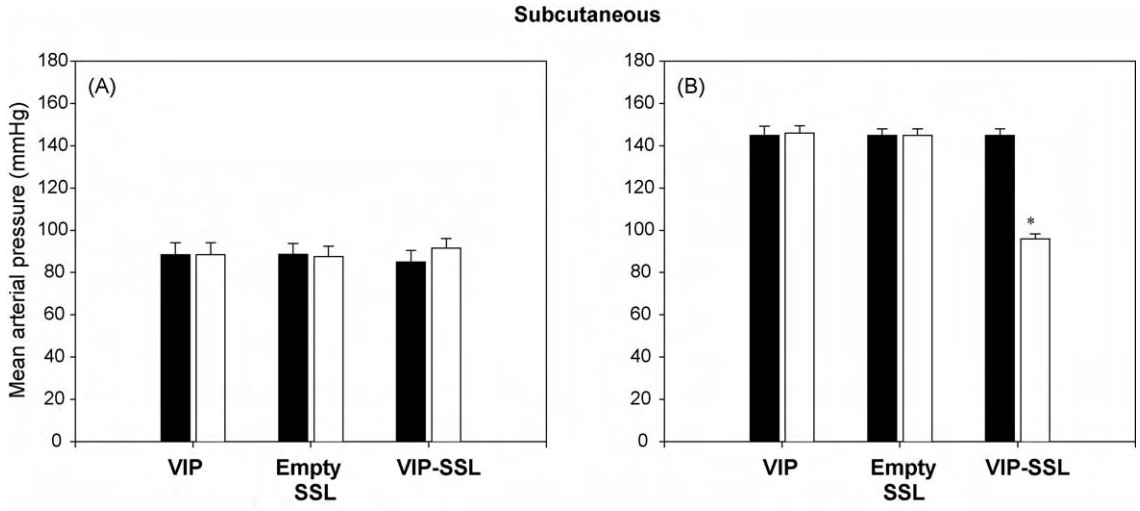

Fig. 3. Effects of a single subcutaneous administration of self-associated VIP with sterically stabilized liposomes (VIP-SSL), VIP alone (each, 0.1 nmol) and empty SSL on mean arterial pressure in control hamsters (A) and spontaneously hypertensive hamsters (B). Closed bars, baseline; open bars, conclusion of the 6-h observation period. Data are means ± S.D. Each group, $n = 4$ animals; $p < 0.05$ in comparison to baseline.

Subcutaneous VIP-SSL, VIP alone (each, 0.1 nmol) and empty SSL had no significant effects on MAP and heart rate in normotensive hamsters (Figs. 3A and 4A; $p > 0.5$). By contrast, subcutaneous VIP-SSL elicited a significant decrease in MAP in hypertensive hamsters that was observed within 20 min and lasted for 6 h (Fig. 3B; $p < 0.05$). Subcutaneous VIP-SSL (0.1 nmol) had no significant effects on heart (Fig. 4B; $p > 0.5$). Subcutaneous VIP alone (0.1 nmol) and empty SSL had no significant effects on MAP and heart rate in hypertensive hamsters (Figs. 3B and 4B; $p > 0.5$).

The new finding of this study is that a single, low-dose intratracheal and subcutaneous administration of biocompatible and biodegradable VIP-SSL normalizes MAP in spontaneously hypertensive hamsters for 6 h. The onset of VIP-SSL-induced responses was within 10–20 min with no further decline in MAP observed once the normative range was reached. VIP-SSL had no significant effects on heart rate suggesting its salutary effects are not related to depressed cardiac function. Importantly, VIP-SSL had no significant effects on MAP and heart rate in normotensive hamsters implying its effects are selective.

The onset of action, magnitude and duration of VIP-SSL-induced responses in spontaneously hypertensive hamsters were similar whether the drug was administered intratracheally or subcutaneously. This implies that liposomal VIP is absorbed rapidly and, most likely, intact from the lung and subcutaneous tissue into the systemic circulation where it evades degradation and uptake by the reticuloendothelial system (Suzuki et al., 1996; Séjourné et al., 1997; Gololobov et al., 1998). This, in turn, improves VIP bioavailability and amplifies its vasoactive effects over a prolonged period of time (Séjourné et al., 1997; Gololobov et al., 1998). Due to its relatively large size (~250 nm), liposomal VIP does not extravasate through the intact resistant arteriolar

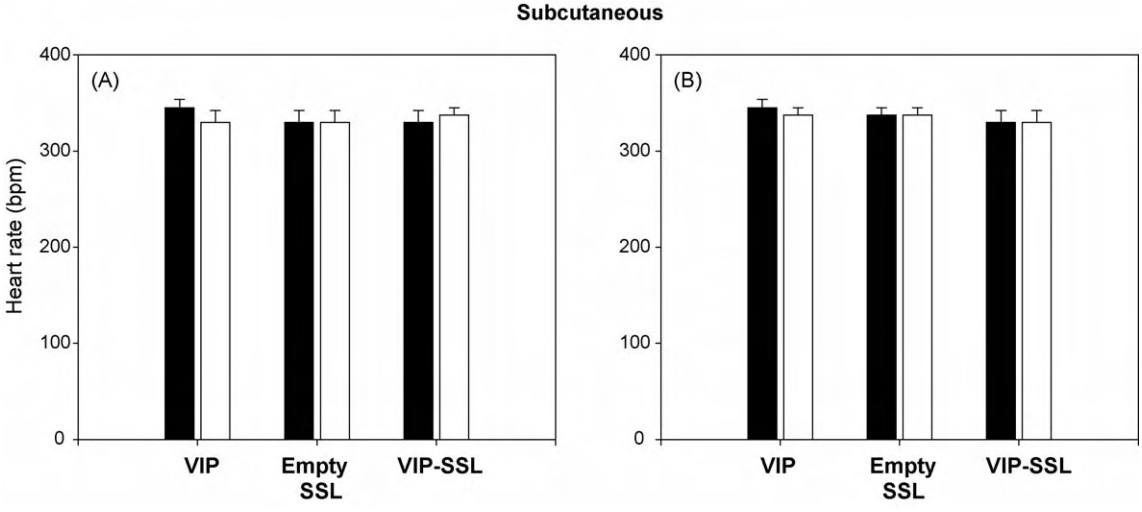

Fig. 4. Effects of a single subcutaneous administration of self-associated VIP with sterically stabilized liposomes (VIP-SSL), VIP alone (each, 0.1 nmol) and empty SSL on heart rate in control hamsters (A) and spontaneously hypertensive hamsters (B). Closed bars, baseline; open bars, conclusion of the 6-h observation period. Data are means ± S.D. Each group, $n = 4$ animals.

wall in normotensive hamsters thereby mitigating its vasorelaxant effects.

In summary, a single intratracheal and subcutaneous administration of low-dose, long-circulating biocompatible and biodegradable liposomal formulation of VIP normalizes MAP in spontaneously hypertensive hamsters for several hours. We suggest that pulmonary and subcutaneous delivery of VIP-SSL should be further developed as peptide nanomedicine for essential hypertension.

Acknowledgement

This study was supported, in part, by NIH grants RO1 AG024026 and RO1 HL72343, VA Merit Review and Department of Defense grant.

References

Cosentino, F., Volpe, M., 2005. Hypertension, stroke, and endothelium. Curr. Hypertens. Res. 7, 68–71.

Gololobov, G., Noda, Y., Sherman, S., Rubinstein, I., Baranowska-Kortylewicz, J., Paul, S., 1998. Stabilization of vasoactive intestinal peptide by lipids. J. Pharmacol. Exp. Ther. 285, 753–758.

Henning, R.J., Sawmiller, D.R., 2001. Vasoactive intestinal peptide: cardiovascular effects. Cardiovasc. Res. 49, 27–37.

Séjourné, F., Rubinstein, I., Suzuki, H., Alkan-Önyüksel, H., 1997. Development of a novel bioactive formulation of vasoactive intestinal peptide in sterically stabilized liposomes. Pharm. Res. 14, 362–365.

Suzuki, H., Noda, Y., Gao, X.-p., Séjourné, F., Alkan-Önyüksel, H., Paul, P., Rubinstein, I., 1996. Encapsulation of vasoactive intestinal peptide into liposomes restores vasorelaxation in hypertension in situ. Am. J. Physiol. 271, H282–H287.

available at www.sciencedirect.com

SCIENCE DIRECT®

journal homepage: www.elsevier.com/locate/peptides

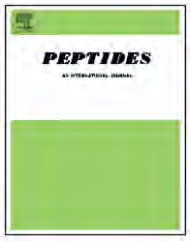

PEGylated phospholipid nanomicelles interact with β-amyloid$_{(1–42)}$ and mitigate its β-sheet formation, aggregation and neurotoxicity in vitro

Ashwini S. Pai [a], *Israel Rubinstein* [a,b,d], *Hayat Önyüksel* [a,c,*]

[a] *Department of Biopharmaceutical Sciences, University of Illinois at Chicago, Chicago, IL 60612, USA*
[b] *Department of Medicine, University of Illinois at Chicago, Chicago, IL 60612, USA*
[c] *Department of Bioengineering, University of Illinois at Chicago, Chicago, IL 60612, USA*
[d] *Jesse Brown VA Medical Center, Chicago, IL 60612, USA*

ARTICLE INFO

Article history:
Received 10 March 2006
Received in revised form
18 April 2006
Accepted 19 April 2006

Keywords:
β-Amyloid aggregation
Alzheimer's disease
DSPE-PEG$_{2000}$
PEGylated phospholipid
Nanomicelles
SHSY-5Y cells
Nanomedicine

Abbreviations:
AD, Alzheimer's disease
APP, amyloid precursor protein
Aβ, beta-amyloid
CD, circular dichroism
CMC, critical micellar concentration
CR, Congo red
DSPE-PEG$_{2000}$, 1,2-distearoyl-*sn*-glycero-3-phosphoethanolamine-*N*-methoxy-poly (ethylene glycol 2000)
EM, electron microscopy

ABSTRACT

β-Amyloid (Aβ) is a hydrophobic peptide that drives the pathogenesis of Alzheimer's disease (AD) due to its aberrant aggregation. Inhibition of Aβ aggregation process is one of the most promising strategies for therapeutic intervention in AD. Here, we demonstrate that sterically stabilized (PEGylated) phospholipid nanomicelles (SSM) are effective in mitigating Aβ-42 aggregation using several deterministic techniques such as (1) Turbidimetry (2) Congo red binding (3) Thioflavine-T binding (4) Laser light scattering and (5) Electron Microscopy. α-Helicity of Aβ-42 is significantly augmented in the presence of SSM as demonstrated by circular dichroism ($p < 0.05$). Cytotoxicity studies, employing human neuroblastoma SHSY-5Y cells, established that PEGylated phospholipid associated peptide demonstrated significantly lower neurotoxicity compared to lipid untreated Aβ-42 ($p < 0.05$). Collectively, our results establish that PEGylated phospholipids abrogate transformation of Aβ-42 to amyloidogenic β-sheeted form and impart neuroprotection in vitro. This study provides a foundation for designing nanoconstructs of PEGylated phospholipid nanomicelles in conjunction with a therapeutic agent for multitargeting the different pathophysiologies associated with AD.

* *Corresponding author at*: Department of Biopharmaceutical Sciences (M/C 865), College of Pharmacy, University of Illinois at Chicago, 833 S. Wood Street, Chicago, IL 60612-7231, USA. Tel.: +1 312 996 2097; fax: +1 312 996 0098.
E-mail address: hayat@uic.edu (H. Önyüksel).

0196-9781/$ – see front matter © 2006 Elsevier Inc. All rights reserved.
doi:10.1016/j.peptides.2006.04.022

MTS, 3-(4,5-dimethylthiazol-2-yl)-5-(3-carboxymethoxyphenyl)-2-(4-sulfophenyl)-2H-tetrazolium
SDS, sodium dodecyl sulfate
SSM, sterically stabilized micelles
ThT, thioflavine-T

1. Introduction

β-Amyloid (Aβ) is a hydrophobic peptide responsible for the development of extracellular neuritic plaques in the brain which are a classical hallmark of Alzheimer's disease (AD). Biochemical and genetic reports have implicated these plaques in the pathophysiological process of AD [23]. A key component of the senile neuritic plaque is a central core containing variants of a 38–43 amino acid peptide commonly referred to as β-amyloid (Aβ) due to its high pre-disposition to form β-sheets [16]. Altered proteolytic processing and sequential cleavage of transmembrane amyloid precursor protein (APP) by secretase enzymes result in formation of small Aβ fragments (~4 kDa) of different lengths, primarily 40 (Aβ-40) and 42 (Aβ-42) residues. These fragments agglomerate to form a cascade of intermediate species (including oligomers and protofibrils) which finally culminate in the development of neurotoxic amorphous β-sheeted fibrillar aggregates [8,15,24]. Although development and progression of AD is characterized by multiple pathogenic events that include neurofibrillary tangles, neuroinflammation and genetic mutations [23,26], there is compelling evidence implicating Aβ-42 aggregation as a pivotal player in the etiology of AD [9]. This canonical view of attributing Aβ as the key player in AD etiology, often referred to as the *Amyloid Hypothesis*, has received almost unanimous acceptance over the last two decades. Several researchers advocate mechanism based therapeutic approaches that target the amyloid cascade through inhibition and clearance of Aβ aggregates. Along these lines, Tramiprosate (ALZHEMED™), an Aβ fibrillogenesis inhibitor has entered Phase III clinical testing in US and Canada [7]. We believe that AD progression can be slowed down significantly if aggregation and transformation of Aβ from a monomeric soluble α-helical form to an insoluble amyloidogenic β-sheeted conformation is inhibited.

When located as an element of APP in the transmembrane region of the cell bilayer, Aβ exhibits non-amyloidogenic α-helical conformation [22]. Aβ aggregation, in part, can be attributed to the loss of this structural context (provided by cell bilayer) on secretase mediated APP cleavage. To this effect, it has been observed that Aβ-42 also exhibits a significant amount of α-helical character in membrane mimicking environments [13]. For example, it has been shown that several hydrophobic proteins and peptides penetrate into the hydrophobic core of sodium dodecyl sulfate (SDS) micelles and adopt α-helical conformation [18,19,31]. However, therapeutic utilization of such membrane mimicking surfactants is greatly limited by their relatively high critical micelle concentration (CMC) and undue toxicity. We have previously demonstrated that several amphiphilic peptides associate with biocompatible and biodegradable nanosized PEGylated phospholipid nanomicelles and change their conformation to α-helix resulting in increased stability and bioactivity [6,29]. PEGylated phospholipid nanomicelles provide a hydrophobic milieu amenable to confine Aβ-42 in non-amyloidogenic α-helix conformation thereby attenuating its aggregation potential.

Sterically stabilized phospholipid nanomicelles (SSM) are formed spontaneously and reproducibly in aqueous environments when polyethylene glycol (PEG) grafted (PEGylated) diacyl lipids are present at super critical micelle concentrations. Steric stabilization refers to the attachment of PEG polymer to phospholipid head groups which renders the micelle "stealth" by providing a physico-mechanical barrier and preventing complement opsonization and liver sequestration [17]. SSM overcome the limitations of conventional detergent micelles due to their much lower CMC (μM versus mM range), hence offering an attractive safety profile [2,17]. DSPE-PEG_{2000} (1,2-distearoyl-*sn*-glycero-3-phosphoethanolamine-*N*-methoxy-poly(ethylene glycol 2000)) that we used in this study is already approved for use in humans by the FDA, albeit for different indications.

The aim of this study was to investigate the biophysical effect of biocompatible nanosized (~14 nm) PEGylated phospholipid nanomicelles on the secondary structure of Aβ-42, its aggregation behavior and neurotoxicity in order to explore their potential as a therapeutic aid for intervention in the *Amyloid Cascade*. We chose to study Aβ-42 fragment amongst several other variants since biochemical analysis of the amyloid plaque demonstrated that Aβ-42 aggregated more rapidly [20] and was responsible for seeding and aggregation of other Aβ species in the amyloid core [10].

2. Materials and methods

2.1. Materials

1,2-Distearoyl-*sn*-glycero-3-phosphoethanolamine-*N*-methoxy-poly(ethylene glycol 2000) (DSPE-PEG_{2000}) was purchased from Northern Lipids (Vancouver, Canada). Thioflavine-T (ThT), Congo red (CR), 1,1,1,3,3,3-hexafluoro-2-propanol (HFIP) and sodium azide were obtained from Sigma–Aldrich (St. Louis, MO). Synthetic Aβ-42 was obtained from American Peptides (Sunnyvale, California). Uranylacetate and other materials required for electron microscopy were purchased from Electron Microscopy Sciences (Hatfield, PA). Buffer and all other reagents used were analytical grade and purchased from Sigma–Aldrich. Water was deionized at 18 MΩ and sterile filtered (0.22 μm) before use. All peptide and lipid samples were high performance liquid chromatography purified and the peptide purity was always greater than 98%.

2.2. Preparation of β-amyloid (Aβ-42)

Stock solution of the peptide was prepared by dissolving the lyophilized peptide in HFIP to a final concentration of 1 mg/ml using a Hamilton syringe equipped with a Teflon plunger [34]. This solution was shaken on a Barnstead Lab Line plate shaker for 2 h at 4 °C, aliquoted into sterile glass vials, HFIP was removed under vacuum in the fume hood and the peptide was stored desiccated at 20 °C until use [32]. Prior to use, each vial was allowed to equilibrate at room temperature for 15 min to avoid drastic temperature alteration leading to condensation.

2.3. Preparation of PEGylated phospholipid containing Aβ-42 samples

We have previously documented the preparation procedure for SSM [6]. In this study, we employed the same protocol with a slight modification. Appropriate amount of DSPE-PEG_{2000} was added to Aβ-42 in HFIP. This mixture was vortexed for 5 min (Thermolyne Maxi Mix II) and solvent was evaporated to form Aβ-42-lipid film. Residual solvent was removed under vacuum. Films were reconstituted in 10 mM HEPES buffer, vacuum sonicated (Fisher Scientific bath sonicator B2200R-1) and incubated at 25 °C (VWR SHEL LAB Incubator) for 2 h. Films were freshly prepared before each experiment. For SSM and Aβ-42 controls, the same procedure was followed without Aβ-42 and SSM, respectively. Size of SSM was ~14 nm as determined by quasi-elastic light scattering (data not shown).

2.4. Experimental procedures

2.4.1. Turbidimetry assay

This experiment was performed as previously described [10] with slight modifications. Samples were prepared as described above (Section 2.3). For control sample containing Aβ-42 in buffer, same procedure was repeated without lipid. A final Aβ-42 concentration of 25 μM was obtained corresponding to Aβ-42: lipid ratio of 1:0–1:100. Sodium azide (0.01%) was added to the buffer to prevent bacterial contamination. The solution was stirred continuously at room temperature in dark using a magnetic stirrer at ~60 rpm. Aliquots were withdrawn at predefined time intervals in a 96-well plate and shaken for 60 s to evenly resuspend the aggregates. Turbidity was measured at 405 nm using a Labsystems Multiskan Plus UV–Vis Microplate Reader.

2.4.2. Congo red (CR) binding assay

β-sheet formation of Aβ-42 in presence and absence of lipid was determined by Congo red binding. Aβ-42 (10 μM) samples were prepared with or without lipid (0.5 mM) as described above. At the end of 2 h, CR (100 μM stock prepared in NaCl, pH 7.4) was added to the Aβ-42 solution to give a final concentration of 10 μM CR. Solutions were vortexed and incubated at 25 °C for 15 min. Absorbance values at 403 and 541 nm were recorded for samples and CR alone preparations using a Perkin-Elmer Lambda 35 UV spectrophotometer in a 1-cm path length cuvette. Background absorbance values of buffer and SSM were subtracted from the respective test solutions. Aggregated Aβ-42 was quantitated as described previously [12] using the equation:

$$\text{Aggregated A}\beta(\mu\text{g/ml}) = ({}^{541\,\text{nm}}\text{A}/4780) - ({}^{403\,\text{nm}}\text{A}/6830) - ({}^{403\,\text{nm}}\text{A}_{\text{CR}}/8620)$$

$^{541\ \text{nm}}$A and $^{403\ \text{nm}}$A are absorbance of peptide sample while $^{403\ \text{nm}}\text{A}_{\text{CR}}$ is the absorbance of CR dye alone. The concentration of aggregated Aβ-42 monomer was then calculated assuming a molecular mass for Aβ-42 of 4514 (obtained from vendor).

2.4.3. Thioflavine-T (ThT) binding assay

The degree of Aβ-42 fibrillization was determined using the fluorescent dye, ThT, which specifically binds to fibrillar conformations [14]. Samples were prepared as described above with final Aβ-42 concentration of 25 μM. At the end of 2 h, 200 μL of sample solution was transferred to 96-well Black Cliniplates (Labsystems). ThT was added to each test sample to a final concentration of 10 μM. Samples were shaken for 30 s prior to each measurement. Relative fluorescence intensity was measured using a SpectraMax Gemini XS Plate Reader (Molecular Devices). Measurements were performed at an excitation wavelength of 445 nm and an emission of 481 nm (pre-determined experimentally). To account for background fluorescence, fluorescence intensity from control solution without Aβ-42 was subtracted from solution containing Aβ-42.

2.4.4. Circular dichroism spectroscopy (CD)

Secondary structure of Aβ-42 in presence and absence of lipids were determined by CD spectroscopy. Samples were prepared as described above (10 μM Aβ-42 and peptide: lipid ratio of 1:50) and scanned at room temperature in a 1 mm path length fused quartz cuvette using a Jasco J-710 Spectropolarimeter (Jasco, Easton, MD) calibrated with d10 camphor sulfonic acid. This service was provided by the Protein Research Lab of Research Resources Center (RRC) of University of Illinois at Chicago. Spectra were obtained from 190 to 260 nm at 1-nm bandwidth, 5 nm step and 1 s response time averaged over 5 runs. Spectra were corrected for buffer or SSM scans and smoothed using manufacturer's Savitzky Golay algorithm. Spectra were deconvoluted and percentage secondary structure was calculated by fitting the data into simulations by SELCON® [27].

2.4.5. Particle size determination by quasi-elastic light scattering

Particle size of aggregates formed by Aβ-42 in presence and absence of phospholipid were analyzed by quasi-elastic light scattering (QELS) using a NICOMP 380 Particle Size Analyzer (Santa Barbara, California) equipped with a 5 mW helium–neon laser at 632.8 nm and a temperature controlled cell holder. Samples were prepared as described previously. Solutions were stirred continuously at ~60 rpm at room temperature. 500 μL of test solution was aliquoted after 2 h and particle size distribution of Aβ-42 (12.5 μM; peptide: lipid ratio of 1:50) aggregates was determined. The mean hydrodynamic particle diameter, d_h was obtained from the Stokes–Einstein relation using the measured diffusion of particles in solution as described previously [2]. Data was analyzed in terms of volume weighted distribution.

2.4.6. *Transmission electron microscopy (TEM)*

The ultrastructural characteristics of Aβ-42 (100 μM) aggregates in presence and absence of lipids were examined under a transmission electron microscope (TEM) (JEOL-JEM 1220, JEOL USA Inc., Peabody, MA) at 100 kV for morphology. Use of this equipment was provided Electron Microscopy Services at RRC-UIC. Samples were prepared as described above and incubated at 25 °C for 72 h. A 5 μL drop of sample was placed on Formvar carbon support film on copper grid (mesh 200) (Electron Microscopy Sciences, Hatfield, PA) stained with 2% uranylacetate for 1 min. Excess stain was removed and samples were dried overnight at room temperature. TEM images were recorded by at 30 000× on a multiscan camera (Gatan Inc., Pleasanton, CA) using the Gatan Digital Micrograph version 2.5 software.

2.4.7. *Cytotoxicity assay*

Human Neuroblastoma SHSY-5Y cell line was used to study the effect of PEGylated phospholipid nanomicelles on Aβ-42 induced toxicity. Cells were cultured in Dulbecco's modified Eagle's medium (DMEM) (Mediatech) supplemented with 4.5 g/L L-glucose, 0.1 mmol/L non-essential amino acids, 2 mmol/L glutamine and 10% fetal bovine serum at 37 °C in 5% CO_2. Cells were plated (5×10^4 per well) in 96 well plates in 150 μL of media. After overnight incubation, cells were washed with serum free media. Serum free media alone or containing one of the following combinations (0.2–4 μM of Aβ incubated for 2 h at 25 °C with or without 0.01–0.2 mM of PEGylated lipid; Aβ-42: lipid ratios of 1:50) were added to the cells. Cells were then incubated for further 12 h at 37 °C in 5% CO_2. Cell viability was tested using MTS (3-(4,5-dimethylthiazol-2-yl)-5-(3-carboxymethoxyphenyl)-2-(4-sulfophenyl)-2H-tetrazolium) assay (Cell Titer 96® Aqueous One Solution Cell Proliferation Assay kit; Promega, Madison, WI) as described in the manufacturer's protocol. In summary, after the end of incubation period cell media was replaced with 100 μL of RPMI-1640 without phenol red. 20 μL of Cell Titer 96 One® solution reagent was added to each well. The plates were incubated at 37 °C for 3 h in humidified, 5% CO_2 atmosphere. Optical density was then read at 492 nm using a UV Spectrophotometric plate reader (Labsystems) and the values obtained for untreated controls were used to define 100% survival.

2.5. *Data and statistical analyses*

Data are represented as mean ± standard deviation (S.D.) for at least three independent determinations. Difference between groups and its statistical significance was determined using two-tailed Student's *t*-test and ANOVA. Statistical analysis was performed using SPSS version 10.0 (Chicago, IL). p value of <0.05 was considered statistically significant.

3. Results

3.1. *PEGylated phospholipid nanomicelles mitigate β-sheet formation and aggregation of Aβ-42 in vitro*

Commercially available synthetic Aβ-42 is usually a heterogeneous mixture of seeds, oligomers and fibrils. To ensure sample homogeneity, HFIP pre-treatment was carried out, thereby facilitating the examination of the effect of PEGylated phospholipid nanomicelles on Aβ-42 aggregation in a more physiologically relevant state. A pilot turbidimetric study was performed to obtain the optimal peptide to lipid (P/L) ratio at which significant inhibition of aggregation was observed. Aβ-42 (25 μM) was incubated with five P/L ratios ranging from 1:25 to 1:100 for 2 h at 25 °C and optical density (OD) measurements were carried out at 405 nm. OD values (Fig. 1) demonstrate a significant retardation in the extent of Aβ-42 aggregation of lipid treated peptide at 1:40, 1:50 and 1:100 P/L ratios. However, saturation was observed at P/L 1:50. Aggregation inhibitory efficacy was not significantly different for P/L ratios of 1:50 and 1:100 and therefore, 1:50 was chosen for further exploratory studies. This value is in good agreement with the value of 1:55 reported previously for Aβ-40 using a lipid bilayer archetype [28]. However, turbidity measurement at 405 nm, per se, is a generic aggregation assay that is not conclusive for detection of amyloid fibrillization process. Therefore, we employed

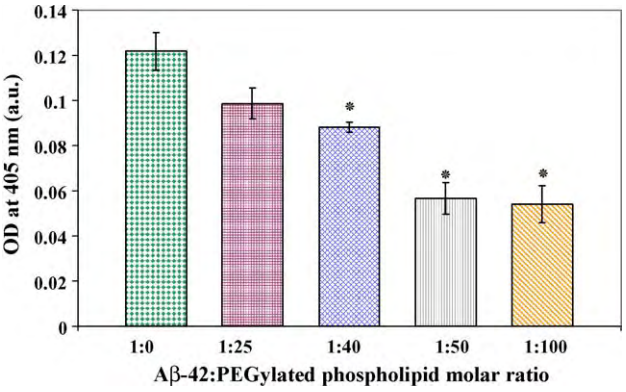

Fig. 1 – Effect of PEGylated phospholipid nanomicelles on Aβ-42 aggregation by turbidimetry assay and determination of optimal peptide: lipid ratio. An increase in OD is directly correlated to aggregation. Data represents mean OD of three independent experiments ($n = 3$, $^*p < 0.05$ compared to Aβ-42 in buffer). Error bars represent standard deviation (S.D.).

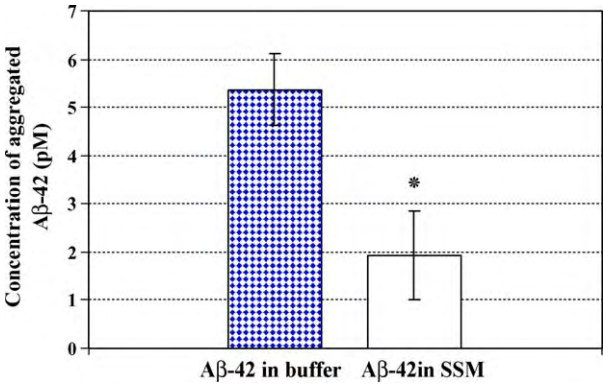

Fig. 2 – Effect of PEGylated phospholipid nanomicelles on Aβ-42 aggregation by Congo red assay. ($n = 3$, $^*p < 0.05$ compared to Aβ-42 in buffer). Error bars represent standard deviation.

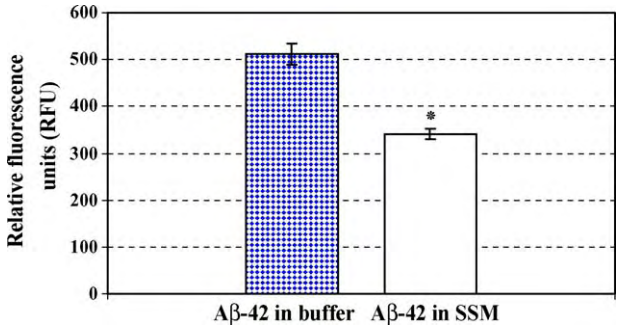

Fig. 3 – Effect of PEGylated phospholipid nanomicelles on Aβ-42 aggregation by fluorometric thioflavine-T assay. Increase in relative fluorescence units (RFU) is proportional to fibril formation ($n = 3$, $^{*}p < 0.05$ compared to Aβ-42 in buffer). Error bars represent standard deviation.

more specific deterministic techniques such as Congo red binding and Thioflavine-T interaction assay to obtain fundamental information regarding the nature of effect of PEGylated phospholipid nanomicelles on Aβ-42 aggregation.

In general, amyloid protein fibrils possess tinctorial dye binding properties owing to their characteristic fibrillar conformations. ThT and CR are two standard dyes used to monitor fibrillogenesis. Binding of ThT to amyloid fibrils causes enhancement of ThT fluorescence, while binding to CR causes a red shift in the absorbance spectrum of the dye. We used CR binding assay to quantify the concentration of aggregated β-sheeted amyloid as described previously [12]. ThT assay was used for determination fibril formation. The results of CR binding assay demonstrated that concentration of aggregated β-sheeted Aβ-42 in PEGylated phospholipid treated sample was reduced almost three-fold (~1.9 pM) ($p < 0.05$) compared to untreated control (~5.8 pM) (Fig. 2). ThT fluorescence spectroscopic assay was then employed to confirm this observation and complementary results were obtained. Relative fluorescence intensity of PEGylated phospholipid treated sample was significantly lower than that of untreated control, indicating significant mitigation of β-sheeted fibril formation in lipid treated samples (Fig. 3).

We postulated that PEGylated phospholipid nanomicelles retard Aβ-42 aggregation by inducing a constructive conformational change in its secondary structure. CD spectroscopy was performed to obtain a qualitative estimate of Aβ-42 secondary structure in the presence of PEGylated phospholipid nanomicelles. CD scans were deconvoluted using SELCON® software to obtain percentage of each secondary structural element. After incubation of the peptide in buffer for 2 h at 25 °C, Aβ-42 exhibited ~38% β-sheeted conformation while α-helicity was insignificant (~1.9%) indicating an onset of aggregation. However, upon incubation with PEGylated phospholipid nanomicelles, a radical alteration in the relative proportions of secondary structural elements was observed. In presence of PEGylated phospholipid nanomicelles, folding of Aβ-42 was significantly changed resulting in very high proportions of α-helicity (~34%) and a concurrent favorable decline in β-sheet conformation (~3.4%) (Table 1). Therefore, it is evinced that in presence of PEGylated phospholipid

Table 1 – Influence of PEGylated lipid micelles on Aβ-42 secondary structure by circular dichroism

	Aβ-42 in buffer[§]	Aβ-42 in SSM[*]
% Alpha helix	1.9 ± 0.25	34.25 ± 0.7
% Beta sheet	38.1 ± 1	3.4 ± 0.5

[*] $p < 0.05$ compared to §.

nanomicelles, transformation of Aβ-42 to pathogenic β-sheets is significantly inhibited and α-helicity is radically enhanced compared to respective untreated Aβ-42 control. This change in the secondary structure of the peptide in presence of PEGylated phospholipid nanomicelles is directly responsible for reduction in the Aβ-42 aggregation rate. Results obtained from CD study concur well with the CR binding and ThT assay which demonstrated that a significant reduction in β-sheeted fibrillar conformation is obtained on treatment with PEGylated phospholipid nanomicelles.

We speculated that the ability of PEGylated phospholipid nanomicelles to attenuate Aβ-42 aggregation could also manifest in reduction of Aβ-42 aggregate size. To obtain comprehensive information on representative dimensions of Aβ-42

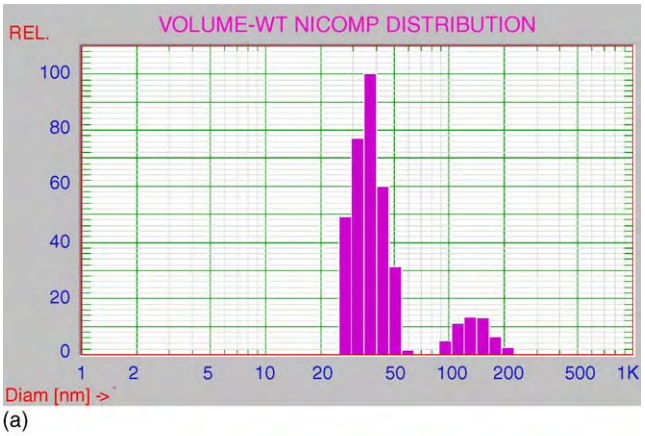

(a)

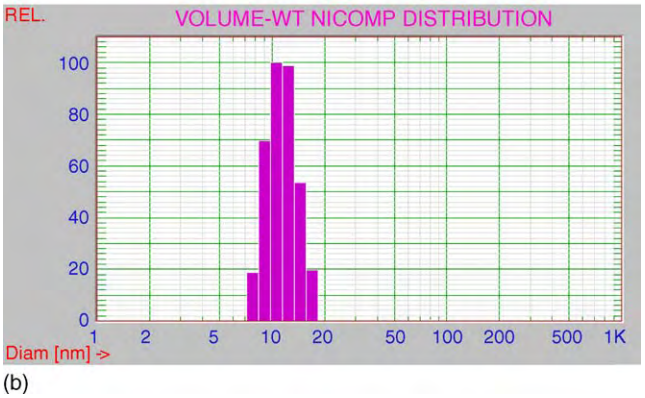

(b)

Fig. 4 – Representative size analysis by quasi-elastic light scattering. (a) Aβ-42 in buffer: After 2 h of incubation, bimodal heterogeneous distribution is observed. Eighty-eight percent of the particles have average diameter of 36.7 nm (±6.2 nm), 12% of the particles have an average size of 134.4 nm (±31.2 nm). (b) Aβ-42 in SSM: after 2 h of incubation, 100% of the particles form a single peak with 11.2 ± 2.3 nm.

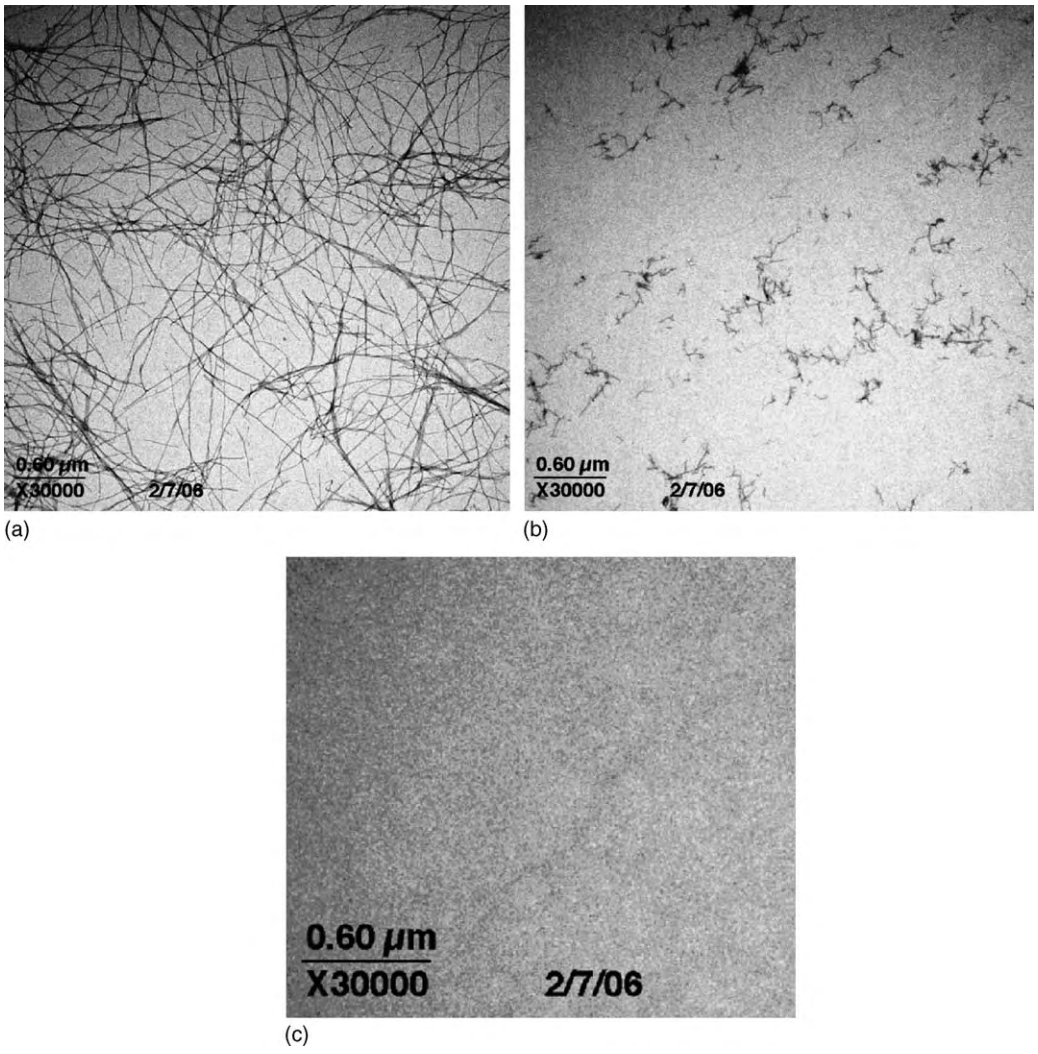

Fig. 5 – Representative electron micrographs of (a) Aβ-42 in buffer, (b) PEGylated phospholipid associated Aβ-42 and (c) SSM.

aggregates, quasi-elastic light scattering was employed. After incubation of Aβ-42 (12.5 μM) in buffer for 2 h, a heterogeneous distribution with dual peaks having a maximum average hydrodynamic diameter of 134.4 nm was observed (Fig. 4(a)). However, in presence of PEGylated phospholipid nanomicelles, the particle size distribution was more homogenous and stable with a single peak at ~12 nm corresponding to the size of PEGylated phospholipid nanomicelles (Fig. 4(b)).

Transmission electron microscopy was employed to determine the effect of PEGylated phospholipid nanomicelles on ultrastructure of Aβ-42 aggregates. Solutions of Aβ-42 (100 μM) were incubated at 25 °C with or without PEGylated phospholipid nanomicelles. After 72 h, samples were placed on copper grids, negatively stained with 2% uranylacetate and visualized under TEM. In absence of PEGylated phospholipid nanomicelles Aβ-42 formed a dense meshwork of elongated fibrils that covered the entire grid area (Fig. 5(a)). Presence of micelles ameliorated fibril growth significantly and much shorter fragments were formed (Fig. 5(b)). The density of these short fragments on each copper grid was much sparse compared to lipid untreated controls.

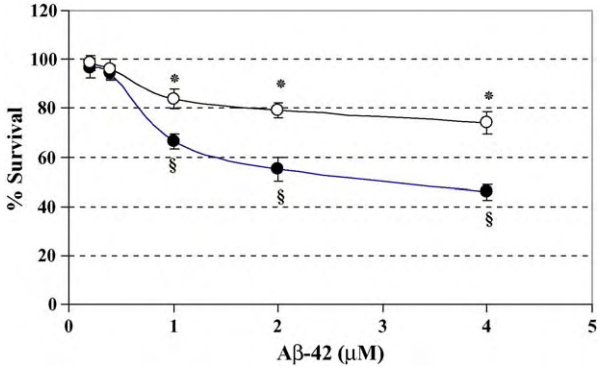

Fig. 6 – Effect of PEGylated phospholipid nanomicelles on Aβ-42 induced cytotoxicity. A significant reduction in Aβ-42 induced cytotoxicity is observed in cells treated with PEGylated lipid associated Aβ-42 ($n = 3$, $^{*}p < 0.05$ compared respective §). Error bars represent standard deviation.

3.2. PEGylated phospholipid nanomicelles attenuate neurotoxicity of Aβ-42 in vitro

Aβ-42 is shown to be toxic to neurons and cause cell death via apoptotic mechanisms [1]. MTS assay provides a good estimate of cell survival based on bioreduction of MTS to aqueous soluble colored formazan crystals accomplished by dehydrogenase enzymes found in metabolically active cells. Cytotoxicity study was carried out using human neuroblastoma SHSY-5Y cell paradigm that possess highly developed neurites and exhibit high sensitivity against Aβ-42 [3]. A series of physiologically relevant Aβ-42 concentrations (0.2–4 μM) were tested. Lipid untreated Aβ-42 demonstrated elevated neurotoxicity above 1 μM concentration. However, when incubated with PEGylated phospholipid nanomicelles, Aβ-42 neurotoxicity was significantly mitigated and percentage survival was increased by almost 30% compared to lipid untreated control (Fig. 6).

4. Discussion

At least 16 different proteins have been identified hitherto that have a high propensity to misfold and form β-sheeted amyloid fibrils leading to toxic gain of function and associated pathologies. Structural context plays a critical role in protein conformational change, their subsequent misfolding and dysregulation. It has been reported that amyloidogenic peptides and proteins contain short stretches of amino acid sequences referred to as ''hot spots'' that facilitate and drive this aggregation process [5]. In its native state, Aβ-42 ''hot spots'' are stabilized in α-helical conformation by the cell membrane bilayer [22]. Therefore, a promising therapeutic strategy to prevent aggregation would be to stabilize this native state of the peptide and coat the ''hot spots'' by providing a steric barrier to prevent their interaction [4]. The objective of this study was to test the hypothesis that PEGylated phospholipid nanomicelles mitigate Aβ-42 aggregation by providing a cell membrane simulating milieu that constrains the peptide in a favorable α-helical conformation preventing its conversion to pathogenic β-sheet form. The lipid monomers (which are in dynamic equilibrium with the micelles) coat the exposed ''hot spots'' reducing any further deleterious peptide–peptide interaction (detailed explanation in Section 4.2). The rationale behind this hypothesis was based on our previous experience with several amphiphilic peptides and proteins [6,11,17,29] and on the observation that Aβ structure examined in membrane mimicking surfactants and organic solvents resembled the native non-pathogenic α-helical structure of transmembrane Aβ in vivo [25,33].

4.1. PEGylated phospholipid nanomicelles attenuate Aβ-42 β-sheet formation, aggregation and neurotoxicity in vitro

CD spectroscopy results demonstrated that α-helicity of Aβ-42 was significantly augmented (almost 17-fold) with a concurrent decline in β-sheet (almost 10-fold) in presence of PEGylated phospholipids. These findings concur with our previous results where hydrophobic amino acid residues of the several amphiphilic peptides interacted with the hydrophobic micelle core and rendered the peptide α-helical [6,29]. To this end, it has also been previously shown using a lipid bilayer paradigm that Aβ interaction with lipid at high P/L ratios, promotes its conformational transition to α-helix [28]. We believe that PEGylated phospholipid nanomicelles provide a hydrophobic environment similar to cell membrane bilayer, making it amenable to interact with the high energy transmembrane residues. This resultant interaction will eliminate unfavorable self peptide-peptide association. Since DSPE-PEG_{2000} is zwitterionic, no significant electrostatic interactions between Aβ-42 and PEGylated phospholipid nanomicelles are possible. To determine the specific nature of the inhibitory effect of PEGylated phospholipid nanomicelles on amyloid fibril formation, CR binding and ThT assay were employed. These techniques established that PEGylated lipids not only induced a favorable conformational change in the secondary structure of Aβ-42 but also reduced the concentration of β-sheeted amyloid fibrillar aggregates significantly (~3-fold).

Using laser light scattering, aggregates up to 134 nm were observed in untreated Aβ-42 control. These results indicate that within 2 h of incubation, the aggregation process is triggered leading to formation of several intermediate amyloid species. The heterogeneity in particle size distribution can be attributed to presence of several different peptide species and their co-existing amalgamates that include oligomers and elongated fibrils. Oligomers (or Aβ derived diffusible ligands-ADDL) are spherical with a diameter of approximately 5 nm while protofibrils range from spherical assemblies of ~5 nm to short rod like sequences up to 200 nm in length [30]. Our results are in conformation with these values reported in literature. It is technically complex to ascertain the nature of aggregates based exclusively on light scattering data. However, a good preliminary estimate can be obtained which can then be combined with more sensitive analytical methods to acquire comprehensive information. No detectable peptide aggregates were formed in lipid treated samples leading to the inference that PEGylated phospholipid nanomicelles inhibit both the rate and extent of Aβ-42 aggregation.

Significantly smaller fibril fragments were seen under TEM in lipid treated samples indicating that fibril elongation rate is considerably slowed down compared to untreated peptide samples that exhibited dense elongated fibrils. Collectively, these in vitro results employing several deterministic techniques lead to the conclusion that PEGylated phospholipid nanomicelles mitigate Aβ-42 aggregation by accommodating Aβ-42 molecule in α-helical conformation resulting in reduced aggregation and amyloidogenecity.

Previously, it has been reported that aggregated β-sheeted Aβ-42 is responsible for eliciting neurotoxicity in cells in culture [3]. In vitro cytotoxicity study demonstrated that PEGylated lipid micelle treated Aβ-42 was significantly less neurotoxic compared to untreated control. We can purport that SSM elicited a constructive conformational change in Aβ-42 to a more favorable α-helix form thereby preventing formation of amyloid toxic species and salvaging neurons from cell death.

4.2. Putative mechanism of action for anti-aggregation property of PEGylated phospholipid nanomicelles

Based on the results obtained in this study we postulate two different mechanisms elucidating how PEGylated lipids might affect the rate of Aβ-42 fibrillogenesis.

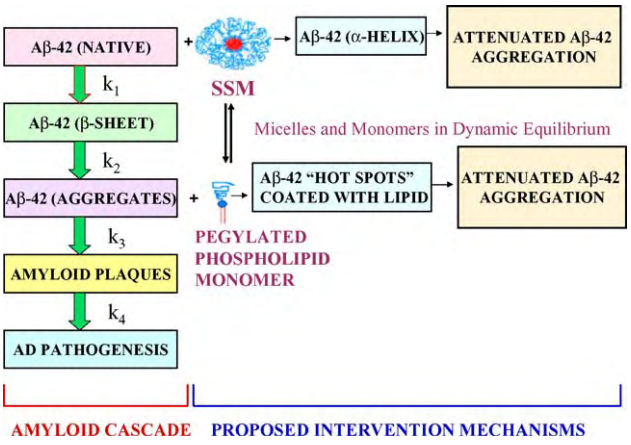

Fig. 7 – Schematic presentation of proposed mechanisms for Aβ-42 interaction with PEGylated phospholipid nanomicelles and its monomers. PEGylated phospholipid nanomicelles provide a hydrophobic environment to preserve Aβ-42 in α-helical conformation; thereby preventing its transformation to pathogenic β-sheeted aggregates (k_1 is significantly reduced). PEGylated phospholipid monomers coat the high energy domains ("hot-spots") on the initial aggregates and avert their further interaction and aggregation (k_3 is significantly reduced).

Firstly, if PEGylated phospholipid nanomicelles are present in the extracellular milieu when Aβ-42 is cleaved, Aβ-42 would interact with the micelles so as to accommodate its hydrophobic amino acid domains in the hydrophobic micelle core in a α-helical conformation. This interaction results in a thermodynamically favorable state of the peptide, preventing β-sheet formation and self-aggregation. To this end, we have demonstrated that Aβ-42 exists in a predominantly α-helical form in presence of PEGylated phospholipid nanomicelles (Table 1).

The second premised mechanism is that PEGylated lipid monomers shield the exposed hydrophobic domains or "hot spots" of the early Aβ-42 aggregates (oligomers and protofibrils) with their hydrophobic acyl chains and avert further aggregate–aggregate or aggregate–monomeric Aβ-42 interaction. PEGylated lipid monomers are ideally suited as aggregation inhibitors of this type because of their two long hydrophobic acyl chains which cover a relatively large hydrophobic surface area compared to conventional surfactants. A schematic illustration of these proposed mechanisms is shown in Fig. 7. By a complementary mechanism, the PEG polymer will also provide steric stability to the lipid associated Aβ-42, surreptitiously hiding it from neighboring Aβ-42 molecules by providing a physico-mechanical barrier. Further verification of the exact mechanism is still under investigation. A recent paper studying the effect of alkyl bromide surfactants on Aβ-40 fibrillogenesis also described analogous mechanisms which substantiate our results [21]. However, we speculate that DSPE-PEG_{2000} nanomicelles may have greater efficacy owing to the presence of two long acyl chains and large PEG polymer as described above. Furthermore, phospholipid nanomicelles are more attractive due to their relatively low CMC resulting in reduced toxicity. To this end, DSPE-PEG_{2000} has been FDA approved for human use in other indications.

5. Conclusion

In conclusion, this study outlines the significant inhibitory effect of PEGylated phospholipid nanomicelles on in vitro aggregation of Aβ-42 as demonstrated by several physicochemical techniques. The innate biophysical properties of Aβ-42 can be manipulated by these lipid moieties either to alter its secondary structure or to shield the hydrophobic "hot spots" responsible for aggregation and thereby curtail their aberrant misfolding. Conventionally, phospholipid nanomicelles have been studied as carriers for challenging chemical entities such as water insoluble drugs and amphiphilic biologics. This study, for the first time, proposes the potential use of PEGylated phospholipid micelles as a therapeutic agent against AD. We are working on developing PEGylated phospholipid nanomicelles as a novel nanomedicine that acts as a bifunctional carrier system to deliver a therapeutic moiety to treat AD while concurrently mitigating Aβ-42 aggregation.

Acknowledgements

We thank Dr. Richard Gemeinhart's Laboratory for the access and use of some equipments in this study. We also thank Dr. Jim Wang for providing us with SHSY-5Y cells. This study was supported, in part, by VA Merit Review grant, NIH grants RO1 AG024026, RO1 HL72323 and DOD grant DAMD 17-02-1-0415. This investigation was conducted in a facility constructed with support from Research Facilities Improvement Program Grant Number C06 RR15482 from the National Center for Research Resources, NIH.

REFERENCES

[1] Allen J, Eldadah B, Huang X, Knoblach S, Faden A. Multiple caspases are involved in beta-amyloid-induced neuronal apoptosis. J Neurosci Res 2001;65(1):45–53.
[2] Ashok B, Arleth L, Hjelm RP, Rubinstein I, Onyuksel H. In vitro characterization of PEGylated phospholipid micelles for improved drug solubilization: effects of PEG chain length and PC incorporation. J Pharm Sci 2004;93(10):2476–87.
[3] Datki Z, Jhász A, Gálfi M, Soós K, Papp R, Zádori D, et al. Method for measuring neurotoxicity of aggregating polypeptides with the MTT assay on differentiated neuroblastoma cells. Brain Res Bull 2003;30:223–9.
[4] Dobson CM. Protein folding and misfolding. Nature 2003;426(6968):884–90.
[5] Fernandez-Escamilla A, Rousseau F, Schymkowitz J, Serrano L. Prediction of sequence-dependent and mutational effects on the aggregation of peptides and proteins. Nat Biotechnol 2004;22(10):1302–6.
[6] Gandhi S, Tsueshita T, Onyuksel H, Chandiwala R, Rubinstein I. Interactions of human secretin with sterically stabilized phospholipid micelles amplify peptide-induced vasodilation in vivo. Peptides 2002;23(8):1433–9.

[7] Geerts H. NC-531 (Neurochem). Curr Opin Investig Drugs 2004;5(1):95–100.
[8] Haass C, Selkoe D. Alzheimer's disease. A technical KO of amyloid-beta peptide. Nature 1998;391(6665):339–40.
[9] Hardy J, Selkoe D. The amyloid hypothesis of Alzheimer's disease: progress and problems on the road to therapeutics. Science 2002;297(5580):353–6.
[10] Jarrett J, Berger E, Lansbury Jr P. The C-terminus of the beta protein is critical in amyloidogenesis. Ann N Y Acad Sci 1993;695:144–8.
[11] Kirchhoff C, Rubinstein I, Ludwig J, Onyuksel H. DSPE-PEG5000 increases physical stability of human IL-2 in vitro. In: Proceedings of the controlled release of bioactive materials 28; 2001. p. 524–5.
[12] Klunk W, Jacob R, Mason R. Quantifying amyloid beta-peptide (Abeta) aggregation using the Congo red-Abeta (CR-abeta) spectrophotometric assay. Anal Biochem 1999;266(1):66–76.
[13] Kohno T, Kobayashi K, Maeda T, Sato K, Takashima A. Three-dimensional structures of the amyloid beta peptide (25–35) in membrane-mimicking environment. Biochemistry 1996;35(50):16094–104.
[14] LeVine III H, Thioflavine T. interaction with synthetic Alzheimer's disease beta-amyloid peptides: detection of amyloid aggregation in solution. Protein Sci 1993;2(3):404–10.
[15] Lorenzo A, Yankner B. Beta-amyloid neurotoxicity requires fibril formation and is inhibited by Congo red. Proc Natl Acad Sci USA 1994;91(25):12243–7.
[16] Masters C, Simms G, Weinman N, Multhaup G, McDonald B, Beyreuther K. Amyloid plaque core protein in Alzheimer disease and Down syndrome. Proc Natl Acad Sci USA 1985;82(12):4245–9.
[17] Onyuksel H, Ikezaki H, Patel M, Gao XP, Rubinstein I. A novel formulation of VIP in sterically stabilized micelles amplifies vasodilation in vivo. Pharm Res 1999;16(1):155–60.
[18] Pervushin K, Orekhov V, Popov A, Musina L, Arseniev A. Three-dimensional structure of (1–71) bacterioopsin solubilized in methanol/chloroform and SDS micelles determined by 15N-1H heteronuclear NMR spectroscopy. Eur J Biochem 1994;219(1/2):571–83.
[19] Rizo J, Blanco F, Kobe B, Bruch M, Gierasch L. Conformational behavior of *Escherichia coli* OmpA signal peptides in membrane mimetic environments. Biochemistry 1993;32(18):4881–94.
[20] Roher A, Lowenson J, Clarke S, Woods A, Cotter R, Gowing E, et al. Beta-amyloid-(1–42) is a major component of cerebrovascular amyloid deposits: implications for the pathology of Alzheimer disease. Proc Natl Acad Sci USA 1993;90(22):10836–40.
[21] Sabate R, Estelrich J. Stimulatory and inhibitory effects of alkyl bromide surfactants on beta-amyloid fibrillogenesis. Langmuir 2005;21(15):6944–9.
[22] Schroeder F, Jefferson J, Kier A, Knittel J, Scallen T, Wood W, et al. Membrane cholesterol dynamics: cholesterol domains and kinetic pools. Proc Soc Exp Biol Med 1991;196(3):235–52.
[23] Selkoe D. Alzheimer's disease: genes, proteins, and therapy. Physiol Rev 2001;81(2):741–66.
[24] Serpell L. Alzheimer's amyloid fibrils: structure and assembly. Biochim Biophys Acta 2000;1502(1):16–30.
[25] Shao H, Jao S, Ma K, Zagorski M. Solution structures of micelle-bound amyloid beta-(1–40) and beta-(1–42) peptides of Alzheimer's disease. J Mol Biol 1999;285(2):755–73.
[26] Smith M, Drew K, Nunomura A, Takeda A, Hirai K, Zhu X, et al. Amyloid-beta, tau alterations and mitochondrial dysfunction in Alzheimer disease: the chickens or the eggs? Neurochem Int 2002;40(6):527–31.
[27] Sreerama N, Woody R. Poly (pro)II helices in globular proteins: identification and circular dichroic analysis. Biochemistry 1994;33(33):10022–5.
[28] Terzi E, Holzemann G, Seelig J. Interaction of Alzheimer beta-amyloid peptide (1–40) with lipid membranes. Biochemistry 1997;36(48):14845–52.
[29] Tsueshita T, Gandhi S, Onyuksel H, Rubinstein I. Phospholipids modulate the biophysical properties and vasoactivity of PACAP-(1–38). J Appl Physiol 2002;93(4): 1377–83.
[30] Walsh D, Klyubin G, Shankar G, Townsend M, Fadeeva J, Betts V, et al. The role of cell derived oligomers of Aβ in Alzheimers disease and avenues for therapeutic intervention. Proteins in disease. Biochem Soc Trans 2005;33(5):1087–90.
[31] Waterhous D, Johnson Jr W. Importance of environment in determining secondary structure in proteins. Biochemistry 1994;33(8):2121–8.
[32] Yoshiike Y, Tanemura K, Murayama O, Akagi T, Murayama M, Sato X, et al. New insights on how metals disrupt amyloid beta-aggregation and their effects on amyloid-beta cytotoxicity. J Biol Chem 2001;276(34):32293–9.
[33] Zagorski M, Barrow C. NMR studies of amyloid beta-peptides: proton assignments, secondary structure, and mechanism of an alpha-helix-beta-sheet conversion for a homologous, 28-residue, N-terminal fragments. Biochemistry 1992;31(24):5621–31.
[34] Zagorski M, Yang J, Shao H, Ma K, Zeng H, Hong A. Methodological and chemical factors affecting amyloid beta peptide amyloidogenicity. Meth Enzymol 1999;309:189–204.

Appendix (12) 33rd Annual Meeting of Control Release Society Meeting, Austria

INTERACTION OF PEPTIDE DRUGS WITH STERICALLY STABILIZED PHOSPHOLIPID MICELLES AT A MOLECULAR LEVEL

Eunjung Jeon[1], Israel Rubinstein[2, 4], Hayat Önyüksel [1,3]
[1]Department of Biopharmaceutical Sciences, [2]Medicine, [3]Bioengineering
University of Illinois at Chicago and [4]Jesse Brown Veterans Affairs Medical Center
Chicago, IL 60612, USA
E-mail address of presenting author: hayat@uic.edu

ABSTRACT SUMMARY

This study explores the peptide drugs-phospholipid micelles interaction and shows that the number of peptide molecules associated with sterically stabilized micelles (SSM) is proportional to the overall increase in α-helicity of the peptide-micellar self-assembly.

INTRODUCTION

Previously we reported that peptide drugs, such as secretin, vasoactive intestinal peptide (VIP) and galanin, were stabilized by pegylated phospholipid micelles, and that incubation of peptide drugs with SSM resulted in increased α-helicity and *in vivo* bioactivity of the peptide drugs[1-5].

The purpose of this study was to determine certain biophysical phenomena underlying the increased α-helicity of peptide drugs when incubated with SSM.

EXPERIMENTAL METHODS

Determination of peptide-phospholipid micelles interactions

Distearoyl-phosphatidylethanolamine-polyet -hyleneglycol-2000 (DSPE-PEG2000) micelles were prepared as described before[1-5]. Briefly, pegylated phospholipid was added to saline (5mM), vortexed for 2min, and then sonicated for 5min. Thereafter it was allowed to equilibrate for 1 hr at 25^{o}C.

For the peptide-phospholipid micelles interaction study, we used four peptide drugs, secretin, VIP, glucagon like peptide-1 (GLP-1) and galanin. A fixed concentration of peptide drugs was incubated with varying concentrations of SSM (molar ratio of lipid to peptide varying from 0 to 200) for 2hr at 25^{o}C. Due to the presence of fluorescent amino acid residues in the peptides, we were able to obtain the fluorescence emission spectra (Em_{max} and λ_{max}) using the SLM Aminco 8000 Spectrofluorimeter. Em_{max} vs. molar ratio of lipid to peptide was plotted to determine the saturation molar ratio. The molar ratio of lipid to peptide, which gave the maximum intensity and no significant change beyond that ratio, was considered as a saturation molar ratio. Using the saturation molar ratio and SSM aggregation number (~90)[6], the number of peptide molecules associated with each SSM was calculated. This value was termed peptide-SSM interaction parameter.

Determination of the extent of α-helicity increase of peptide-micellar self-assembly

The α-helicity of GLP-1 in saline and in SSM (at the saturation molar ratio of lipid to peptide) was determined by the circular dichroism measurement as described previously[1-2;4]. Briefly, CD spectra were acquired at 25^{o}C on Jasco J-710 spectropolarimeter using a 1 mm pathlength quartz cuvette. The spectra were obtained between the wavelengths of 190-260nm at the speed of 50nm/min. Percentage α-helicity for GLP-1 in saline and SSM was calculated using the software Selcon (Softwood, Brookfield, CT). The data for secondary structure of secretin, VIP and galanin in saline and SSM were obtained from our recent work[1-2;4]. The increase in α-helicity of peptide-micellar self-assembly was determined from the difference of α-helicity in saline and in the presence of SSM. This value was used as a parameter indicating conformational change in peptide-micellar self-assembly.

RESULTS AND DISCUSSION

In this study, we characterized the interactions of four peptide drugs with SSM to obtain the interaction parameter (A), which is specific to the each peptide drug (Table 1). We also determined the α-helicity of peptide drugs in saline and SSM, calculated the extent of α-helicity increase of peptide-micellar self-assembly and termed this value as the conformational change parameter (B) (Table 2). The parameter (A) was directly correlated to the parameter (B) as shown in Figure 1. This linear correlation indicates that the α-helicity increase of peptide drugs in SSM is not related to augmented peptide folding in the presence of SSM, but is related to increased number of peptide molecules associated with SSM.

Peptide drugs	Saturation molar ratio of lipid to peptide	Number of peptide molecules /micelle* (A)
Secretin	10	9
VIP	20	4.5
GLP-1	40	2.25
Galanin	60	1.5

Table 1. Saturation molar ratios of lipid to peptide (n=3, averaged value) and theoretical calculation of number of peptide molecules/micelle (*: SSM aggregation number is 90[6])

Peptide drugs	Saline	SSM	Increased α-helicity (B)
Secretin[2]	4.0±2.0%	35.0±6.4%[&]	8.75
VIP[4]	5.0±1.0%	27.0±2.0%[&]	5.4
GLP-1	11.2±1.0%	32.6±7.3%[&]	2.91
Galanin[1]	8.3±1.0%	13.0±0.5%[&]	1.56

Table 2. Percentage α-helicity (at 25°C) of peptide drugs in saline and SSM, and increased α-helicity of peptide-micellar self-assembly (n=3, mean±SEM, [&]p<0.05 in comparison to its respective control)

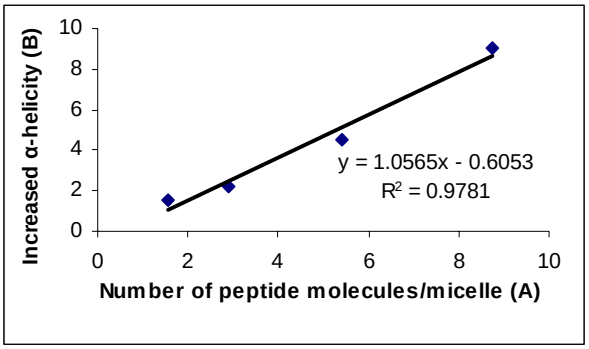

Figure 1. Correlation between average number of peptide molecules/micelle (A) and increased α-helicity (B)

CONCLUSIONS

We studied the peptide-phospholipid micelles interactions using fluorescence technique and determined the number of peptide molecules associated with a micelle. The peptide-SSM interaction parameter was directly correlated to the conformational change parameter. Based on this correlation, we conclude that number of associated peptide molecules with SSM is proportional to the α-helicity increase when peptide drugs are incubated in SSM. However, to confirm this relationship between two parameters, additional studies using larger number of peptide drugs are required.

REFERENCES

1. Dagar, S., et al, *Peptides* 24, 1373-1380 (2003)
2. Gandhi, S., et al, *Peptides* 23, 201-204 (2002)
3. Gandhi, S., et al, *Peptides* 23, 1433-1439 (2002)
4. Rubinstein, I., et al, *Peptides* 20, 1497-1501 (1999)
5. Onyuksel, H. et al, *Pharm Res.* 16, 155-160 (1999)
6. Ashok, B., et al, *J. Pharm. Sci.* 93, 2476-2497 (2004)

ACKNOWLEGEMENTS

This work was supported in part by Department of defense grant BCRP, No. DAMD 17-02-1-0415, a VA merit Review and NIH grants R01 AG024026, R01 HL72323 and C06RR15482.

NANOSIZED STERICALLY STABILIZED PHOSPHOLIPID MICELLES ATTENUATE β-AMYLOID AGGREGATION AND NEUROTOXICITY IN VITRO

Ashwini S. Pai[1], Israel Rubinstein [1,2,4] and Hayat Önyüksel[1,3]
[1]Departments of Biopharmaceutical Sciences, [2] Medicine, and [3]Bioengineering, University of Illinois at Chicago and [4]Jesse Brown VA Medical Center, Chicago, Illinois 60612, USA
E-mail address of presenting author: hayat@uic.edu

ABSTRACT SUMMARY

We determined the physicochemical interactions between sterically stabilized phospholipid micelles (SSM) and β-amyloid (Aβ-42): a hydrophobic peptide implicated in the pathophysiology of Alzheimer's disease (AD). We found that SSM attenuates formation of β-sheeted Aβ-42 aggregates. Neurotoxicity of SSM-associated Aβ-42 is significantly lower than that of Aβ-42 alone. Given this data, SSM represents a novel nanomedicine candidate to treat early stages of AD.

INTRODUCTION

Current paradigms implicate the aberrant aggregation of hydrophobic β-amyloid (Aβ-42) peptide in the pathogenesis of Alzheimer's disease (AD)[1.] This misfolding results in production of highly neurotoxic intermediate species[2]. Hence, drugs that could circumvent this process may prove beneficial in early stages of AD. To this end, membrane mimicking surfactants, such as sodium dodecyl sulfate (SDS) inhibit Aβ-42 aggregation by constraining the peptide in its non amyloidogenic soluble α-helix conformation[3]. However, clinical use of SDS is vastly limited by its toxicity. To overcome this limitation, we attempted to determine whether biocompatible and biodegradable nanosized (~15nm) sterically stabilized micelles (SSM) composed of 1,2-distearoyl-glycero-3-phosphoethanolamine-N-methoxy- poly(ethylene glycol 2000) (DSPE-PEG_{2000})developed in our laboratory attenuate Aβ-42 aggregation and neurotoxicity in vitro.

EXPERIMENTAL METHODS

Sample preparation

SSM were prepared as previously described[4] with a slight modification. Briefly, DSPE-PEG_{2000} was added to Aβ-42 dissolved in hexafluoroisopropanol and vortexed. Aβ-42-lipid film was formed, dried, reconstituted in buffer, and incubated at 25°C for 2 h. Aβ-42 control samples were prepared similarly without lipid.

Congo Red (CR) binding assay

We used Congo red dye binding assay to quantify formation of β-sheeted amyloid as described earlier[5]. Samples of Aβ-42 (10 μM) with or without SSM were prepared as described above (peptide: lipid molar ratio of 1:50) and CR (10 μM) was added. Samples were incubated at 25ºC for 15 min. OD values at 403 and 541 nm were recorded using a Perkin Elmer Lambda 35 UV spectrophotometer. Aggregated Aβ-42 was quantified as described previously[5].

Particle size analysis by light scattering

To obtain detailed information on representative dimensions of Aβ-42 aggregates, dynamic light scattering was employed. Particle size of Aβ-42 with or without SSM was determined (peptide: lipid molar ratio 1:50) at several time points. Aliquots were periodically measured using quasielastic light scattering (QELS) with a NICOMP 380 Particle Size Analyzer. Data were analyzed in terms of volume weighted distribution and weighted average was calculated.

Cytotoxicity assay

Human neuroblastoma SHSY-5Y cells were seeded (5 x 10^4/well) in 96 well plates containing 150 μL of DMEM. After overnight incubation, cells were washed with serum free media. A range of physiological Aβ-42 concentrations (0.2-4.0 μM of Aβ-42) were pre-incubated either with SSM (10-200 μM) or buffer for 2 h at 25 ºC. Serum free media alone or containing above mixtures were then added to cells and incubated for further 12 h at 37 °C. Cell viability was determined by the MTS assay according to the manufacturer's protocol.

Data and statistical analysis

Data are expressed as means ± standard deviation. Statistical analysis was carried out using Student's *t*-test and ANOVA. $p<0.05$ was considered statistically significant.

RESULTS AND DISCUSSION

CR dye is frequently used to monitor amyloid fibrillogenesis. Binding of amyloid fibrils to CR dye causes a red shift in the absorbance spectrum of the dye. Results of the CR binding assay demonstrated that SSM-treated Aβ-42 showed a significant ($p<0.05$) ~ 3 fold reduction in the concentration of aggregated β-sheeted Aβ-42 (~1.9 pM) compared to control (~5.5 pM) (*Fig1).*

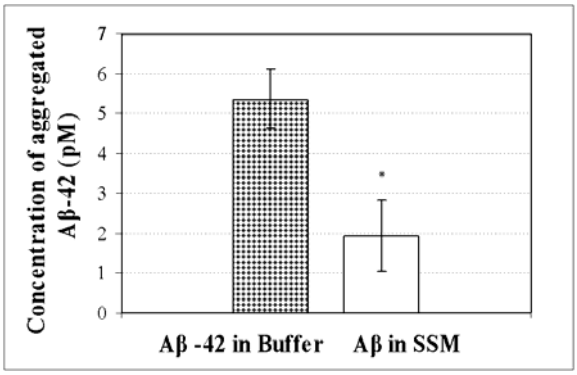

Fig.1 Effect of SSM on the Aβ-42 aggregation by Congo red assay (n=3; *p<0.05 compared to Aβ-42 alone).

Observation of Aβ-42 aggregation kinetics demonstrated that both the rate and extent of Aβ-42 aggregation was significantly ($p<0.05$) attenuated in presence of SSM *(Fig 2)*. Particle size distribution was heterogeneous with multiple peaks ranging from nanometer to micron scale. This heterogeneity can be attributed to presence of several different sized peptide aggregates (oligomers, protofibrils) co-existing together. Oligomers are spherical with a diameter of ~ 5nm, protofibrils range from spherical assemblies of ~ 5nm to short rod like sequences up to 200 nm in length while elongated fibrils extend into micron range[6]. Results of our light scattering study conform favorably with this. In presence of SSM, no detectable aggregates were observed indicating that association with lipid, radically reduced aggregation propensity of Aβ-42.

Aβ-42 is toxic to neurons and causes cell death through apoptotic mechanisms. SSM untreated Aβ-42 elicited neurotoxicity at >1μM. However, when incubated with SSM, Aβ-42 toxicity was significantly ($p<0.05$) attenuated *(Fig 3)*.

CONCLUSIONS

This study shows that Aβ-42 interacts avidly with biocompatible and biodegradable nanosized sterically stabilized phospholipid micelles resulting in attenuation of Aβ-42 aggregation and neurotoxicity in vitro.

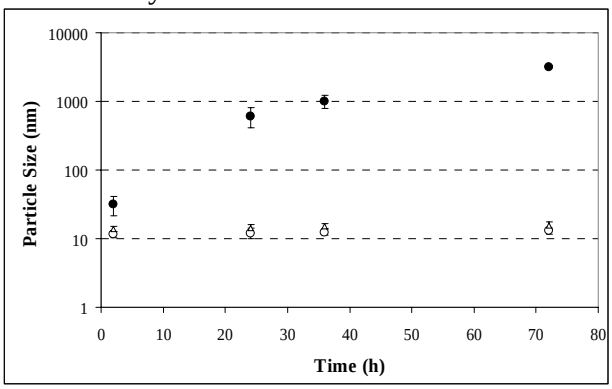

Fig.2 Effect of SSM on Aβ-42 aggregate growth by laser light scattering. (n=3; * $p<0.05$ compared to Aβ-42 alone). Open circles-Aβ-42 in SSM; Closed circles-Aβ-42 in buffer; Open triangles-SSM in buffer.

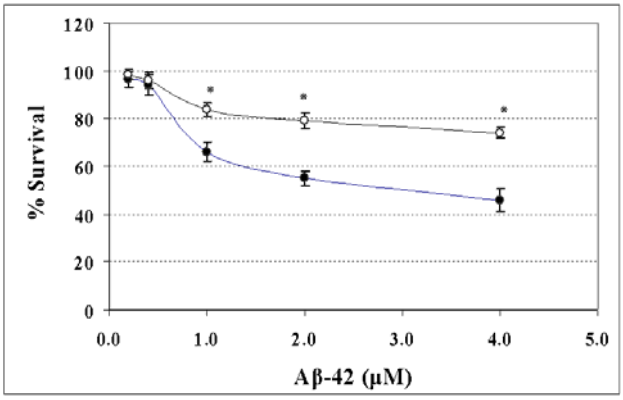

Fig.3 Effect of SSM on Aβ-42 induced cytotoxicity (n=3; *p<0.05 compared to Aβ-42 alone). Open circles-Aβ-42 in SSM; Closed circles-Aβ-42 in buffer**.**

REFERENCES

1. Selkoe, *Physiol. Rev*. 2001;**81**(2):741-766.
2. Lorenzo et al., *Proc Natl Acad Sci* 1994;**91**(25):12243-12247.
3. Poulsen et al., *J Struct Biol*. 2000 ; **130**: 142-52.
4. Gandhi et al., *Peptides*. 2002; **23**: 1433-9.
5. Klunk et al., *Anal Biochem.*1999; **266**:66-76.
6. Walsh et al., *Biochemical Society Transactions.* 2005; **33:1087**-090.

ACKNOWLEDGEMENTS

This study was supported in part by DOD grant BCRP, No. DAMD 17-02-1-0415, VA Merit Review and NIH grants RO1 AG024026, RO1 HL72323 and C06RR15482.

Appendix (14) 33rd Annual Meeting of Control Release Society Meeting, Austria

REAL TIME TRACKING OF ACTIVELY TARGETED PHOSPHOLIPID MIXED MICELLES TO HUMAN BREAST CANCER CELLS USING QUANTUM DOTS

Israel Rubinstein[1,2,4], Imre H. Soos[3], Hayat Onyuksel[1,3]
[1]Departments of Biopharmaceutical Sciences, [2]Medicine, and [3]Bioengineering University of Illinois at Chicago, and [4]Jesse Brown VA Medical Center, Chicago, Illinois 60612, U.S.A.
E-mail address of corresponding author: IRubinst@uic.edu

SUMMARY

We optically tracked accumulation of human vasoactive intestinal peptide-targeted biocompatible and biodegradable sterically stabilized phospholipid mixed micelles (VIP-SSMM) in cultured human MCF-7 breast cancer cells in real time using hydrophobic CdSe/ZnS quantum dots. We found that quantum dots encapsulated into VIP-SSMM accumulated significantly faster and in greater quantity in MCF-7 cells than did quantum dots in SSMM alone. We suggest that VIP-SSMM could be used as an actively targeted nanosized drug delivery platform for breast cancer.

INTRODUCTION

We have previously shown that paclitaxel-loaded, human vasoactive intestinal peptide-targeted biocompatible and biodegradable sterically stabilized phospholipid mixed micelles (VIP-SSMM) constitute an efficacious and safe nanomedicine for breast cancer over-expressing VIP receptors[1-3]. However, the mechanisms whereby these nanocarriers are internalized in target cells are uncertain. To begin to address this issue, we incorporated hydrophobic quantum dots[4] (QD) into the core of SSMM and VIP-SSMM and optically tracked their accumulation into human breast cancer cells (MCF-7) over-expressing VIP receptors.

EXPERIMENTAL METHODS

Encapsulation of quantum dots into sterically stabilized phospholipid mixed micelles

Red emitting (λ_{em}=620nm, diameter~5nm) CdSe/ZnS core shell QD were obtained from Evident Technologies (Troy, NY).

Sterically stabilized phospholipid mixed micelles (SSMM size~15nm) were prepared as previously described in our laboratory[1]. Briefly, distearoyl-phosphatidylethanolamine-polyethyleneglycol-2000 (DSPE-PEG2000) and egg phosphatidylcholine (EPC) (molar ratio, 90:10; final lipid concentration, 5 mM) were dissolved in chloroform. Quantum dots dissolved in toluene (80 µg/mL) were added to the mixture, vortexed and evaporated under argon and vacuum. The resulting film was dried under vacuum overnight. Thereafter, HEPES buffer (10 mM, pH 7.4) was added to each flask, vortexed, sonicated and allowed to equilibrate in the dark for 2 h at 25 ºC. Human VIP (final concentration of 3.0 µM) was then incorporated into SSMM as previously described[3].

Cell culture

Adherent human MCF-7 cells (ATCC, Manassas, VA) were incubated in 5% CO_2 at 37ºC in complete growth medium supplemented with 10% FBS. Cells were seeded onto 12 mm glass cover slips in 24-well tissue culture plates at a density of 15,000 cells/well and allowed to grow for 3 days. On the day of the experiment, the media was replaced with culture media containing SSMM-QD or VIP-SSMM-QD and incubated for various time intervals. In another series of experiments, 30 µM human VIP was added to the culture media 30 min before exposure of cells to SSMM-QD or VIP-SSMM-QD.

Cell imaging

At the conclusion of the incubation period, cells were washed with serum-free media and PBS, stained, and fixed with 4% paraformaldehyde. Wheat germ agglutinin (WGA; Molecular Probes, Eugene, OR) and DAPI were used to outline the cell membrane and nucleus, respectively. Cover slips were then mounted onto glass slides and sealed.

Images of cells were obtained using an Olympus IX70 inverted fluorescent microscope and a CCD camera. To localize QD within cells,

optical z-stack sections were obtained using a Zeiss LSM 510 Axiovert 1000 laser scanning confocal microscope with argon UV laser excitation wavelength of 364 nm.

A normalized fluorescence signal value was determined by comparing the ratio of the red signal from QD in an image frame to the number of cells visible in that frame. All images were taken under identical exposure conditions. Five images were used to compute a mean for each individual time point.

Data and statistical analyses

Data are expressed as means ± standard deviation. Statistical analysis was performed using ANOVA and Tukey's post-hoc test. $P<0.05$ was considered statistically significant.

RESULTS AND DISCUSSION

We found that QD encapsulated into VIP-SSMM accumulated faster and in greater quantity in human MCF-7 cells than did QD in SSMM alone (Figure 1; $p<0.05$). After 2-h incubation, cells exposed to VIP-SSMM had a 1.8-fold higher normalized fluorescence signal than did SSMM (Figure 1; $p<0.05$). Pre-treatment of cells with excess free VIP to saturate VIP receptors significantly attenuated the fluorescence signal in MCF-7 cells exposed to VIP-SSMM-QD but not to SSMM-QD alone (Figure 1; $p<0.05$). Confocal microscopy revealed that cells incubated with VIP-SSMM had significantly higher accumulation of QD within their cytoplasm relative to cells exposed to SSMM alone (n=3; $p<0.05$). Taken together, these data indicate that uptake and internalization of VIP-SSMM nanoparticles into MCF-7 cells are time-dependent phenomena mediated, in part, by VIP receptors.

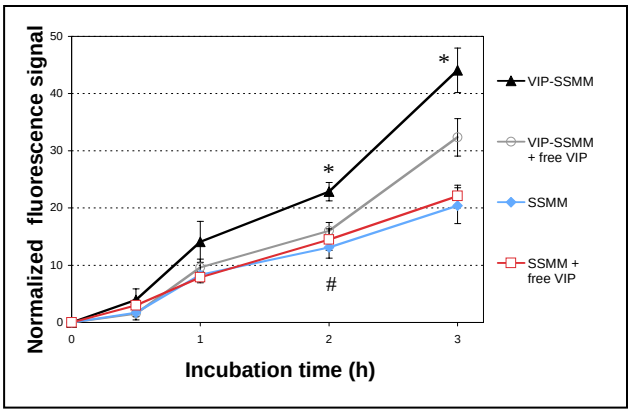

Figure 1. Normalized fluorescence signal of VIP-SSMM-QD and SSMM-QD in human MCF-7 cells with and without pre-exposure to excess free VIP (30 µM). Each group, n=3 separate experiments; *p<0.05 for VIP-SSMM as compared to SSMM; #p<0.05 for VIP-SSMM as compared to VIP-SSMM + free VIP.

CONCLUSIONS

Quantum dots encapsulated into biocompatible and biodegradable VIP-SSMM accumulated significantly faster and in greater quantity in MCF-7 cells than did quantum dots in SSMM alone. We suggest that VIP-SSMM could be used as an actively targeted nanosized drug delivery platform for breast cancer.

ACKNOWLEGEMENTS

This work was supported, in part, by DOD grant BCRP, #DAMD 17-02-1-0415, VA Merit Review and NIH grants R01 AG024026, R01 HL72323 and C06RR15482.

REFERENCES

1. Krishnadas, A., et al, *Pharmaceutical Research*, 20, 297-302 (2003)
2. Ashok, B., et al, *Journal of Pharmaceutical Sciences*, 93, 2476-2487 (2004)
3. Dagar, S., et al, *Journal of Controlled Release*, 74, 129-134 (2001)
4. Alivisatos, P., et al, *Annu. Rev. Biomed. Eng.* 7, 55-76 (2005)

Appendix (15)

Journal of
Nanoscience and Nanotechnology
Vol. 6, 2996–3000, 2006

Camptothecin in Sterically Stabilized Phospholipid Nano-Micelles: A Novel Solvent pH Change Solubilization Method

Otilia M. Y. Koo[1], Israel Rubinstein[1,2,4], and Hayat Onyuksel[1,3,*]

Departments of [1]Biopharmaceutical Sciences, [2]Medicine, and [3]Bioengineering, University of Illinois at Chicago, USA
[4]Jesse Brown VA Medical Center, Chicago, IL 60612, USA

Camptothecin (CPT) is a topoisomerase I inhibitor that acts against a broad spectrum of cancers. Unfortunately clinical application of CPT is limited by insolubility, instability, and toxicity problems. To circumvent these delivery problems of CPT, we propose biocompatible, targeted sterically stabilized micelles (SSM) as nanocarriers for CPT (CPT-SSM). SSM composed of polyethylene glycol (PEGylated) phospholipids are attractive nanocarriers for CPT delivery because they are sufficiently small to extravasate through the leaky microvasculature of tumor and inflamed tissues for passive targeting. The purpose of this study was to develop a novel method of preparing CPT-SSM based on its pH dependent, reversible carboxylate-lactone conversion chemistry. CPT carboxylate was added to SSM at pH 5 that favored the formation of active but hydrophobic CPT lactone for spontaneous association with SSM. The kinetics of CPT conversion and CPT-SSM formation, and the effect of varying CPT-PEGylated phospholipid molar ratio on CPT-SSM properties and CPT solubilization were evaluated. CPT converted gradually from the carboxylate form to lactone, and CPT-SSM were formed after 12 h incubation. The mean size of CPT-SSM was ~14 nm. CPT solubilization (~12 μg/ml) and other CPT-SSM micelle properties did not change significantly with increasing CPT to PEGylated phospholipid molar ratios using this novel method, unlike the coprecipitation/reconstitution technique previously reported. This reproducible CPT solubilization in SSM was attributed to avoidance of drug aggregate formation by this method. The advantages of our solvent pH change method to prepare CPT-SSM support further investigations of this approach to other hydrophobic drugs similar to CPT in chemistry and also CPT molecular solubilization in other nanocarriers.

Keywords: Camptothecin, PEGylated Phospholipids, Nano-Micelles, Solubilization, pH Change.

1. INTRODUCTION

Camptothecin (CPT) is a potent anticancer agent that is active against a broad spectrum of cancers, including ovarian, colon, breast, and lung cancers.[1–3] However, clinical use of CPT is hampered by poor aqueous solubility and instability under physiologic conditions and its potential to cause toxic side effects such as hemorrhagic cystitis and myelosuppression.[4–6] Previously, we developed sterically stabilized micelles (SSM) as targeted drug nanocarriers for CPT.[7] SSM are long circulating nanocarriers due to their polyethylene glycol outer corona that reduce opsonization and clearance by the mononuclear phagocytic system.[8] SSM are of an ideal size range (~13–16 nm) for passive targeting to cancer and inflamed tissues by selective extravasation though leaky microvasculature (pore size, ~100–300 nm)[9] but not through normal (pore size, <5 nm) microvascular wall. SSM form spontaneously in an aqueous environment when diacyl lipid-polyethylene glycol (PEG) phospholipids exist at concentrations above the critical micelle concentration (CMC).[10,11] These phospholipid molecules are biocompatible and biodegradable[12] and hence, safe for human use. Although PEGylated phospholipids have a negatively charged phosphodiester group, zeta potential of PEGylated phospholipid micelles was found to be close to neutral, about −9.0 mV due to the "hidden charge effect."[13] Many researchers concurred that this effect resulted from the PEG moiety moving the plane of shear further away from the lipid/water interface.[13,14] This effect resulted in almost neutral zeta potentials for sterically stabilized micelles loaded with drug and other nano-carriers (e.g., liposomes) surface-modified with PEGylated phospholipids.[13]. Previously, when we prepared CPT-loaded SSM by the conventional

*Author to whom correspondence should be addressed.

1533-4880/2006/6/2996/005 doi:10.1166/jnn.2006.460

coprecipitation/reconstitution method, we observed formation of a second population of nano-sized sterically stabilized particles (SSP) when drug to PEGylated phospholipids molar ratio exceeded a critical molar ratio.[7] This may impact reproducibility of drug solubilization when drug-PEGylated phospholipid molar ratios greater than the critical ratio were used. We hypothesize that SSPs were sterically stabilized drug nanoparticles coated by PEGylated phospholipids that prevent their further precipitation and remain suspended in aqueous medium as a clear solution. Even though SSPs can be attractive to be used as a sustained release nanomedicine,[15] our goal was to solubilize CPT in molecular state in SSM.

The purpose of this study was to prepare CPT-SSM formulations devoid of SSPs by a novel method based on reversible, pH-dependent chemical conversion of CPT from relatively water soluble carboxylate to water-insoluble active lactone form that associates spontaneously with SSM. At pH 5, the active, hydrophobic lactone form of CPT predominates, while at pH $\geq$ 7, the inactive, soluble carboxylate form predominates.[16] Our aim was to obtain a homogeneous formulation of a single population of CPT-SSM and reproducible CPT solubilization at a molecular level that will not be affected by CPT-PEGylated phospholipid molar ratios used during preparation.

2. MATERIAL AND METHODS

2.1. Chemicals

Camptothecin (99% purity, M.W. 348.3) was a gift from Boehringer Ingelheim Fine Chemicals (Ingelheim, Germany). Poly (ethylene glycol 2000)-conjugated diastearoyl phosphatidylethanolamine (DSPE-PEG_{2000}) was purchased from Northern Lipids Inc. (Vancouver, B.C., Canada). Buffer and all other reagents used were analytical grade and purchased from Sigma-Aldrich (St Louis, MO). Water was deionized at 18 MΩ-cm and sterile filtered before use.

2.2. Preparation of CPT-SSM

CPT-SSM were prepared using DSPE-PEG_{2000} concentration of 5 mM, and varying molar ratios of CPT : DSPE-PEG_{2000} (0.003 : 1 to 0.057 : 1). Accurately weighed amounts of CPT based on the molar ratios to be studied, were first dissolved in 0.01 N NaOH for 12 h at 4 °C. Concentrations of the CPT carboxylate solutions were measured by reversed-phase high performance liquid chromatography using the conditions described in 2.4. The CPT carboxylate solution was then added drop wise within 1 min to 5 mM DSPE-PEG_{2000} in 0.01 M acetate buffer (pH 5.0), and the vial was shaked gently lengthwise for 1 min. The resulting dispersions were incubated at 25 °C in the dark for up to 24 h. Aliquots at fixed time intervals were removed after gentle shaking and centrifuged (13,000 g) to remove any excess precipitated drug before characterization. All dispersions were prepared in triplicates.

2.3. Size Analysis and Morphologic Features

CPT-SSM particle size and morphology under transmission electron microscope (TEM) were determined as described previously.[7] Particle size was measured by quasi- elastic light scattering (QELS) using a NICOMP 380 particle size analyzer (Santa Barbara, CA), equipped with a 5 mW helium-neon laser at 632.8 nm. Mean diameters of the particles in the aqueous dispersions were calculated using the Stokes-Einstein equation by the NICOMP CW380 software.

The CPT-SSM aqueous dispersions were observed under TEM (Jeol JEM-1220, Jeol USA Inc., MA) at 100 kV for morphology. A 0.05 ml drop of sample was placed on the formvar carbon support film (grid mesh 200) and stained with 1% uranylacetate (pH 4.5) for 1 min. Excess stain was removed and sample was air dried at room temperature. TEM images were recorded by a multiscan camera (Gatan Inc., CA) using the Gatan Digital Micrograph version 2.5 software.

2.4. HPLC analysis for CPT concentrations

Concentration of solubilized CPT in the aqueous dispersions was measured by reversed-phase HPLC using conditions modified from literature.[17] Experiments were performed at ambient temperature at a flow rate of 1 ml/min using a HPLC setup that consisted the following: ThermoFinnigan Spectra System P2000 pump, Spectra System AS3500 Autosampler and Spectra Focus Forward Optical Scanning Detector. Injection volumes of 20 μl were used and the mobile phase was acetonitrile-10 mM potassium phosphate (45 : 55 v/v, pH 7.0). Separations were achieved on an Agilent Zorbax SB-C18 reverse-phase column (250 × 4.6 mm, 5 mm). UV detection was achieved at a wavelength of 365 nm. A calibration curve was produced based on the average peak area of standard injections of CPT lactone and carboxylate. All injections were performed in triplicates.

2.5. Fluorescence Emission Spectroscopy

A shift in CPT fluorescence peak emission towards a lower wavelength is indicative of CPT movement from the aqueous medium into a more hydrophobic environment.[18] Thus, fluorescence emission experiments would demonstrate the association of CPT with SSM since SSM provided a more hydrophobic environment for CPT. Fluorescence emission spectra of CPT in the absence of phospholipids and in SSM were recorded at a scan rate of 1 nm/s with a SLM-Aminco 8000 spectroflourimeter (Edison, NJ) at an excitation wavelength of 360 nm using

parameters described previously.[7] Samples were measured in cuvets of 1 cm pathlength at ambient temperature. Fluorescence emission spectra for each sample were obtained in duplicates, each system was repeated three times (i.e., 3 samples/system).

2.6. Data and Statistical Analyses

Formulation and characterization data are expressed as means ± SD. Differences between groups were compared using one-way ANOVA followed by Scheffe's post-hoc tests. All statistical analyses were performed using the SPSS program (version 10.0, Chicago, IL). $P < 0.05$ was considered statistically significant.

3. RESULTS AND DISCUSSION

3.1. Kinetics of CPT Carboxylate to Lactone Conversion

The conversion of CPT carboxylate to lactone for loading into DSPE-PEG_{2000} SSM at predetermined time intervals was observed by the relative peak changes of the two forms on the HPLC chromatogram (Fig. 1). Confirmation of chemical conversion of CPT was also evident from the shift in peak fluorescence emission wavelength toward a lower wavelength, which will be discussed in the following section. The kinetics of CPT carboxylate to lactone conversion for preparation of CPT-SSM (DSPE-PEG_{2000} concentration = 5 mM, CPT : DSPE-PEG_{2000} molar ratio = 0.028 : 1) is illustrated in Figure 2. Added CPT carboxylate (50 μg/ml) decreased almost linearly in the first 5 h of incubation, and after 10 h only 1.52 ± 0.17 μg/ml remained. From the CPT lactone concentration versus time profile (Fig. 2), CPT lactone solubilized concentration increased as carboxylate concentration decreased during the first 3 h. However, a supersaturated solution of CPT lactone in SSM existed between 3 to 5 h, when the solubilized lactone concentration was approximately 32 μg/ml. Within the next 5 h (i.e., 5 to 10 h of incubation), the supersaturated lactone concentration decreased to steady concentrations (11–12 μg/ml). Solubilized CPT lactone concentrations did not change significantly between 10 h and 72 h ($n = 3$, $p > 0.05$). This implied that more than 10 h is required to achieve equilibrium CPT lactone concentrations as CPT-SSM. Thus, at least 12 h are required to form CPT-SSM using solvent pH change preparation. Unlike other methods to prepare nanoparticulate systems, this method is simple and involved only mixing and incubation of the CPT carboxylate and DSPE-PEG_{2000} micelle solution. Furthermore, organic solvents or heating were not required. The major limitation of this method was the lengthy incubation (~12 h) required to prepare CPT-SSM compared to the conventional method of coprecipitation/reconstitution where CPT-SSM is formed immediately upon buffer addition to the molecular film of coprecipitated drug and phospholipids.[7]

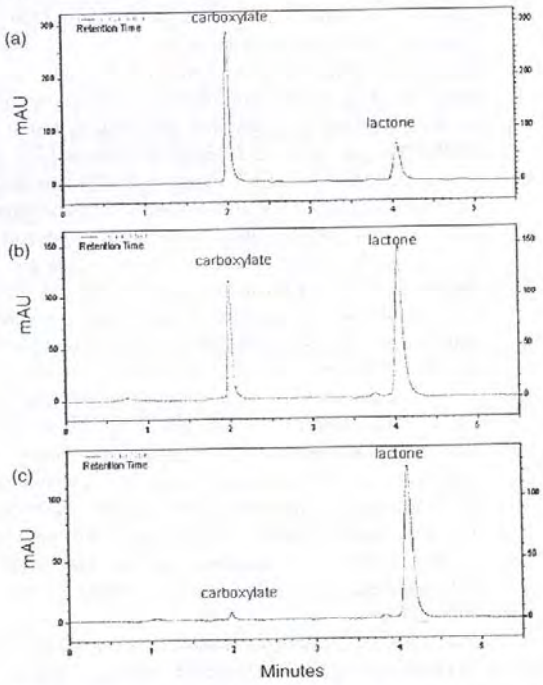

Fig. 1. Representative HPLC chromatograms illustrating the conversion of CPT carboxylate to lactone for the formation of CPT-SSM with (a) 0.5 h, (b) 3 h, and (c) 10 h incubation.

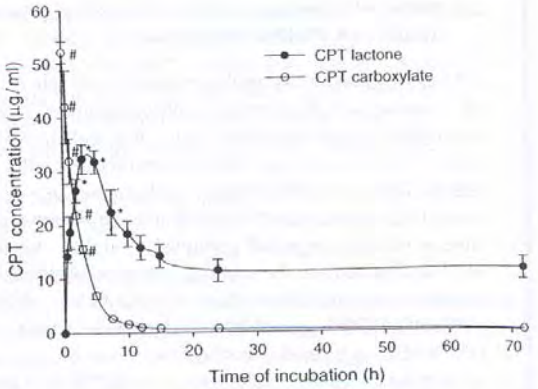

Fig. 2. Concentration-time profile of the conversion of CPT carboxylate to lactone for the preparation of CPT-SSM. DSPE-PEG_{2000} concentration = 5 mM, initial added CPT : DSPE-PEG_{2000} molar ratio = 0.028 : 1, (•) represents CPT lactone concentrations; (○) represents CPT carboxylate concentrations. *, # indicated significantly different lactone and carboxylate concentrations, respectively from 72 h (ANOVA, $p < 0.05$). $n = 3$ separate experiments and error bars represent S.D. (these are smaller than symbols for CPT carboxylate when time of incubation ≥7.5 h).

3.2. Effect of Increasing CPT-DSPE-PEG$_{2000}$ Molar Ratio on CPT-SSM Properties

CPT-SSM prepared using this method were spherical and of a narrow size distribution as observed under TEM and quasi-elastic light scattering (Figs. 3(a) and (b)). Micelle size (~14 nm) did not change significantly with initial added CPT to DSPE-PEG$_{2000}$ molar ratio ($n = 3$, $p > 0.05$) (Fig. 3(c)), and CPT-SSM micelle diameters were similar to those reported previously.[7] Unlike the phenomenon observed for the coprecipitation/reconstitution formulation method, where there was formation of SSP at CPT : DSPE-PEG$_{2000}$ = 0.014 : 1 and above (using 5 mM DSPE-PEG$_{2000}$),[7] in this method there was no appearance of SSP up to CPT : DSPE-PEG$_{2000}$ = 0.057 : 1. This was attributed to the slow conversion of CPT carboxylate to the hydrophobic lactone form to be loaded into the micelles. Once the saturation limit of CPT lactone in SSM at a fixed phospholipid concentration was exceeded, drug particles were formed at a slow enough rate to form precipitates larger than the nanosize range, thus they were not sufficiently sterically stabilized by the PEGylated phospholipids. Consequently, the large CPT precipitates were removed from the aqueous dispersions by centrifugation, leaving a system containing only CPT-SSM.

CPT solubilization in SSM (11–12 μg/ml) did not change significantly with increasing CPT-phospholipid molar ratios up to 0.057 : 1 ($n = 3$, $p > 0.05$) (Fig. 4). The use of molar ratios above the CPT : DSPE-PEG$_{2000}$ critical molar ratio of 0.014 : 1 at 5 mM DSPE-PEG$_{2000}$ (as determined in the coprecipitation/reconstitution method) did not result in formation of drug nanosized particles (SSP). Consequently, there was no increase in CPT solubilization with increasing CPT-phospholipid molar ratios due to SSP in this method. A comparison of CPT solubilization in SSM by the 2 methods is illustrated in Figure 4. Using 5 mM DSPE-PEG$_{2000}$, up to a 12-fold increase in CPT solubilization compared to CPT alone in buffer was achieved. This was a higher CPT solubilization when compared to other micellar systems used at their safe concentrations, e.g., 4-fold for Pluronic micelles[20] and 5-fold for Tween micelles[17] CPT and its analogs exhibit this pH-dependent carboxylate-lactone conversion, therefore, we anticipate that this method of solubilization can also be investigated for other CPT analogs as well as other nanocarrier systems. Using a similar approach of pH change, silatecan 7-t-butyldimethylsilyl-10-hydroxycamptothecin has also been formed and associated with a chemically modified beta-cyclodextrin.[21] Our data are significant in demonstrating the kinetics of CPT carboxylate-lactone conversion and that CPT solubilization behavior in SSM and micelle properties were not influenced by varying initial CPT-PEGylated phospholipid molar ratios due to elimination of SSP formation.

Fluorescence emission spectra of CPT in the absence of DSPE-PEG$_{2000}$ are illustrated in Figure 5, where the fluorescence peak emission wavelength shifted towards a lower wavelength when CPT converted from the water soluble carboxylate form to the hydrophobic lactone form.

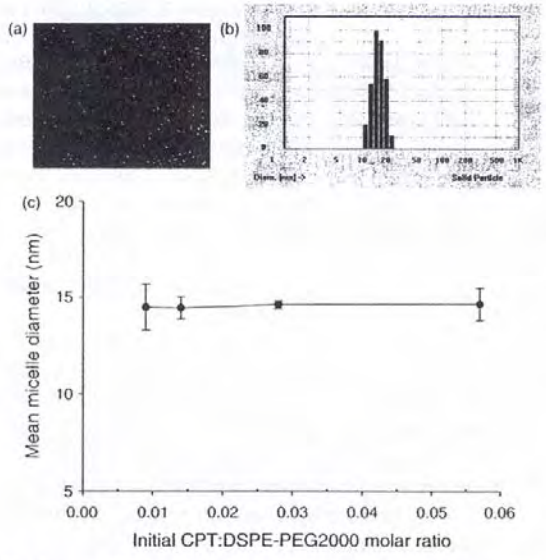

Fig. 3. (a) CPT-SSM spherical morphology observed under TEM; and (b) size and size distribution of CPT-SSM. DSPE-PEG$_{2000}$ concentration = 5 mM, initial added CPT : DSPE-PEG$_{2000}$ molar ratio = 0.028 : 1; (c) Mean micelle diameter with increasing initial added CPT : phospholipid molar ratio (DSPE-PEG$_{2000}$ concentration = 5 mM). No significant change in micelle diameter with CPT : phospholipid molar ratio was observed (ANOVA, $p > 0.05$). $n = 3$ separate experiments and error bars represent S.D.

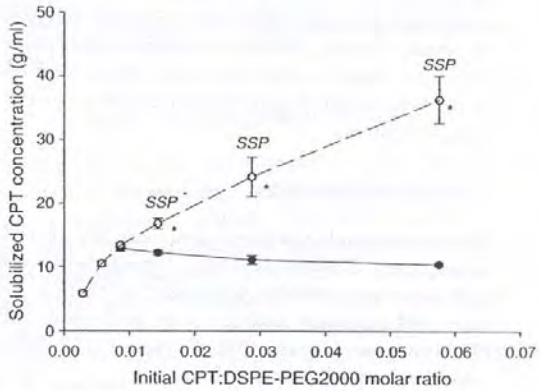

Fig. 4. Comparison of solubilized CPT concentration in SSM with increasing initial added CPT : phospholipid molar ratio (DSPE-PEG$_{2000}$ concentration = 5 mM), prepared by (•) solvent pH change and (○) coprecipitation/reconstitution. No significant change in solubilized CPT concentration in SSM with CPT : phospholipid molar ratio by solvent pH change was observed (ANOVA, $p > 0.05$). *indicated significant increase in CPT solubilization due to SSP in addition to CPT-SSM (ANOVA, $p < 0.05$) by coprecipitation/reconstitution (This profile (—) is taken from Ref. 7). $n = 3$ separate experiments and error bars represent S.D.

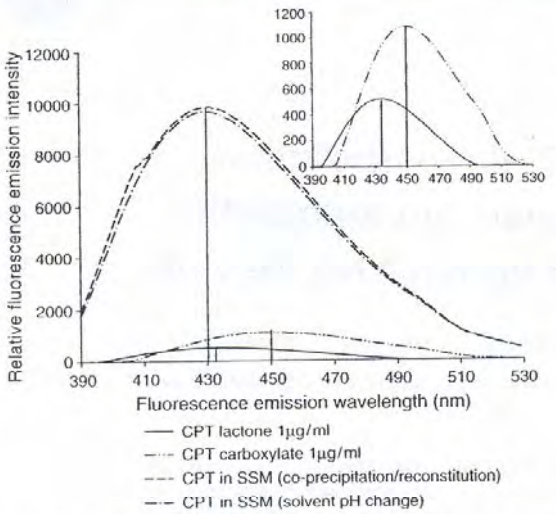

Fig. 5. Averaged CPT fluorescence emission spectra of CPT (1 μg/ml) lactone (—) and carboxylate (····) in the absence of phospholipids [spectra are magnified and depicted in the inset]; CPT in SSM (DSPE-PEG2000 concentration = 5 mM, CPT:DSPE-PEG2000 = 0.009:1), prepared by (—) coprecipitation/reconstitution and (---) solvent pH change. $n = 3$ separate experiments.

Fluorescence emission spectra of CPT associated with SSM indicated a further significant shift in fluorescence peak emission wavelength (429.9 ± 0.4 nm; $n = 3$) compared to CPT in buffer (434.7 ± 0.6 nm; $n = 3$). This was similar to liposomes[22] where CPT fluorescence peak emission wavelength shifted towards a lower wavelength when it moved from the aqueous medium into a more hydrophobic environment. There was no significant difference in fluorescence peak emission wavelength of CPT in SSM with increasing CPT:DSPE-PEG_{2000} molar ratios ($n = 3$, $p > 0.05$) and also with CPT in SSM prepared by co-precipitation/reconstitution preparation (430.1 ± 0.7 nm; $n = 3$) (Fig. 5).[7] Therefore, using both formulation methods molecular CPT was loaded into the same region of the micelles, and thus existed in a region of similar polarity within the micelle.

4. CONCLUSIONS

We have developed and tested an improved method to prepare nano-sized CPT-SSM. A homogeneous population of CPT-SSM was prepared after incubation and conversion of CPT soluble carboxylate to active hydrophobic lactone in the presence of empty SSM. A 12-fold increase in CPT solubilization in SSM was achieved compared to CPT in buffer. Formation of SSPs was avoided; therefore, solubilization behavior of CPT in SSM was not influenced by SSPs formation above the critical CPT-PEGylated phospholipid molar ratio as observed with the coprecipitation/reconstitution method. The advantages of this method support its further development and testing for hydrophobic CPT analogs that have similar chemistry. Lastly, our data from this study suggest that CPT solubilization into other nanocarrier systems using the same solvent pH change principles is worth investigating as well.

Acknowledgments: This work was supported, in part, by a VA Merit Review grant, Department of Defense grant BCRP, No. DAMD 17-02-1-0415 and NIH grants RO1 AG024026 and RO1 HL72323. This investigation was conducted in a facility constructed with support from grant C06RR15482 from the NIH National Center for Research Resources. O. M. Y. Koo is a recipient of the UIC Fellowship 2004–2005. We thank Dr. Gemeinhart for using his laboratory equipment during this study.

References and Notes

1. M. K. Clements, S. Wasi, and S. S. Daoud, *Anticancer Drugs* 7, 851 (1996).
2. E. A. Natelson, B. C. Giovanella, C. F. Verschraegen, K. M. Fehir, P. D. De Ipolyi, N. Harris, and J. S. Stehlin, *Ann. N. Y. Acad. Sci.* 803, 224 (1996).
3. N. H. Oberlies and D. J. Kroll, *J. Nat. Prod.* 67, 129 (2004).
4. R. Garcia-Carbonero and J. G. Supko, *Clin Cancer Res.* 8, 641 (2002).
5. U. Schaeppi, R. W. Fleischman, and D. A. Cooney, *Cancer Chemother. Rep* 3, 25 (1974).
6. C. L. Erickson-Miller, R. D. May, J. Tomaszewski, B. Osborn, M. J. Murphy, J. G. Page, and R. E. Parchment, *Cancer Chemother Pharmacol.* 39, 467 (1997).
7. O. Koo, I. Rubinstein, and H. Onyuksel, *Nanomedicine.* 1, 77 (2005).
8. A. N. Lukyanov, Z. Gao, L. Mazzola, and V. P. Torchilin, *Pharm Res.* 19, 1424 (2002).
9. S. H. Jang, M. G. Wientjes, D. Lu, and J. L. Au, *Pharm Res.* 20, 1337 (2003).
10. L. Arleth, B. Ashok, H. Onyuksel, P. Thiyagarajan, J. Jacob, and R. P. Hjelm, *Langmuir* 21, 3279 (2005).
11. B. Ashok, L. Arleth, R. P. Hjelm, I. Rubinstein, and H. Onyuksel, *J. Pharm. Sci.* 93, 2476 (2004).
12. P. K. Working and A. D. Dayan, *Hum Exp Toxicol.* 15, 751 (1996).
13. O. Garbuzenko, S. Zalipsky, M. Qazen, and Y. Barenholz, *Langmuir* 21, 2560 (2005).
14. M. C. Woodle, M. S. Newman, and J. A. Cohen, *J. Drug. Target.* 2, 397 (1994).
15. B. E. Rabinow, *Nat. Rev. Drug. Discov.* 3, 785 (2004).
16. J. H. Beijnen, H. Rosing, W. W. ten Bokkel Huinink, and H. M. Pinedo, *J. Chromatogr.* 617, 111 (1993).
17. R. Cortesi, E. Esposito, A. Maietti, E. Menegatti, and N. C., *Int. J. Pharm.* 159, 95 (1997).
18. T. G. Burke, A. K. Mishra, M. C. Wani, and M. E. Wall, *Biochemistry.* 32, 5352 (1993).
19. D. Needham, T. J. McIntosh, and D. D. Lasic, *Biochim. Biophys. Acta.* 1108, 40 (1992).
20. R. Barreiro-Iglesias, L. Bromberg, M. Temchenko, T. A. Hatton, A. Concheiro, and C. Alvarez-Lorenzo, *J. Control. Rel.* 97, 537 (2004).
21. T. X. Xiang and B. D. Anderson, *Pharm Res.* 19, 1215 (2002).
22. T. G. Burke, A. E. Staubus, and A. K. Mishra, *J. Amer. Chem. Soc.* 114, 8318 (1992).

Received: 15 December 2005. Revised/Accepted: 16 March 2006.